Optimal Performance-Based Control of Structures against Earthquakes Considering Excitation Stochasticity and System Nonlinearity

DISSERTATION

Presented in Partial Fulfillment of the Requirements for the Degree Doctor of Philosophy in the Graduate School of The Ohio State University

By

Omar El Khoury, M.S., B.E.

Graduate Program in Civil Engineering

The Ohio State University

2017

Dissertation Committee:

Dr. Abdollah Shafieezadeh, Advisor

Dr. Natassia Brenkus

Dr. Halil Sezen

Dr. Wei Zhang

Abstract

Natural disasters are one of the constant challenges for designing new and strengthening existing infrastructures. Such hazards in the past have incurred significant loss of life and economic damage; therefore, further research is warranted in this area to enhance the health and minimize the cost of maintaining and upgrading infrastructures, improve residents' comfort, and enable achieving higher levels of life safety. To this end, the field of hazard mitigation and control focuses on performance improvement, safety, and cost effectiveness of structures mostly through minimizing large deformations of seismic-excited structures and suppressing the damage and collapse in dynamic systems due to excessive vibrations.

Past developments in active and semi-active control designs, such as the commonly used state space controllers (e.g. linear quadratic regulator for fully observed systems and linear quadratic Gaussian for partially observed systems), consider linear feedback strategies. Meanwhile, such control strategies require linearization, and the system is usually linearized based on linear elastic properties. The control force is proportional to the state space vector and the dynamics and constraints of control devices are mainly ignored. The objective functions have restrictive forms, and are solely dependent on a second order convex function of the response variables. To overcome the aforementioned shortcomings, this dissertation develops new stochastic control algorithms for active and semi-active control strategies. This research concentrates on the development of frameworks that

incorporate nonlinearity of the system, uncertainty of the excitation, and constraints and dynamics of the control device. Control designs are developed based on different objective functions such as higher order polynomials of response variables, reliability of the structure, and life cycle cost of the system considering hazard risks in seismic prone areas.

In particular, a nonlinear sliding mode control algorithm based on stochastic linearization is developed; this method supports higher order objective functions and therefore enhances the ability of designers to achieve design objectives. The proposed control algorithm is designed, optimized, and tested on a seismically excited multi-span bridge equipped with semi-active magnetorheological dampers. Next, a stochastic control algorithm is presented based on a proposed stochastic averaging method called enhanced stochastic averaging. This method conserves the nonlinear behavior of the system and the stochastic nature of the excitation in optimal control design. In order to directly minimize the probability of failures, the stochastic control algorithm is extended to a reliability-based control algorithm. These control algorithms are implemented in a system with nonlinear soil-structure interactions. Furthermore, a risk-based control methodology is developed to minimize life cycle cost of a nonlinear multi-story building subjected to seismic excitations. The findings of these proposed control methodologies are found to be superior to conventional control techniques. This doctoral research aims at filling a major gap in smart control technology in terms of conserving nonlinearity and stochasticity in control design. Moreover, they provide explicit optimization processes based on reliability and risk. Future investigations include advancing the proposed methods and applying them to different structural systems subjected to various hazard types.

Dedication

Dedicated to my family and friends.

Acknowledgments

My PhD pursuit at The Ohio State University was a delightful journey full of challenges and growth on the personal and professional levels. I would like to express my deepest appreciation to my advisor, Dr. Abdollah Shafieezadeh, who mentored me, guided me, motivated me, encouraged me, and advocated for me during the past four years. I would like to thank the Department Chair Dr. Dorota Grejner-Brzezinska for the opportunity to continue my education at Ohio State and my former advisor Dr. Hojjat Adeli for the wonderful experience in the first year of my PhD. Special thanks to Ms. Nancy Kaser for the encouragement and empathetic support. I would also like to acknowledge my defense and candidacy committee members including Dr. Wei Zhang, Dr. Ethan Kubatko, Dr. Halil Sezen, and Dr. Natassia Brenkus, who gave me insightful feedback and advice about my research direction and my future endeavors.

My experience was fulfilling because I met wonderful people such as my friends and colleagues in RAMSIS. I joined different organizations on-campus and off-campus including fellowships, cultural clubs, and my church. I am blessed to have met so many people and have built everlasting relationships and friendships. In addition, I sincerely thank my gracious family for their sacrifice and my faithful friends back home for their wholehearted love. My last and foremost thanks and praises go to the Lord Jesus Christ for through Him I can do all things (Philippians 4:13).

Vita

Sep. 2004 to June 2008 .....B.E. Civil Engineering, Department of Civil, Environmental and Geodetic Engineering, Notre Dame University, Lebanon

August 2008 to August 2010 .....M.S., Department of Civil Engineering, North Dakota State University

August 2008 to August 2009 .....Graduate Teaching Assistant, Department of Civil Engineering, North Dakota State University

August 2009 to August 2010 .....Graduate Research Assistant, Department of Civil Engineering, North Dakota State University

Feb. 2011 to July 2012 .....Structural Engineer, D.G. Jones, Lebanon

August 2012 to Present .....Ph.D., Department of Civil, Environmental and Geodetic Engineering, The Ohio State University

August 2012 to July 2013 .....Graduate Fellow, Graduate School, The Ohio State University

August 2013 to July 2014 .....French Fellow, Department of Civil, Environmental and Geodetic Engineering, The Ohio State University

July 2014 to Present .....PhD Candidate, Department of Civil, Environmental and Geodetic Engineering, The Ohio State University

August 2014 to Present .....Graduate Teaching Associate, Department of Engineering Education, The Ohio State University

Publications

Journal Papers

El-Khoury, O., Shafieezadeh, A., and Fereshtehnejad, E. (2017), "Risk-Based Control Based of Nonlinear Structures." Structural Control and Health Monitoring, In Preparation.

El-Khoury, O. and Shafieezadeh, A. (2017b), "Reliability-Based Control Strategies for Nonlinear Hysteretic Systems Using Enhanced Stochastic Averaging Approach." Earthquake Engineering and Structural Dynamics, In Preparation.

El-Khoury, O. and Shafieezadeh, A. (2016). A Stochastic Averaging-based Optimal Control Method for Nonlinear Systems: Application to a Building with Soil-structure Interactions. Engineering Structures, Vol. 127, No. 15, pp. 635-644.

El-Khoury, O., Shafieezadeh, A., Kim, C., Hur, J. E., and Heo, G. H. (2016), "Mitigation of the Seismic Response of Multi-Span Bridges Using MR Dampers: Experimental Study

of a New SMC-Based Controller." Journal of Vibrations and Control, DOI: 10.1177/1077546316633540.

El-Khoury, O., Kim, C., Shafieezadeh, A., Hur, J. E., and Heo, G. H. (2015), "Experimental study of the semi-active control of a nonlinear two span bridge using stochastic optimal polynomial control." Smart Materials and Structures, Vol. 24, No.6, pp. 1-15.

El-Khoury, O. and Adeli, H. (2013), "Recent Advances on Vibration Control of Structures under Dynamic Loading." Archives of Computational Methods in Engineering, Vol. 20, No.4, pp.353-360.

Conference Papers

El-Khoury, O., Kim, C., Shafieezadeh, A., Hur, J. E., and Heo, G. H. (2015), "Shake Table Tests of Stochastic Optimal Polynomial Control of Two Span Bridge Equipped with MR Dampers."12th International Conference on Applications of Statistics and Probability in Civil Engineering, Vancouver, Canada, July 12-15, 2015, peer reviewed.

El-Khoury, O. and Shafieezadeh A. (2015), "A Constrained Nonlinear Stochastic Optimal Control for Dynamic Systems."12th International Conference on Applications of Statistics and Probability in Civil Engineering, Vancouver, Canada, July 12-15, 2015, peer reviewed.

Fields of Study

Major Field: Civil Engineering

Table of Contents

List of Tables

List of Figures

List of Abbreviations

Chapter 1

u: Control Force
$\boldsymbol{k}$: Constant gain matrix
X: State space vector
$\dot{\mathbf{X}}$: Time derivative of **X**
$\boldsymbol{Q}$: Semi-positive definite matrix
$\boldsymbol{R}$**:** Positive definite matrix

Chapter 2

x: Displacement
$\dot{x}$: Velocity
$\ddot{x}$: Acceleration
$f(x, \dot{x})$: Nonlinear restoring force
$\ddot{x}_{\mathrm{e}}$: External excitation
ξ: Equivalent damping ratio
ω: Fundamental angular frequency
$n_i(t)$: White noise excitation of *i*th DOF

Chapter 3

X: State space vector
$\mathbf{A}_{\mathbf{state}}$: System matrix
$\dot{\mathbf{X}}$: Time derivative of **X**
u: Control Force
$\mathrm{G}(\mathbf{X}, \mathbf{u}, t)$: Nonlinear term
$\mathbf{F_e}$**:** Excitation vector
B: Location matrix of controllers
$\mathbf{Q_1}$: Semi-positive weighting matrix
S: Sliding surface
$\dot{\mathbf{S}}$: Time derivative of **S**
Y: State space vector for converted system
D: Orthogonal transformation matrix
$\dot{\mathbf{Y}}$**:** Time derivative of **Y**

$\mathbf{B_T}$: Transformed sub-location matrix
μ: positive parameter
HOT: Higher order terms
F_j: Rubber bearing force of jth component
k_j: Stiffness of the jth rubber bearing
$\alpha_{\dot{x}_{MR}}$: Pre-yield factor of the jth rubber bearing of the damping component
$\alpha_{z_{MR}}$: Pre-yield factor of the jth rubber bearing of the hysteretic component
z_j: Evolutionary component for hysteresis of jth component
$\dot{z}_j$: Time derivative of z_j
A_{BW_j}, β_{BW_j}, and γ_{BW_j}: parameters that control the shape of the loop
i_c: Current of MR damper
F_{impact}: Impact force
k_h: Impact stiffness
y_{12}: Relative displacement between two adjacent nodes
$\dot{y}_{12}$: Time derivative of y_{12}
ξ: Damping constant
g_p: Gap distance
o: Hertz coefficient
Δv_{12}: Relative velocity before impact
c_h: Nonlinear damping coefficient
¥: Constant for the pounding model (= 0.6 for concrete)
U: Linear displacement vector
Z: Evolutionary vector
C_j: Linearized parameter of the velocity term
K_j: Linearized parameter of the hysteretic term
∂: Partial differential operator
E(...): Expectation of …
M: Mass matrix of bridge
$\mathbf{C_d}$: Damping matrix of bridge
$max^{+}_{x_{12_C}}$: Maximum of the positive relative displacement of span A with respect to span B
$max_{x_{12_C}}$: Maximum absolute relative displacement of span A with respect to span B
| ... |: Absolute value of …
R_{coil}: Resistance of coil wire of MR damper

Chapter 4

m_i: Mass of the ith DOF
x_i: Displacement of the ith DOF
$\dot{x}_i$: Velocity of the ith DOF
$\ddot{x}_i$: Acceleration of the ith DOF

z_i: Evolutionary variable for modeling hysteresis of the ith DOF
$\tau_{x_i}(x_{i-1}, x_i, x_{i+1})$: Coupled function dependent on the displacements
$\tau_{z_i}(z_{i-1}, z_i, z_{i+1})$: Coupled function dependent on the evolutionary variables
k_i: Stiffness component of the ith DOF
α_{z_i}: Level of nonlinearity of the ith DOF (≤ 1)
c_i: Damping coefficient of the ith DOF
$\pounds_E(x_1, x_2, \dots, x_p, z_1, z_2, \dots, z_p)$: Potential energy of the system
E: Energy of the system
$\pounds_E(x_1, x_2, \dots, x_p, z_1, z_2, \dots, z_p)$: Potential energy of the system
$\mathrm{IND}(x_1, x_2, \dots, x_{i-1}, x_{i+1}, \dots, x_p, z_1, z_2, \dots, z_{i-1}, z_{i+1}, \dots, z_p)$: Component of energy that is independent of the variables z_i and x_i
e: Energy per mass of the system
$\pounds_e(x_1, x_2, x_p, z_1, z_2)$: Potential energy per mass of the system
$\pounds_1(x_1, x_2)$: Potential energy component dependent on displacement of the 2-DOF system
$\pounds_2(z_2)$: Potential energy component dependent on evolutionary variable of the 2-DOF system
$v(\dot{x}_1, \dot{x}_2)$: Kinetic energy per mass of the system
B: Brownian motion
σ_0: Standard deviation of the excitation
$\mathrm{d}B/dt$: Time derivative of B
$c_2{}''$: Damping component and is equal to $c_1 + c_2$
$\emptyset_0$, $\emptyset_1$, $\emptyset_2$, and $\emptyset_3$: Integration operators
Δ_{drift}: Mean of the weighted residues of drift component
$\Delta_{\mathrm{diffusion}}$: the mean of the weighted residues of diffusion component
δ_{drift}: Error measure of drift
$\delta_{\mathrm{diffusion}}$: Error measure of diffusion
$W(\dot{x}_1, \dot{x}_2)$: Weighted function of weighted residual method
K_w: Weighting coefficient
$\sigma_0{}'$ and c': Equivalent parameters of intensity and damping, measures, respectively
$\overline{M'}_{\mathrm{drift}}$: Drift component
$\overline{\sigma'}^2_{\mathrm{diffusion}}$: Diffusion component
$p_{\mathrm{s}}(e)$: Stationary probability distribution function of energy
λ_{e}: Constant to ensure that the integration of the PDF function over the entire domain yields one
G: Shear modulus
v_{p}: Poisson ratio
$\emptyset_{\mathrm{a}}$: Angle of friction
ρ_{s}: Soil density
J: Objective function
PLF: Peaks of the lateral forces
$\mathrm{A_{BW}}$ and γ_{BW}: Bouc Wen parameters that control the shape of the loop

Chapter 5

m_i: Mass of the ith DOF
x_i: Displacement of the ith DOF
$\dot{x}_i$: Velocity of the ith DOF
$\ddot{x}_i$: Acceleration of the ith DOF
z_i: Evolutionary variable for modeling hysteresis of the ith DOF
$\tau_{x_i}(x_{i-1}, x_i, x_{i+1})$: Coupled function dependent on the displacements
$\tau_{z_i}(z_{i-1}, z_i, z_{i+1})$: Coupled function dependent on the evolutionary variables
k_i: Stiffness component of the ith DOF
α_{z_i}: Level of nonlinearity of the ith DOF (≤ 1)
c_i: Damping coefficient of the ith DOF
$£_E(x_1, x_2, \dots, x_p, z_1, z_2, \dots, z_p)$: Potential energy of the system
E: Energy of the system
$£_E(x_1, x_2, \dots, x_p, z_1, z_2, \dots, z_p)$: Potential energy of the system
$\mathrm{IND}(x_1, x_2, \dots, x_{i-1}, x_{i+1}, \dots, x_p, z_1, z_2, \dots, z_{i-1}, z_{i+1}, \dots, z_p)$: Component of energy that is independent of the variables z_i and x_i
e: Energy per mass of the system
$£_e(x_1, x_2, x_p, z_1, z_2)$: Potential energy per mass of the system
$£_1(x_1, x_2)$: Potential energy component dependent on displacement of the 2-DOF system
$£_2(z_2)$: Potential energy component dependent on evolutionary variable of the 2-DOF system
$v(\dot{x}_1, \dot{x}_2)$: Kinetic energy per mass of the system
B: Brownian motion
σ_0: Standard deviation of the excitation
$\mathrm{d}B/dt$: Time derivative of B
$c_2{}''$: Damping component and is equal to $c_1 + c_2$
$\emptyset_0$, $\emptyset_1$, $\emptyset_2$, and $\emptyset_3$: Integration operators
Δ_{drift}: the mean of the weighted residues of drift component
$\Delta_{\text{diffusion}}$: Mean of the weighted residues of diffusion component
δ_{drift}: Error measure of drift
$\delta_{\text{diffusion}}$: Error measure of diffusion
$W(\dot{x}_1, \dot{x}_2)$: The weighted function of weighted residual method
K_w: Weighting coefficient
$\sigma_0{}'$ and c': Equivalent parameters of intensity and damping, measures, respectively
$\overline{M'}_{\text{drift}}$: Drift component
$\overline{\sigma'^2}_{\text{diffusion}}$: Diffusion component
$p_{\mathrm{s}}(e)$: Stationary probability distribution function of energy
λ_{e}: Constant to ensure that the integration of the PDF function over the entire domain yields one
G: Shear modulus

v_p: Poisson ratio
$\emptyset_a$: Angle of friction
ρ_s: Soil density
J: Objective function
PLF: Peaks of the lateral forces
A_{BW} and γ_{BW}: Bouc Wen parameters that control the shape of the loop
u: Control force
$V(t,e)$: Value function
$L(t,e,\bar{u})$: Performance index
$L'(e,u)$: Stationary performance index
$V'(e)$: Stationary value function
ρ: Discount factor
R: Positive gain factor
$\theta(e) = s_1 e + s_2 e^2$: Convex polynomial function
$h_1,\ldots,h_n$: Coefficients of n collocation nodes
$\varphi_1(e), \ldots, \varphi_n(e)$: Independent basis functions of of n collocation nodes
v_{SLQR}: Positive coefficient of stochastic linear quadratic regulator

Chapter 6

m_i: Mass of the ith DOF
x_i: Displacement of the ith DOF
$\dot{x}_i$: Velocity of the ith DOF
$\ddot{x}_i$: Acceleration of the ith DOF
z_i: Evolutionary variable for modeling hysteresis of the ith DOF
$\tau_{x_i}(x_{i-1}, x_i, x_{i+1})$: Coupled function dependent on the displacements
$\tau_{z_i}(z_{i-1}, z_i, z_{i+1})$: Coupled function dependent on the evolutionary variables
k_i: Stiffness component of the ith DOF
α_{z_i}: Level of nonlinearity of the ith DOF (≤ 1)
c_i: Damping coefficient of the ith DOF
$\pounds_E(x_1, x_2, \ldots, x_p, z_1, z_2, \ldots, z_p)$: Potential energy of the system
E: Energy of the system
$\pounds_E(x_1, x_2, \ldots, x_p, z_1, z_2, \ldots, z_p)$: Potential energy of the system
$\mathrm{IND}(x_1, x_2, \ldots, x_{i-1}, x_{i+1}, \ldots, x_p, z_1, z_2, \ldots, z_{i-1}, z_{i+1}, \ldots, z_p)$: Component of energy that is independent of the variables z_i and x_i
e: Energy per mass of the system
$\pounds_e(x_1, x_2, x_p, z_1, z_2)$: Potential energy per mass of the system
$\pounds_1(x_1, x_2)$: Potential energy component dependent on displacement of the 2-DOF system
$\pounds_2(z_2)$: Potential energy component dependent on evolutionary variable of the 2-DOF system
$v(\dot{x}_1, \dot{x}_2)$: Kinetic energy per mass of the system
B: Brownian motion

σ_0: Standard deviation of the excitation
$\mathrm{d}B/dt$: Time derivative of B
$c_2{}''$: Damping component and is equal to $c_1 + c_2$
$\emptyset_0$, $\emptyset_1, \emptyset_2$, and $\emptyset_3$: Integration operators
Δ_{drift}: the mean of the weighted residues of drift component
$\Delta_{\mathrm{diffusion}}$: the mean of the weighted residues of diffusion component
δ_{drift}: Error measure of drift
$\delta_{\mathrm{diffusion}}$: Error measure of diffusion
$W(\dot{x}_1, \dot{x}_2)$: The weighted function of weighted residual method
K_w: weighting coefficient
σ_0' and c': Equivalent parameters of intensity and damping, measures, respectively
$\overline{M'}_{\mathrm{drift}}$: Drift component
$\overline{\sigma'^2}_{\mathrm{diffusion}}$: Diffusion component
$p_{\mathrm{s}}(e)$: Stationary probability distribution function of energy
λ_{e}: Constant to ensure that the integration of the PDF function over the entire domain yields one
G: Shear modulus
v_{p}: Poisson ratio
$\emptyset_{\mathrm{a}}$: Angle of friction
ρ_{s}: Soil density
J: Objective function
PLF: Peaks of the lateral forces
$\mathrm{A_{BW}}$ and γ_{BW}: Bouc Wen parameters that control the shape of the loop
u: Control force
$V(t, e)$: Value function
$L(t, e, \bar{u})$: Performance index
$L'(e, u)$: Stationary performance index
$V'(e)$: Stationary value function
ρ: Discount factor
R: Positive gain factor
$\theta(e) = s_1 e + s_2 e^2$: Convex polynomial function
h_1,…,h_n: Coefficients of n collocation nodes
$\varphi_1(e), \ldots, \varphi_n(e)$: Independent basis functions of of n collocation nodes
$\mathrm{v_{SLQR}}$: Positive coefficient of stochastic linear quadratic regulator
L_1 and L_2: Objective functions of first level and second level optimizations in CRC method
L_0: Objective functions in URC method
$P(e \geq e_c)$: Probability of failure
$g(e) = j_0 + j_1 e + j_2 e^2$: Second order polynomial function in URC method
DR: Maximum drift
H: Story height

Chapter 7

$\boldsymbol{G_{state}(X)}$: Nonlinear term of state space form
$\mathbf{X}$: State space vector
$\mathbf{A_{state}}$: System matrix
$\dot{\mathbf{X}}$: Time derivative of $\mathbf{X}$
$\mathbf{F_e}$: Excitation vector
LCC: Life cycle cost
ICC:Initial construction cost
RC: Replacement cost
E(Loss): Total annual loss
AMC: Annual maintenance cost
K_γ^n: Cumulative discount factor for *n* years
γ_{df}: Discount factor
$P(\mathrm{EQ})$: Annual probability of at least one earthquake occurrence
v_{EQ}: Mean annual rate of hazard occurrence
$\mathrm{E}(\mathrm{Loss}|DS_i)$: Average cost of the estimated loss or equivalently the repair cost required to restore the structure to its initial condition for a particular damage state i (DS_i)
$\lambda_{\mathrm{AR}}(\mathrm{PGA})$: Mean annual rate of exceedance
$f(IM)$: Annual probability density function of the intensity measure IM
$P(\mathrm{PGA})$: Annual probability of the peak ground acceleration PGA
b_h: Drift threshold for the *h*th damage state
$P_\emptyset(b_{h-1} \leq DR \leq b_h)$: Failure interval corresponding to drift between b_{h-1} and b_h
$P(DS_h|IM)$: Probability of failure corresponding to the *h*th damage
$g_p(\emptyset_1, \dots, \emptyset_s)$: Probability density function of the uncertain parameters $(\emptyset_1, \dots, \emptyset_s$
$v_{\mathrm{CR}}(\emptyset)_{\Sigma_{b_h}}$: Total crossing rate for the *h*th damage state
$v_{b_{h-1}}^m$: Crossing rate for the *h*th damage state at the *m*th story
$\bar{v}_{\mathrm{DR}}\ (\emptyset)_{\Sigma}^{b_h}$: Averaged total crossing rate for b_h
$\bar{v}_{b_{h-1}}^m$: Average crossing rate for the *h*th damage state at the *m*th story
σ_{DR_m}: Standard deviations of drift
$\sigma_{\dot{DR}_m}$: Standard deviations of time differential DR_m at the *m*th story
HOT: Higher order terms
$\mathbf{S_{COV}}$: Covariance matrix solved by Lyapunov equation
$\mathrm{C}_{\mathrm{controller}}$: Controller cost
ICo: Initial controller cost
AC: Actuator cost
IAC: Installation cost
WSC: Cost of wireless data acquisition
SHCC: Cost of a servo hydraulic controller
AMCC: Annual controller maintenance costs

$\boldsymbol{K_u^*}$: Optimal control gain
$\mathbf{u}$: Control Force
$\mathbf{B}$: Location matrix of controllers
$\boldsymbol{P_{R-LQR}}$: Positive definite matrix for R-LQR case
$\boldsymbol{P_{URR}}$: Positive definite matrix for URR case
$H(j\omega)$: Frequency response function
$n(t)$: White noise
ζ_g and ω_g: Angular frequency and the damping content, respectively for Kanai-Tajimi filter

Chapter 1: Introduction

1.1. Motivation

Natural disasters are one of the constant challenges to designing new or strengthening existing infrastructure. For instance, earthquakes are still demolishing cities such as the case in Haiti in 2010 (316,000 fatalities and $8 billion damage) (Guha-Sapir et al., 2011). Structural engineers are motivated to develop resilient infrastructure designs; ones that can ensure structural safety, serviceability, and comfort.

Hazard Mitigation and Control (HMC) is one of the solutions to design resilient structures that can withstand natural disasters. HMC uses smart control devices to attenuate specific response variables, such as alleviating lateral and torsional response of a long span bridge subjected to heavy wind. On the community level, research in HMC can enhance the health and minimize the cost of maintaining and upgrading infrastructures, improve residents' comfort, and enable achieving higher levels of life safety. To achieve these goals, this research concentrates on minimizing damage to structural and nonstructural components through actions that affect pre-, during, and post- hazard performance of systems. The research indirectly results in reducing initial cost, retrofitting cost, repair time, and injuries and casualties.

1.1.1 Background

Over the past few decades, various structural control devices, including passive, active, and semi-active controllers have been developed to mitigate various critical responses of structures. Passive devices do not require power to operate during earthquakes or other hazards and often include supplementary dampers to dissipate the energy of systems. More common forms of these systems are tuned mass damper (TMD) (Figure 1-1b), tuned liquid column damper (TLCD) (Figure 1-1c), and base isolation systems. These dissipative devices are considered to be reliable, but they are effective only for a limited range of external excitations (Symans et al., 2008). Furthermore, they are unable to adapt to changes in the structural properties and to the nature of external excitations (Debbarma et al., 2010; Chakraborty et al., 2012; Soto and Adeli, 2013; Soto and Adeli, 2014). To overcome these shortcomings, active devices (e.g. active mass damper, hydraulic actuators) were developed which are capable of adjusting to a wide range of operating conditions. However, they require a large amount of power, may induce instability problems in structures (Du et al., 2008), and may cost more than passive control devices. Semi-active devices provide a compromise between the features of active and passive devices. These systems have gained attention and widespread acceptance in the control engineering community for their robustness and stability, in addition to adaptability and low (battery-operated) power requirements. Semi-active technology increases the overall reliability, stability, and efficacy of the control system (Corbi et al., 2013). Both semi-active and active systems are effective for a wide range of excitations as opposed to passive schemes that are effective for a limited bandwidth only (Yoshida and Dyke, 2005; Guo et

al., 2009; Fan et al., 2009). Semi-active systems include, among others, magnetorheological (MR) dampers (Figure 1-1e), variable friction dampers (Figure 1-1d), and negative stiffness devices (NSD) (Figure 1-2a), (Ozbulut and Huberlaus, 2011), among others. Moreover, hybrid control systems are introduced to combine different control systems and hence improve their performance, efficiency, and stability (Bahar et al., 2010; Chang and Spencer, 2010). An example of a hybrid system is depicted in Figure 1-2b where a semi-active NSD is combined with a TLCD system on the roof. This system is expected to provide improved vibration attenuation compared with a stand-alone NSD system shown in Figure 1-2a. Some of the diverse applications of smart control systems are listed below:

- Mitigating inter-story drifts and story accelerations in multi-story buildings (Figure 1-1a).
- Minimizing roof displacements in high-rise buildings (Figure 1-1b).
- Reducing torsional displacements of irregular structures (Figure 1-1c).
- Alleviating the impact of pounding of adjacent structures such as multi-span bridges (Figure 1-1e).
- Attenuating vertical accelerations in vehicles (Spencer and Nagarajaiah, 2003; Korkomaz, 2011; El-Khoury and Adeli, 2013; Soto and Adeli, 2013).

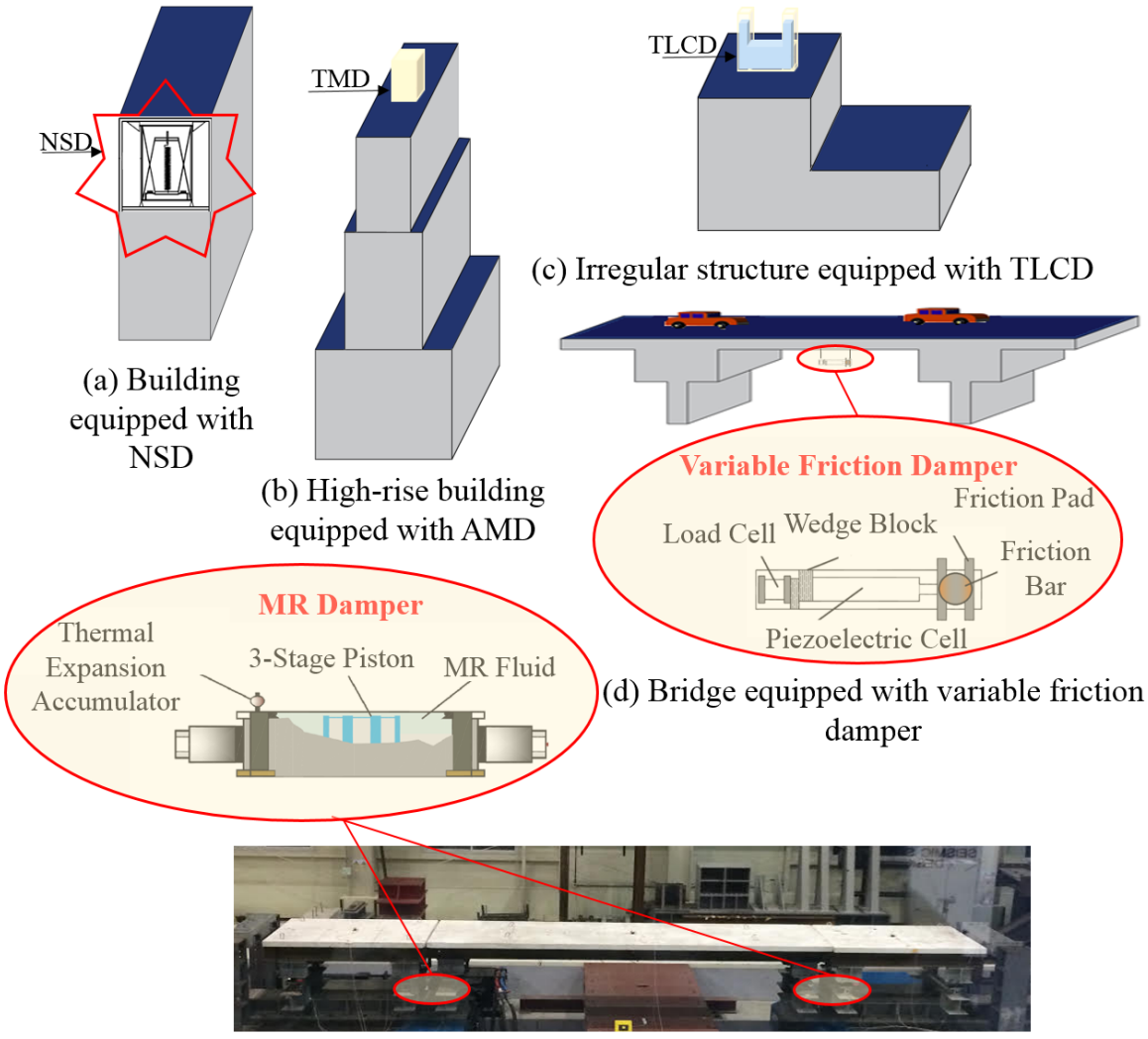

(a) Building equipped with NSD

(b) High-rise building equipped with AMD

(c) Irregular structure equipped with TLCD

(d) Bridge equipped with variable friction damper

(e) Three-span bridge equipped with MR dampers

Figure 1-1 Civil engineering applications of control engineering.

To summarize, passive control systems have been well developed and tested over the past few decades. Meanwhile, the current frontier of research in this area is active and especially semi-active control of structures. Such control problems are complex and require integration of several different hardware and software technologies such as smart materials, adaptive dampers, actuators, sensors, and control and signal processing algorithms with

structural designs. Herein, the research is focused on active and semi-active control strategies and algorithms. In the next sections, the objectives and scopes of research (Section 1.2) and the dissertation content (Section 1.3) are discussed.

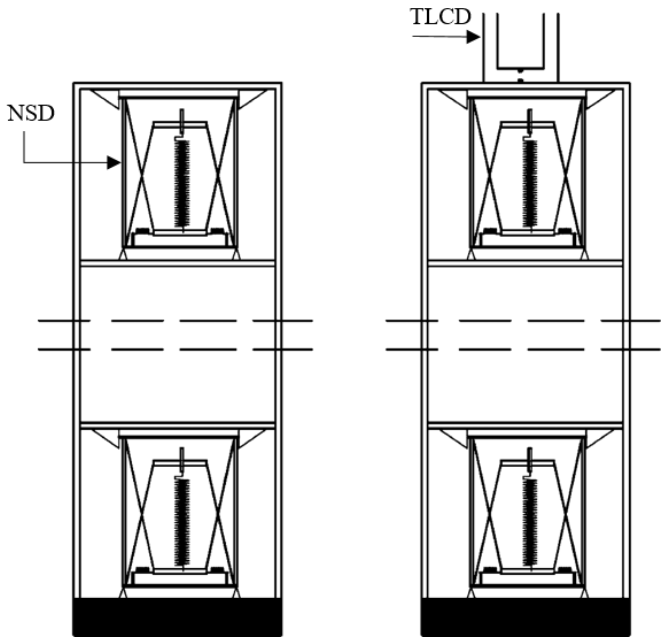

(a) (b)

Figure 1-2 (a) NSD system and (b) a hybrid TLCD and NSD system.

1.2. The Objectives and Scope of Research

In semi-active and active control designs, systems subjected to external excitations are monitored via a set of sensors that measure critical structural responses as shown in Figure 1-3a. Then, the central processing unit (CPU) estimates the full state responses and determines the control command. Subsequently, the control command is fed to the control device and the corresponding force is applied to the system. An example for a control system developed for a two span bridge equipped with semi-active MR dampers to mitigate

bridge responses especially poundings under seismic excitations is depicted in Figure 1-3b. In this example, an observer and a controller system are designed and optimized for a representative dynamic model of the bridge. During seismic excitations, the control system calculates the optimal input current for MR dampers given the measured structure responses. MR dampers then react to the input current and induce a stabilizing force in the structural system. This process continues until the end of seismic excitation.

Conventional linear feedback controllers such as linear quadratic regulator (LQR) for fully observed systems and linear quadratic Gaussian (LQG) controller for partially observed systems have been used extensively in control problems. In these methods, the control force, $\mathbf{u}$, of the system is determined as $-\boldsymbol{k}\mathbf{X}$, where $\boldsymbol{k}$ is the constant gain matrix and $\mathbf{X}$ is the state space vector. The gain matrix is determined by minimizing a second degree polynomial cost function, $(\mathbf{X}^{\boldsymbol{T}}\boldsymbol{Q}\mathbf{X} + \mathbf{u}\boldsymbol{R}\mathbf{u})$, where $\boldsymbol{Q}$ and $\boldsymbol{R}$ are semi-positive and positive definite matrices, respectively, that are defined by the designer to indicate the relative importance of reducing various responses of the structure and the control force. Such control algorithms are easy to implement and are relatively effective in mitigating the response of structures (See Aldemir et al., 2012; Karimi et al., 2013). However, a major limitation of these methods is that they produce optimal solutions for only linear systems and their application to nonlinear systems requires linearization of the system. In such cases, the derived control forces may not be optimal. As for the linearization of the systems, majority of studies have used linear elastic properties of systems in the LQR/LQG designs. This approach does not conserve the stochasticity of excitations and nonlinearity of the system behavior in response to high intensity stochastic excitations.

To overcome the shortcomings of conventional control strategies, the primary research goal here is to develop effective nonlinear stochastic control frameworks for nonlinear dynamic systems. These frameworks entail mitigating the vibrational effects, reducing the extent of damage, and minimizing the likelihood of failure and the life cycle cost. Herein, the development of control framework involves: (1) proper characterization of the nonlinearity and stochasticity of the system, and dynamics and constraints of the control device and (2) well-defined control design objective functions for systems of interest using measures such as drift, acceleration, reliability, cost, etc. To develop the aforementioned process, the following topics are studied in this dissertation:

- The treatment of nonlinearity and stochasticity in the control design using stochastic linearization (El-Khoury et al., 2015; El-Khoury et al., 2016) and stochastic averaging (El-Khoury and Shafieezadeh, 2016).
- The expansion of the conventional control objectives to higher order convex functions and incorporation of the dynamics and constraints of controllers (El-Khoury et al., 2015; El-Khoury et al., 2016).
- A nonlinear stochastic control based on stochastic averaging of energy envelope that enables the incorporation of nonlinearity of the system, stochasticity of the excitation, and unrestricted objective function of control design (El-Khoury and Shafieezadeh, 2016; El-Khoury and Shafieezadeh, 2017a).
- The development of a reliability-based control algorithm based on stochastic averaging of energy envelope that minimizes the probability of failure of nonlinear systems (El-Khoury and Shafieezadeh, 2017b).

- The optimization of control systems within a risk management framework such that the life cycle cost of structures is minimized (El-Khoury et al., 2017). This control optimization explicitly minimizes structures' life cycle cost which consists of the initial cost, the cost of maintaining and upgrading the structure, and finally direct and indirect costs of repairing the structures following hazards. This control algorithm implicitly minimizes casualties and improves residents' comfort as well.

  All of the above studies enable achieving a more reliable and resilient system.

1.3. The Dissertation Outline

The rest of the dissertation consists of seven chapters with the following content:

- Chapter 2 presents a review of model characterization techniques and control design strategies in the literature and discusses their strengths and shortcomings.
- Chapter 3 develops a nonlinear sliding mode control design approach using concepts from optimal polynomial control (SMC-OPC) and applies it to multi-span bridges equipped with semi-active MR dampers. The chapter presents simulation as well as large scale shake table experiment results.
- Chapter 4 presents development of an advanced stochastic averaging method of energy envelope, called enhanced stochastic averaging (ESA) and implements this approach for estimation of probabilistic features of responses of a single story building supported on a nonlinear foundation.
- Chapter 5 introduces new stochastic control algorithms that implement ESA within optimal control designs and applies this method for the system discussed in Chapter 4.

- Chapter 6 presents development of a reliability-based control, where minimizing the probability of failure of the structure estimated via ESA is considered the primary objective.
- Chapter 7 proposes a risk-based control framework to minimize the life cycle cost of structures and applies the method to a multi-story nonlinear building.
- Chapter 8 summarizes the research, draws general conclusions, and highlights some future research needs.

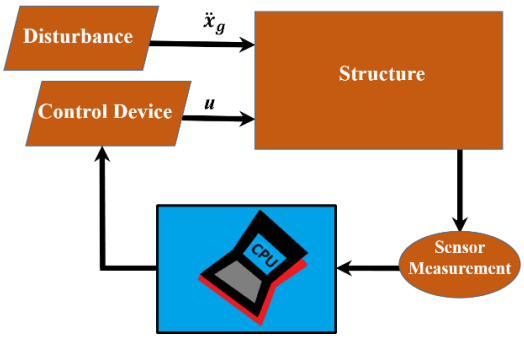

(a)

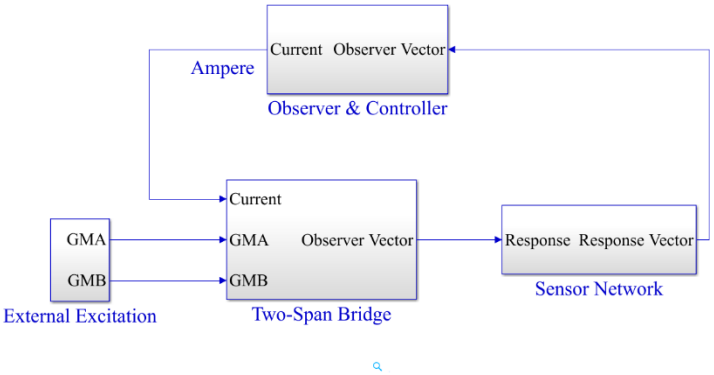

(b)

Figure 1-3 (a) Schematic of controlled systems and (b) Simulink model of two span bridge subjected to seismic excitation.

Chapter 2: Challenges of Control Design of Structures under Hazard Excitation

2.1 Introduction

The complex behavior of civil engineering structures during a hazard event and the vulnerabilities of these assets have been extensively studied with the purpose of improving the design and providing effective mitigation options to reduce the potential of various types of damage and catastrophic failures (Berke et al., 2012). In hazard mitigation and control (HMC), the goal primarily is to develop and evaluate control methods that lead to more resilient designs for various civil engineering structures. HMC research addresses different objective such as

- Adapting to sudden events by considering stochasticity and nonlinearities in different components and excitations (Connor et al., 2014; Tu et al., 2014; Yildiz et al., 2015).
- Reducing the peaks and root mean square of response variables such as acceleration and displacements in dynamic systems (Cha et al., 2013; Xiang et al., 2014; Rahman et al., 2015).
- Maximizing the reliability and minimizing life cycle cost of special buildings (Yuen and Taflanidis, 2003; Scruggs and Taflanidis, 2006; Taflanidis and Beck, 2009)

- Minimizing power consumption of control devices and optimizing the number, the locations, and the reliability of control devices used in the controlled system (El-Khoury et al., 2015; Yildiz et al., 2015; El-Khoury et al., 2016).

Meanwhile, one major challenge of systems under extreme loadings (e.g. earthquakes) is nonlinearity. In this context, it is commonly argued that the purpose of the application of control strategies is to reduce the structural response and limit the extent of nonlinearities so that the system remains nearly linear elastic during the hazard. However, hazards are stochastic events with characteristics that are not fully known prior to the occurrence. This complicates the design of a controller that can ensure a linear system behavior or a behavior with limited nonlinearity. Also in some applications, the goal of the control strategy is to reduce the likelihood of extreme responses in critical demand measures to limit the potential of extensive damage in the system, while accepting presence of nonlinear behavior in the system response. This strategy will allow for more cost-effective solutions based on structural control. However, this strategy poses a challenge considering that control algorithms are normally designed for systems with linear models. Two primary aspects are essential to ensure good control performance: proper characterization of the system and control device and well-defined control design objectives as depicted in Figure 2-1.

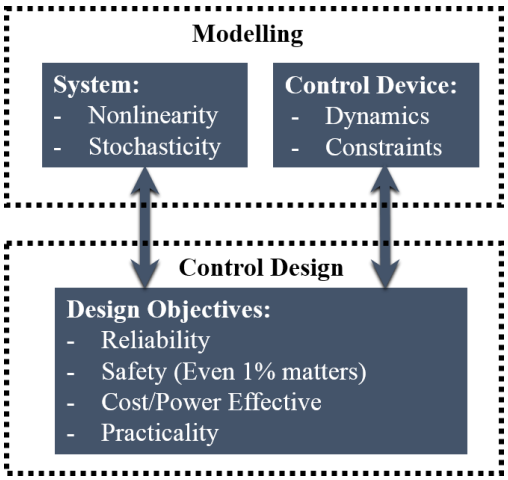

Figure 2-1 Factors in obtaining a successful control design optimization.

In this chapter, these aspects are discussed in achieving the aforementioned objectives: (1) characterization of the system through deterministic and stochastic approximations and (2) the advancement of control algorithms (linear and nonlinear; deterministic and stochastic). Presented in the subsequent sections are the model characterization techniques (Section 2.2) , the control algorithms (Section 2.3), minimization of the probability of failure and extent of loss, the reliability-based control (Section 2.4) and the risk-based control (Section 2.5). The concluding section elaborated the direction of the present research (Section 2.6).

2.2 Model Characterization

Model characterization and response prediction of dynamic systems have posed challenges in many fields of science and engineering. Natural or engineered systems may exhibit nonlinear behavior in their dynamic response; these responses are often uncertain due to the stochasticity in input excitations and other sources (Benjamin and Cornell, 2014). In

control design, incorporating the stochasticity or uncertainty of the excitation and the nonlinearity of the dynamic system is one of the major objective to ensure an optimal control performance. For instance, nonlinear systems can be treated using a variety of different methods (Socha, 2005a; Socha 2005b; Zhu, 2006; Chopra, 2007; Socha, 2007). Traditionally, the system is linearized according to linear elastic assumptions. For instance, a single degree of freedom (DOF) dynamic system is designated as:

$$\ddot{x} + f(x, \dot{x}) = \ddot{x}_{\mathrm{e}} \tag{2.1}$$

where x, $\dot{x}$, and $\ddot{x}$ are displacement, velocity, and acceleration respectively, $f(x, \dot{x})$ is the nonlinear restoring force, and $\ddot{x}_{\mathrm{e}}$ is the external excitation. $f(x, \dot{x})$ is linearized to $2\xi\omega\dot{x} + \omega^2 x$, where ξ and ω are the equivalent damping ratio and fundamental angular frequency, respectively (Chopra, 2007). Such a method does not incorporate the intensity of external excitation in the linearization process. Consequently, probabilistic methods are adopted in nonlinear stochastic dynamic systems to incorporate the properties of the external excitations. In the following subsections, two methods of model characterization are explained: deterministic and stochastic linearization (2.3.1) and stochastic averaging (2.3.2).

2.2.1 Deterministic and Stochastic Linearization

The system matrix in a nonlinear structure is not fixed, and depends on the response of the structure. To generate simplified models for such systems, linearization techniques were developed (Socha, 2005a; Socha 2005b; Chopra, 2007; Socha, 2007; Anh et al., 2015). This class of methods aims at determining parameters of an equivalent linear model by minimizing the error between the responses of the nonlinear and linear systems. A common

objective function for these purposes is the mean square error. The fitting process can be stochastic, where the probabilistic nature of the excitation is considered, or deterministic, where the excitation is assumed to be known a priori.

Conventionally, initial linear elastic properties of systems have been used extensively to present the dynamic behavior of nonlinear structures. This deterministic approach can yield acceptable predictions of system responses in structures that experience very limited nonlinearity. Since such linearization methods do not consider the intensity of external excitation in the linearization process, they may yield poor response predictions when the system is subjected to large excitations and therefore experiences large nonlinearities.

To overcome this limitation, stochastic linearization was introduced for nonlinear hysteretic systems. It is noteworthy that hysteretic nonlinearity is commonly observed in civil engineering structures (Priestley et al., 2007). The hysteretic components in the system matrix can be replaced by equivalent linear time invariant models; the residual errors arising from the linearization process can then be minimized (Wen, 1980). Stochastically linearized models better predict the response of nonlinear structures compared to linear elastic models (Basili and Angelis, 2007; Basili et al., 2013). Basili and Angelis (2007) optimized a passive control design for adjacent structures equipped with viscous dampers. Stochastic linearization was carried out to solve nonlinear equations of motion of the nonlinear system subjected to artificial ground motions generated using a Kanai-Tajimi filter (Kanai, 1957; Tajimi, 1960). Generally, stochastic linearization is easy to implement for simple systems with few degrees of freedom, but it becomes very complicated for multi-degree-of freedom systems. Stochastic linearization faces a number of limitations with regard to the stability of produced solutions, and in dealing with high

degree of freedom systems and structures with large nonlinearity. These limitations stem from the fact that obtaining coefficients of linearized models requires solving a system of nonlinear algebraic equations in the case of stationary response and a system of differential equations in the case of non-stationary response (Socha, 2005a; Socha, 2005b; Socha, 2007).

2.2.2 Stochastic Averaging

As an alternative to linearization techniques, stochastic averaging is a proven solution that provides higher accuracy, since it retains the intrinsic nature of nonlinearity in the system behavior as well as effects of stochasticity in input excitations (Bellizzi et al., 2001). Stochastic averaging has been used for system identification and control design in different domains such as structural engineering (Zhu et al., 2004; Cheng et al., 2006; El-Khoury and Shafieezadeh, 2015), geotechnical engineering (Tartakovsky et al., 1999), earth and environmental sciences (Cai, 2009), and physics (Deng et al., 2011).

Stochastic averaging can be used to derive approximate probabilistic solutions to problems involving lightly damped systems (Zhu, 2006). Such systems can be considered as diffusive Markovian processes with a transition probability density function (PDF) governed by the Fokker-Planck-Kolmogorov (FPK) equation. The drift and diffusion components of the FPK equation are derived by applying stochastic calculus. Subsequently, the PDF of system responses is computed by solving the FPK equation, and this can be used for response prediction of variables such as low and high order moments of energy, displacements, and velocities. In this aspect, three methods of averaging have been proposed (Zhu, 2006): standard stochastic averaging, the averaging method of

coefficients in FPK equation, and stochastic averaging of energy envelope. The first two methods were developed to derive the solution of FPK equation by averaging it with respect to time. The third method transforms the dynamic system into the Hamiltonian domain (in stochastic averaging of energy envelope, the total energy of the system is known as the Hamiltonian). Common response variables of dynamic systems e.g. displacements and velocities are often rapidly varying quantities, while energy envelopes of systems are slowly varying quantities. This method exploits this feature to average the rapidly varying processes to yield the averaged Itô equations for slowly varying processes. This method can be applied to lightly damped systems subjected to weak excitations (Zhu, 2006). Additional features of stochastic averaging of energy envelope include lower computational demand and simpler parameter analysis compared to other stochastic averaging methods, since the dimension of the FPK differential equation is reduced (Zhu et al., 2002).

In general, multi-DOF systems of interest can be either integrable or non-integrable. Integrable systems are identified by uncoupled potential energies, where each DOF corresponds to an independent Hamiltonian. The integrable system is then averaged and the PDF of the Hamiltonian can be derived (Zhu et al., 2002; Huang and Zhu, 2004). On the other hand, non-integrable systems include coupled potential energies, where the entire system can only be represented by a single Hamiltonian (Huang and Zhu, 2009) for all DOFs. Stochastic averaging of energy envelope has been used for response prediction (Stafford et al., 2009; Xu et al., 2013) and reliability estimation (Chen and Zhu, 2009) for both integrable and non-integrable systems. For example, Zhu et al. (2004) applied this method to the linear model of a tall building subjected to wind loadings that were simulated

as filtered white noise. To simplify the analysis, the system was converted from a non-integrable system to an integrable system using linear modal analysis. The averaging was applied to the derived integrable system and a controller was designed accordingly. Stochastic averaging of energy envelope was also implemented for system representation of single DOF hysteretic systems subjected to white noise excitations (Cheng et al., 2006). This technique was further extended to support systems subjected to other types of excitations such as Poisson excitation (Zeng and Zhu, 2011), Gaussian and Poisson excitation (Jia et al., 2014), combined harmonic and real noise excitation (Chen and Zhu, 2011), and fractional Brownian excitation (Xu et al., 2013).

Stochastic averaging of energy envelope is considered to be superior to stochastic linearization because of the following reasons:

- More capable control solutions can be achieved using stochastic averaging versus various linearization methods because the intrinsic non-linearity in the original system is retained in the averaged system (Zhu and Huang, 2004).
- The frequency content characterization is conserved in stochastic averaging, while for linearized systems, this may not be true (Soize, 1995; Bellizi and Bouc, 1999a; Bellizi and Bouc, 1999b).
- Better estimations for probabilistic measures such as stationary probability density functions and higher order moments of responses are achieved using stochastic averaging compared to stochastic linearization.

In addition, an averaged system model via stochastic averaging is a close representation of nonlinear system dynamics, however, this is not the case for linearized models. Therefore a nonlinear feedback control in stochastic linearization in order to yield optimal

results requires repeating the linearization procedure when the control force or excitation intensity, among other factors, change. On the other hand, the control forces can be embedded in the stochastic averaging without requiring further derivation and iterations.

2.3 Control Algorithms

In this section, several feedback control designs are discussed. The linear optimal state space control, known as linear quadratic regulator and linear quadratic Gaussian is elaborated in Section 2.3.1. In order to introduce higher order cost functions, the optimal polynomial control algorithm is presented in Section 2.3.2. Then to improve robustness, sliding mode control is introduced in Section 2.3.1. To incorporate stochasticity and nonlinearity of the system, a family of stochastic controllers based on stochastic averaging of energy envelope is included in Section 2.3.4. These methods are compared to uncontrolled systems, passive systems, and systems equipped with bang-bang control method (Lim et al., 2003) which is a feedback controller that switches between two states of control.

2.3.1 Linear Quadratic Regulator/Gaussian

Traditionally, the most commonly used optimal control algorithms are linear quadratic regulator for fully observed systems (LQR) and linear quadratic Gaussian (LQG) for partially observed systems. These algorithms are considered to be linear feedback strategies, where the control force is proportional to the state space vector and the minimization cost function is a second order convex function (Aldemir et al., 2012; Karimi et al., 2013; Lei and Lin, 2012; Li et al., 2010b; El-Khoury and Adeli, 2013). To date, LQR

is still being adopted for research in active and semi-active control because of its simple implementation and satisfactory results.

For instance in active control, Alavinasab et al. (2006) used LQR algorithm for a three story building equipped with actuators. Li et al. (2010b) designed LQG control algorithm for an eight story shear frame subjected to earthquake ground motions. Karimi et al. (2013) examined a 20 story flat slab building equipped with 20 actuators that were controlled by an LQR algorithm. This approach was introduced to improve the structural response. Lei et al. (2012) suggested an LQG controller to reduce the seismically induced response of a 20-story benchmark linear structure. Amini et al. (2013) presented a design for a 10-story shear frame equipped with active tuned mass dampers using LQR control algorithm and particle swarm optimization. The objective was to reduce torsional deformation of irregular structures subjected to earthquake excitations. Kim et al. (2013) adopted the LQR control algorithm in tall structures equipped with active tuned mass dampers subjected to strong winds (e.g. Aldemir et al., 2012; Tse et al., 2012).

For the semi-active control method, Yoshida et al. (2003) performed shaking table experiments on a two story asymmetric building model equipped with MR dampers subjected to earthquake disturbance to reduce torsional motions. Ohtori et al. (2004) studied seismic control of nonlinear benchmark buildings equipped with semi-active LQG control algorithm based on clipped optimality. The suggested control algorithm improved the reliability and reduced peak damage performance compared to uncontrolled structure. Here, reliability is measured as the conditional probability that the damage measures do not exceed the specified values. Similarly, Christenson and Emmons (2005) used LQR

control algorithm in a three story building equipped with MR damper under seismic excitation. Bitaraf and Huberlaus (2013) implemented semi-active LQR control in a 20-story nonlinear building to reduce the damage in the structure. From this review, it can be realized that these control algorithms can be implemented for different disturbances (wind and earthquake) and various structures (high and medium rise buildings and bridges). However, a limitation of LQR and LQG in active and semi-active technology is that their objective functions has a restricted form and only contains polynomial functions of second degree.

2.3.2 Optimal Polynomial Control

To release the form of the objective function to contain higher (≥ 2) order convex functions, optimal polynomial control (OPC) algorithm was derived. This algorithm introduced by Agrawal and Yang (1996) generalizes the LQR algorithm through inclusion of higher order convex polynomials in the objective function. The OPC control force is composed of two components: a linear LQR component and a set of nonlinear higher order components. In that respect, LQR strategy can be perceived as a special case of OPC method. In general, it is expected that a second level optimization yields nonzero OPC gain matrices, and therefore provides a better performance compared to LQR method. In addition, nonlinear optimal control laws such as OPC are more robust than the linear optimal control law in dealing with uncertainties (Christofides and El-Farra, 2005). Similar to LQR, OPC requires linearization of the nonlinear structure. Studies have implemented stochastic linearization techniques which consider the stochasticity of the excitation and replace the nonlinearity in system components by equivalent linear time invariant models.

Peng et al. (2010) implemented polynomial chaos expansions in nonlinear optimal control of dynamic systems. This expansion estimates the probability distributions of the responses of interest in the structure. They implemented this strategy for an OPC algorithm in a base-excited Duffing oscillator and compared the performance to LQR and Lyapunov control algorithms. Peng et al. (2013) generalized the control strategy to include serviceability, system comfort, and control device workability. A probabilistic control algorithm was suggested for an eight story shear frame equipped with actuators. The control strategy showed a noticeable reduction in the inter-drift of stories, in addition to an optimized efficiency compared to passive and uncontrolled systems. These control methods (LQR, LQG, and OPC) provide optimal solutions for linear systems subjected to white noise. However as stated earlier, these control algorithms do not consider the characteristics of the external disturbance. In reality, actual systems can be highly nonlinear, and external disturbances such as wind and earthquakes are stochastic phenomena, which can be characterized using their probabilistic properties. In addition, these methods are not immune to structure uncertainty, which is encountered in structures subjected to various hazards. In the next section, a family of robust controller known as sliding mode control are discussed to improve adaptability of the control design.

2.3.3 Sliding Mode Control

In order to provide an adaptive control performance, a class of robust control design strategies, known as Sliding Mode Control (SMC), was introduced by Vadim Utkin in the seventies (Utkins, 1977; Utkins, 1992; Fridman et al., 2011). The goal of SMC design was to drive the response trajectory into a pre-defined surface. Primarily, stability was

considered in the SMC design, which follows the trajectory of the sliding surface during the overall duration of the extreme event. Other attractive features included adaptability, efficacy, practical implementation, and good performance in the face of modeling uncertainty.

The SMC algorithm is not based on a minimization procedure such as conventional feedback methods. However, the SMC design is known to be a two-step procedure. The first step involves the sliding surface design. After that, a control law is selected to drive the response variables to the defined sliding curve. Yang et al. (1994) derived linear sliding surfaces based on a regular form transformation and an LQR methodology. The surface designs were analyzed on linear elastic systems (Yang et al., 1995a) and hysteretic systems (Yang et al., 1995b). The control design showed performance improvements; in addition, it was shown to be robust when the stiffness of the structure was varied within 10 percent of the original value. Yang et al. (1996) tested the sliding surface design on seismically excited building. It was shown that the SMC design provided better peak response reduction as compared to traditional feedback LQR control algorithms (Wu and Yang, 1997).

The control law presented by Yang et al. (1994) could not be implemented unless the external excitation is deterministic. To resolve that issue, Adhikari and Yamaguchi (1997) replaced the feedforward component that depends on the excitation, by a Heaviside function that compensates for the stochastic disturbance. The Heaviside component is a source of chattering, which causes damage to mechanical components of actuators. As a result, this discontinuous component was replaced by a tangent-hyperbolic smooth function. Alternatively, Cai et al. (2000) preserved the Heaviside component but omitted

the linear component of the control design. Both design strategies have shown a good performance in terms of reduction in peak response values, and have been considered to various actively and semi-actively controlled multistory buildings (Yang et al., 2004; Fan et al., 2009; Li et al., 2010a) and bridges (Lim et al., 2003; Lee and Chen, 2011a; Lee and Chen, 2011b). However, these linear sliding surfaces are restrictive forms and limit the performance of controllers in terms of both response reduction and control force minimization for nonlinear systems. To address these limitations, a new nonlinear sliding mode control is proposed in Chapter 3 which utilizes optimal polynomial strategy to design nonlinear sliding surfaces.

2.3.4 Stochastic Control Algorithms Using Stochastic Averaging of Energy Envelope

To implement stochastic averaging in control design, Zhu et al. (2000) introduced a nonlinear optimal control based on stochastic averaging of energy envelope for a hysteretic column equipped with an active device. The system was converted to energy domain where the linear and hysteretic displacement and velocity of the structure were reduced to an energy component in the form of a convex function of potential and kinetic energies. This method outperforms OPC control algorithm in terms of efficiency and response reduction. Furthermore, Zhu et al. (2001) used the nonlinear feedback control algorithm in single and multiple DOFs. The paper presented a derivation of the HJB equation for a 2-DOF nonlinearly damped system. This method assumes the convex cost and value functions to be dependent on energy components. The method predetermines the form of both functions and solves the dynamic equation accordingly.

In another effort, Zhu and Ying (2002) considered a partially observed five story structure equipped with an active control device. The nonlinear stochastic control was implemented and compared to both LQG and uncontrolled states. The result showed a better response mitigation compared to linear feedback controller. Ying et al. (2003) suggested a design of hysteretic column equipped with MR damper. A clipped stochastic optimal control was adopted to solve the dynamic programming equation, and better efficiency was achieved compared to semi-active clipped LQG control algorithm. Zhu et al. (2004) implemented the nonlinear stochastic control in a 40 story structure subjected to strong wind excitations. Ying et al. (2004) applied the nonlinear stochastic control for coupled building structures (20 story and 10 story adjacent structures) equipped with active control devices. In that research, stochastic averaging method was used to reduce the higher dimension of the original state. They concluded that more response reduction was achieved for high random excitation intensities compare with conventional LQG control algorithm. Furthermore, Ying et al. (2005) implemented the nonlinear control algorithm for a structure equipped with hybrid control devices including a semi-active MR damper and a passive tuned liquid column damper.

Gao (2006) investigated active stochastic control of a smart truss bridge subjected to stationary random excitations. A mathematical model was developed based on the dissipation of energy where the objective criterion was to minimize structural displacements. Luo and Zhu (2006) proposed a nonlinear stochastic control strategy for jacket-type offshore truss structures subjected to wave forces. This nonlinear stochastic control algorithm was derived according to stochastic averaging strategy. The results

reported better performance compared with LQG control and uncontrolled states. The authors state that by using the stochastic averaging, the problem dimension was reduced by half. Cheng et al. (2006) explored the nonlinear stochastic controller in comparison to stochastic linearized system equipped with a LQG controller. In the suggested control algorithm, the MR damper could achieve the active control force without clipping (e.g. Zhu, 2006; Chen and Zhu, 2009). Ying et al. (2007) developed a bounded nonlinear stochastic control for a structure equipped with MR damper which yields a smoother control force compared with bang-bang control algorithm with increased efficiency. Liu and Zhu (2007) considered delayed feedback control based on stochastic averaging. Zhao and Zhu (2010) developed a nonlinear stochastic control for a cable-stayed bridge equipped with MR dampers. Then, the nonlinear control algorithm was compared with bang-bang control where improved controlled responses were observed. Zhu and Zhu (2011) designed nonlinear stochastic feedback controllers for Hamiltonian systems. In the analysis, they verified that the transient solution converges to the stationary probability density function as time goes to infinity.

A primary drawback for this control algorithm that is based on stochastic averaging is that real-world systems are generally non-integrable and nonlinear. Conventional stochastic averaging methods for such systems neglect effects of off-diagonal damping terms, consider a lumped contribution of the diagonal entries rather than their individual effects, and treat external stochastic excitations on applied DOFs as independent processes (Gu et al., 2012; Gu and Zhu, 2014). These constraints may limit the application of stochastic averaging as nonlinear systems often do not satisfy these conditions. To address

the present shortcomings, Chapter 4 proposes a new strategy called enhanced stochastic averaging to derive an equivalent nonlinear stochastic system for which the application of stochastic averaging yields accurate results. Furthermore, Chapter 5 develops a nonlinear stochastic optimal control algorithm based on the enhanced stochastic averaging method of energy envelope to mitigate the response of nonlinear hysteretic systems. The performance of the suggested control algorithm is compared to that of uncontrolled and conventional control cases.

2.4 Reliability-Based Control

Over the past few decades, reliability has gained great attention in the design of structural systems against natural hazards (Frangopol et al., 2014). Structural reliability is commonly defined as the probability of demand not exceeding a predefined limit that represents the capacity of the structure. The limit state functions are often established using engineering demand parameters such as maximum inter-story drift, maximum absolute acceleration, and maximum shear force (Ghobarah, 2004). Using these functions, reliability analysis enables probabilistic assessment of the ability of a system to meet a set of performance criteria, while accounting for various uncertainties that may affect the system's performance. Reliability concepts can therefore be employed in control design to effectively enhance the performance of systems under external disturbances such as natural hazards. However, research in hazard mitigation and control has been dedicated extensively to minimize particular response variables of interest. In conventional feedback controllers, reliability as a performance metric is not explicitly considered. For example, LQR and LQG algorithms are widely used feedback controllers that minimize the second order

moments of the response variables of interest. LQG and LQR also provide simple and fairly acceptable designs for performance improvement of systems (Shafieezadeh et al., 2008; Shafieezadeh and Ryan, 2011). However in LQR/LQG, minimizing the variance of responses of interest does not directly correspond to improving the reliability of the system (Scruggs et al., 2006; Taflanidis et al., 2007). Consequently, new control strategies had to be developed based on reliability concepts.

To incorporate reliability in the control design, Yuen and Beck (2003) developed a reliability-based control strategy for a shear building model equipped with an actuator device. The control force was determined such that the likelihood of failure estimated via crossing rate is minimized. The limit states were defined in terms of bounds on inter-story drifts and absolute accelerations. In addition, the feedback control force was considered to be linear with respect to the state vector. Scruggs et al. (2006) applied this reliability-based control strategy to optimize the seismic performance of active base isolation systems. Restrictions on the control gain matrix (e.g. a negative definite matrix or a diagonal matrix with negative entries) were enforced to ensure that a stable dissipative force is applied to the structure. Numerical results indicated that their control algorithm provided higher reliability than the LQR method. Similar approaches have been used for passive control (Chakraborty and Roy, 2011), active control (Yuen and Beck, 2003; Scruggs et al., 2006; Taflanidis et al., 2008a; Taflanidis and Scruggs, 2010), and semi-active control (Taflanidis et al., 2007; Taflanidis et al., 2008b) of systems. In these studies, optimization procedures are applied to either linearized system models (Taflanidis et al., 2008a) or the original nonlinear model of the system (Taflanidis et al., 2008b). In the case of controllers for linearized system models, objective functions can be evaluated and optimized analytically.

For nonlinear system models, objective functions have been determined and minimized through numerical simulations. The first approach may not yield optimal control designs as the nonlinear behavior of the system is not directly accounted for in the control design process. In the second approach, extensive numerical simulations may be required to capture the nonlinear stochastic behavior of the systems. This together with additional runtimes needed for numerical optimization procedures may result in significant computational demands

To investigate the essentials of reliability-based design, in Chapter 6, a set of reliability-based control algorithms using stochastic averaging of energy envelope are proposed. The objective function includes the probability of failure which is defined as the likelihood of a key demand parameter exceeding a predefined limit. Figure 2-2 shows a smaller likelihood of failure for the optimally controlled system compared to the -uncontrolled case.

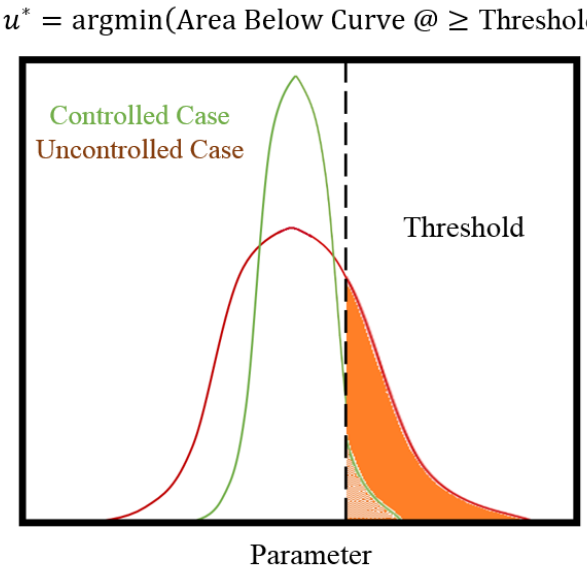

Figure 2-2 PDF of uncontrolled and reliability-based control algorithm (optimal control force = u^*).

2.5 Risk-Based Control

Design of structural systems, especially in hazard prone areas, should account for potential of extreme hazard events. Although they have low probability of occurrence, they may have significant and lasting consequences (Norio et al., 2011). Some consequences include a high number of human casualties and/or extensive levels of physical damage that may lead to collapse, and dysfunctionality of the system. Civil engineers face a challenge to propose a final design that must be serviceable, safe, and economical during its lifetime. The measures of safety, serviceability, reliability, and resilience of structural systems require a detailed research in the dynamic properties of the system. In this context, smart control of structures against natural hazards can be a possible performance-based design to optimize the safety and serviceability of the system. For instance, the objective of smart control technologies for buildings and other structures has been primarily minimization of various structural responses.

While above objectives will very likely reduce the probability of damage and the risk to the systems, the derived control strategies may not yield optimal solutions in terms of the risk and the overall life cycle cost. In particular, these performance objectives have not been incorporated directly into the design process of control algorithms. As a result, a decision-making framework is essential to choose the best alternative among options such as conventional designs (without control) and new designs equipped with control devices, considering costs of installation and maintenance of control systems. For instance, the number of actuators and their corresponding locations in a particular system can be selected based on the life cycle cost criterion. In addition, the control algorithms can be optimized

based on the different cases and the results can be depicted as shown in Figure 2-3. The stakeholder may decide to go with the optimal design that corresponds to the smallest life cycle cost.

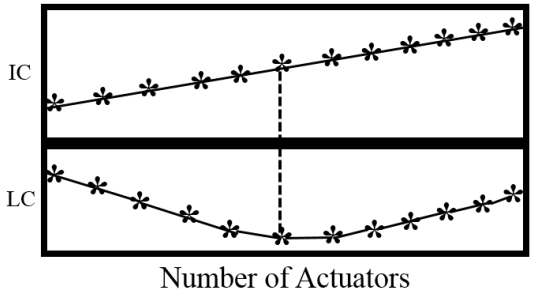

Figure 2-3 Trendlines of number of actuators versus life cycle cost (LC) and initial cost (IC).

Recently, risk-based metrics such as life cycle cost have been added to the passive control objective functions (Taflanidis and Beck, 2009; Gidaris and Taflanidis, 2015). For instance, Taflanidis and Beck (2009) presented an analytical probabilistic framework that estimates and optimizes the life cycle cost for systems equipped with passive dissipative devices. The framework was implemented in a four-story reinforced concrete building. Gidaris and Taflanidis (2015) applied the aforementioned work to shear frame buildings equipped with fluid viscous dampers. In the design process, some challenges arise due to many factors such as uncertainty. Taflanidis and his fellow researchers accounted for uncertainty in the structural stiffness, damping, and mass, on one hand, and stochasticity in the occurrence and intensity of critical hazards on the other hand. In fact, the life cycle cost was computed by a stochastic, multi-dimensional integral over the uncertain

parameters. However, this increased the complexity of incorporating uncertainty with larger systems.

Chapter 7 presents a novel risk-based control design framework for seismically excited nonlinear multi-DOF structures. The proposed method properly accounts for likelihoods of hazards of various intensities during the lifetime of the structure, the fragility of the system for multiple discrete damage states, and the likely consequences associated with each damage state to determine the hazard risks for the structure. These along with initial costs of implementation of control systems and their maintenance constitute the life cycle cost of the structure which is probabilistically incorporated in the proposed control design method.

2.6 Direction for Present Research

This chapter discussed the current state-of-the-art and challenges in active and semi-active control designs particularly focusing on (1) the characterization of the uncertainty of the system, excitation and the nonlinearity in the system, and modeling the dynamics and constraints of the controller and (2) the integration of flexible objective functions to optimize the performance of the system. Conventional linearization techniques and novel stochastic averaging methods were explained for different systems. Mainly, stochastic averaging methods are capable of conserving nonlinearity and stochasticity characteristics compared to conventional linearization techniques. For control design, conventional approaches based on selecting restrained objective functions and on designing sliding mode curves were also described. In addition, stochastic control designs based on stochastic averaging of energy envelope were highlighted in various disciplines. Other topics

included reliability-based control frameworks and risk-based frameworks that entail minimizing explicitly the likelihood and the cost of damage following a hazard event.

Addressing these challenges may require further extensive studies on reliability, resilience, flexibility, practicality, constructability, and cost-effectiveness aspects of control systems. From the results of the literature review, it is found that proper modeling of nonlinearity of the system and further optimizing the controller's performance are needed. Therefore, the following areas have been explored in this dissertation:

- Characterizing systems accurately based on linear or nonlinear stochastic equations rather than using convectional linear deterministic strategies.
- Enhancing conventional control methods by applying stochastic linearization methods, including flexible objective functions, incorporating controller dynamics and constraints, and conducting second level optimizations to select optimal weighing functions.
- Designing a flexible control algorithm that can integrate nonlinearity, stochasticity, and high-order objective functions using stochastic averaging of energy envelope and applying it to real civil engineering applications.
- Developing analytical (versus simulation-based) frameworks for control of nonlinear stochastic systems.

A chart is created for the research directions in this dissertation in Figure 2-4. The red dashed line corresponds to research covered in this dissertation. The current research includes enhancing existing conventional methods (sliding mode control), and developing novel methods to improve performance of stochastic averaging of energy envelope in analytically characterizing systems' behavior, incorporating reliability and risk measures

in control design, and discussing their applicability to civil engineering systems. Future interests are depicted in Figure 2-4 and explained in Section 8.2; These entail enhancing the current methodologies, developing new ones, applying them to complex civil engineering structures and various hazard events, and expanding the spectrum of applications of the developed algorithms to other disciplines.

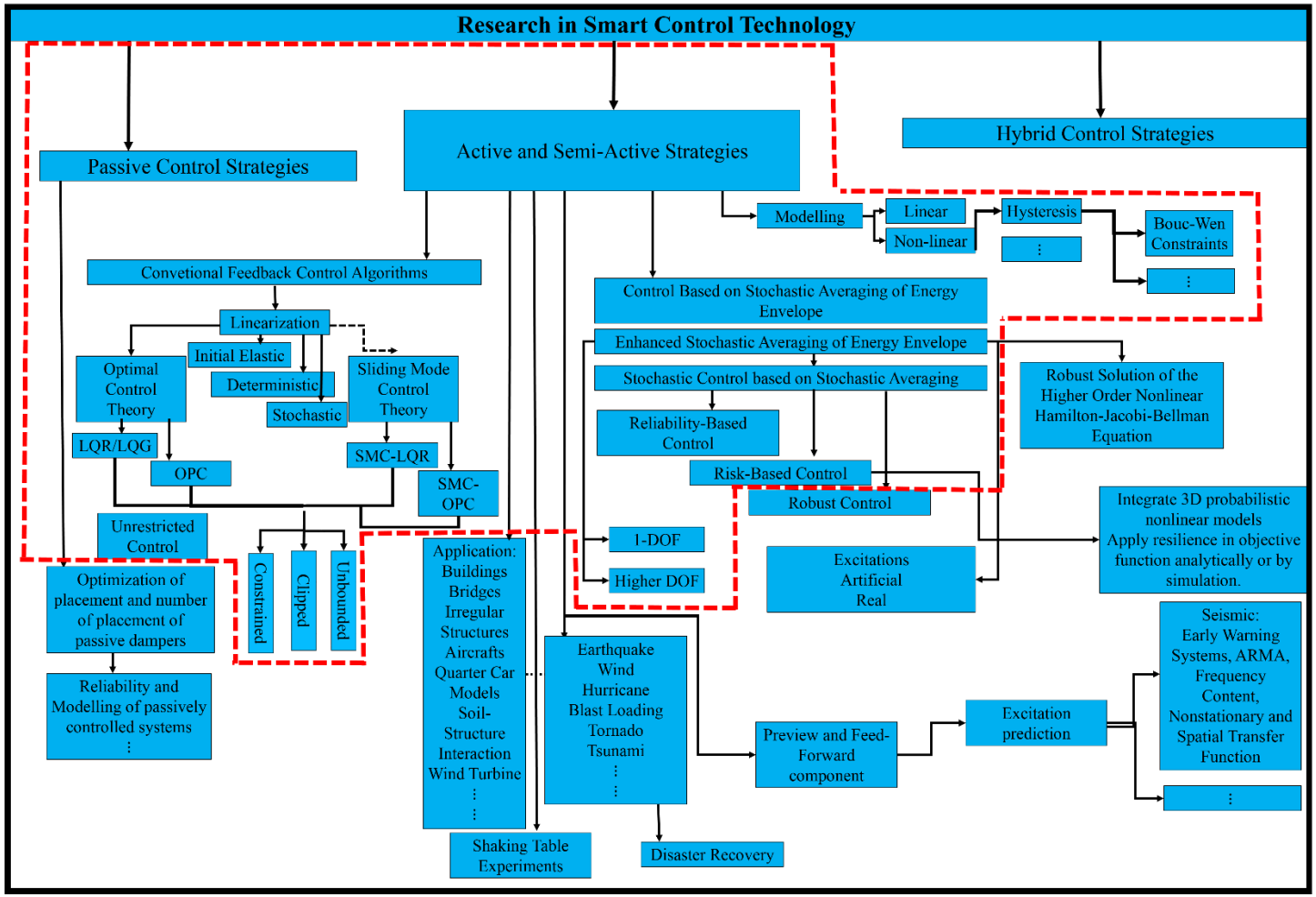

Figure 2-4 Research topics and directions.

Chapter 3: Nonlinear Sliding Mode Control: Shaking Table Experiments on Seismically Excited Multi-Span Bridges Equipped with Semi-active MR Dampers

3.1 Introduction

Semi-active technology has been suggested by researchers to combine properties of both passive and active systems. In semi-active systems, physical parameters of passive systems can change with a small power requirement as opposed to active systems which require a significant amount of power to apply external forces to structures. Furthermore, semi-active devices are efficient for a wide range of excitations compared to passive devices that are only effective for a limited bandwidth.

One of the widely used semi-active devices is magnetorheological (MR) dampers. MR dampers are used in various control problems to:

- Minimize the torsional effects in irregular buildings (Yoshida and Dyke, 2005).
- Suppress the impact of pounding in highway bridges (Guo et al., 2009).
- Reduce excessive displacements of seismically excited base isolated systems (Fan et al., 2009).
- Decrease the acceleration of wind-excited tall buildings (Aly and Zasso, 2011).
- Attenuate vertical vibrations of quarter car models (Prabakar et al., 2013).

MR dampers are considered to be controllable magnetic field devices. They consist of a hydraulic cylinder that contains magnetically polarizable particles suspended within MR fluid (Figure 1-2e). The damping forces are delivered by subjecting the fluid to a magnetic field. MR dampers exhibit high yield stress and operate at wide temperature ranges (Çeşmeci and Engin, 2010; Metered et al., 2010) which are attractive features for control applications. In that respect, MR dampers are employed which exhibit desirable features such as robustness, stability, adaptability, and low power requirements as compared to passive and active systems (Agrawal et al., 2003; Leavitt et al., 2006; Yang and Cai, 2016). However, one main challenge in designing control algorithms for this type of semi-active dampers arises from the nonlinear behavior of the device and the constraints on achievable control forces.

To overcome the complexity of nonlinearity in the system and MR damper and the constraints of the corresponding damper, a new semi-active control algorithm is developed. The control algorithm is called sliding mode control (SMC) based on an optimal polynomial control (OPC) approach (SMC_OPC). The SMC-OPC control force that is derived for an active system is adjusted for MR dampers using a force saturation level and the direction of the motion. This nonlinear SMC is expected to yield better peak response reduction compared to linear SMC surface design at no additional cost as discussed in Section 2.3.3. In general, the proposed semi-active control design is intended to provide a balance between the performance of the controlled system and the power consumption of the controller. The former objective relates to the serviceability and reliability of the structural systems, whereas the latter corresponds to the performance of the control device (Bajaj et al., 2014). In this respect, during large seismic events where safety and reliability

of structures are the major concerns, the performance of the semi-active controller converges to that of the passive-on controller but with considerably reduced power consumption.

The proposed semi-active control algorithm is analyzed and tested using shaking table tests on a three span bridge with a total length of 12 meters equipped with two MR dampers attached between adjacent spans. First, a comprehensive step-by-step procedure is presented for the control design. This is followed by modeling nonlinear bridge components to capture hysteretic responses and pounding. Then, a statistical linearization approach is implemented to provide an equivalent linear model, while accounting for the uncertainty in the system response due to seismic disturbances. Next, clipped-optimal SMC is designed according to a second level optimization that determines the optimal semi-positive definite weighting matrices. The design is tested using shaking table tests of a three span bridge subjected to a scaled Kobe (KB) ground motion. In the testing procedure, the MR dampers are set to minimum and maximum current values, as well as the optimal current determined from semi-active control strategy. The results are elaborated for small and large scaled Kobe earthquake ground motions at different controlled states: uncontrolled structure (the bridge without MR dampers), passive-off (where the input current is set to zero at all times during earthquakes), passive-on (where the input current is set to a maximum value at all times during earthquakes), and semi-active case (in which the input current ranges between minimum and maximum values according to the proposed clipped SMC-OPC algorithm). The performance of these control cases is compared to maximum absolute displacements of the decks, maximum relative displacements between adjacent deck segments and between deck segments and abutments, and finally the

maximum absolute acceleration of deck segments. The primary control objective is to reduce maximum relative displacements that control the likelihood of damage due to pounding. Another goal of the control system is to reduce the maximum absolute displacements and the peak accelerations for mitigating damage to supports (Johnson et al., 2008; Saiidi et al., 2012) and enhancing riding comfort (Kwon et al., 1998; Ni et al., 2001; Yau, 2009). The different control cases of the MR dampers considered in this study exhibit various attributes such as the adaptability to earthquake characteristics, the reduced power consumption in semi-active state, the suboptimal response reduction in passive-on state, and the functionality of the MR dampers when no power is available in the passive-off state.

The rest of the chapter is arranged as follows: Section 3.2 presents a detailed derivation of the novel control algorithm called SMC-OPC for the semi-active control of the system. Next, characteristics of the case study bridge along with modeling techniques for the rubber bearings, MR dampers, and pounding behavior and their validation with experimental results are explained in Section 3.3. Section 3.4 describes the procedure for stochastic linearization of the system and optimization of the clipped semi-active control design. Shaking table experiment results for the proposed SMC-OPC method along with uncontrolled, passive-on, and passive-off cases are presented in Section 3.5. Conclusions and results of the study are summarized in Section 3.6.

3.2 Methodology

In this section, a state space based nonlinear SMC-OPC is initially proposed and derived for the active control of a fully observed system. Then, the considerations of semi-active

control and partial observability are accounted in the design implementation for the particular system in Section 3.4. In that respect, a general linearized system subjected to stochastic disturbance is assumed and represented in state space form as:

$$\dot{\mathbf{X}} = \mathrm{G}(\mathbf{X}, \mathbf{u}, t) = \mathbf{A_{state}X} + \mathbf{Bu} + \mathbf{F_e} \tag{3.1}$$

where $\mathbf{X}$ is the response vector and $\mathbf{A_{state}}$ is the system matrix which is derived using mass, damping, and stiffness components of the dynamic system. In addition, the system matrix can include models for the dynamics of the passive-off component of the control device and stochastically linearized models for the nonlinear behavior of the system. In Equation (3.1), $\mathbf{F_e}$ and $\mathbf{B}$ represent the excitation vector and the location matrix of controllers. The control component, $\mathbf{u}$, denotes the force vector applied by active or semi-active controller. Unlike the case in conventional LQR and LQG methods, the design of SMC is not based on a minimization procedure. Instead, the SMC design is known to be a two-step procedure. The first step involves the design of the sliding surface. Then, a control law is selected to drive the response variables to the defined sliding surface. In order to design linear SMC forces, an optimal sliding surface can be obtained based on minimizing a LQR performance index, L_{LQR}, with semi-positive weighting matrix, $\mathbf{Q_1}$**:**

$$L_{LQR} = \int_0^\infty \mathbf{X^T Q_1 X} dt \tag{3.2}$$

The corresponding linear sliding surface is represented by:

$$\mathbf{S} = \mathbf{PX} \tag{3.3}$$

where $\mathbf{P}$ is to be determined according to LQR method in order to force the system state trajectory to move along a stable manifold (Utkin, 1992; Yang et al., 1994; Adhikari and Yamaguchi, 1997). To enhance the transient response, this study proposes extending the

sliding surface to include higher order nonlinear terms; this extension is expected to improve vibration mitigation of the system. As a result, the performance index is expanded to include Higher Order Terms (HOT) to:

$$L_{OPC} = \int_{\mathbf{0}}^{\infty} (\mathbf{X^T Q_1 X} + \text{HOT})\, dt \tag{3.4}$$

where the terms, $\mathbf{Q_1}$ and HOT are defined later in Equation (19). First, to design the sliding surface, the state space system in Equation (3.1) is converted into the so-called regular form of transformation (Utkin, 1992). The converted system of the state space vector, $\mathbf{Y}$, is represented by:

$$\dot{\mathbf{Y}} = \widehat{\mathbf{A}}_{\mathbf{state}}\mathbf{Y} + \widehat{\mathbf{B}}\mathbf{u} + \widehat{\mathbf{F}}_{\mathbf{e}} \; ; \mathbf{Y} = \mathbf{DX} \tag{3.5}$$

where $\mathbf{D}$ is the orthogonal transformation matrix. The system is transformed and represented with new state space system, defined by $\widehat{\mathbf{A}}_{\mathbf{state}}$ $(= \mathbf{DA_{state}D^{-1}})$, $\widehat{\mathbf{B}}$ $(= \mathbf{DB})$, $\widehat{\mathbf{F}}_{\mathbf{e}}(= \mathbf{DF_e})$. The new system matrices can be partitioned as:

$$\mathbf{Y} = \begin{Bmatrix} \mathbf{Y_1} \\ \mathbf{Y_2} \end{Bmatrix}, \widehat{\mathbf{A}}_{\mathbf{state}} = \begin{bmatrix} \widehat{\mathbf{A}}_{\mathbf{state_1}} & \widehat{\mathbf{A}}_{\mathbf{state_{12}}} \\ \widehat{\mathbf{A}}_{\mathbf{state_{21}}} & \widehat{\mathbf{A}}_{\mathbf{state_2}} \end{bmatrix}, \widehat{\mathbf{B}} = \begin{bmatrix} \mathbf{0} \\ \mathbf{B_T} \end{bmatrix}, \text{and } \widehat{\mathbf{F}}_{\mathbf{e}} = \begin{Bmatrix} \widehat{\mathbf{F}}_{\mathbf{e_1}} \\ \widehat{\mathbf{F}}_{\mathbf{e_2}} \end{Bmatrix} \tag{3.6}$$

where $\mathbf{B_T}$ is the transformed sub-location matrix. Assuming that the vector, Y, is an N-dimensional transformed response vector and u is a P-dimensional control force vector, the vector, $\mathbf{Y_1}$, includes the (N-P) components that are independent of the control force. The remaining P components of $\mathbf{Y}$ form the vector $\mathbf{Y_2}$. This approach enables designing a state space-based surface that is explicitly a function of only $\mathbf{Y_1}$ and $\mathbf{Y_2}$. As a result, the system in Equation (3.5) can be rewritten as:

$$\dot{\mathbf{Y}}_{\mathbf{1}} = \widehat{\mathbf{A}}_{\mathbf{state_1}}\mathbf{Y_1} + \widehat{\mathbf{A}}_{\mathbf{state_{12}}}\mathbf{Y_2} + \widehat{\mathbf{F}}_{\mathbf{e_1}} \tag{3.7a}$$

$$\dot{\mathbf{Y}}_{\mathbf{2}} = \widehat{\mathbf{A}}_{\mathbf{state_{21}}}\mathbf{Y_1} + \mathbf{B_T u} + \widehat{\mathbf{A}}_{\mathbf{state_2}}\mathbf{Y_2} + \hat{\mathbf{F}}_{\mathbf{e_2}} \tag{3.7b}$$

In the design of the sliding surface using OPC, $\mathbf{Y_1}$ and $\mathbf{Y_2}$ play the role of the state vector and the control force of a traditional system, respectively. The term $\widehat{\mathbf{A}}_{\mathbf{state_{12}}}\mathbf{Y_2}$ can be considered virtually as a control force and substituted by $\mathbf{B'}\boldsymbol{u'}$, therefore:

$$\dot{\mathbf{Y}}_{\mathbf{1}} = \widehat{\mathbf{A}}_{\mathbf{state_1}}\mathbf{Y_1} + \mathbf{B'u'} + \hat{\mathbf{F}}_{\mathbf{e_1}} \tag{3.7c}$$

where $\mathbf{B'}$ is the location matrix and $\mathbf{u'}(=\mathbf{Y_2})$ is the virtual control force. Referring to El-Khoury et al. (2015), the performance index of system in Equation (7a) is represented by:

$$L_{OPC} = \int_{\mathbf{0}}^{\infty} \left(\mathbf{Y_1^T Q_{11} Y_1} + \mathbf{Y_2^T Q_{22} Y_2} + \left(\mathbf{Y_1^T M Y_1}\right)\left(\mathbf{Y_1^T Q_{33} Y_1}\right) + \bar{h}(\boldsymbol{Y_1})\right) dt \tag{3.8c}$$

The semi-positive definite matrices, $\mathbf{Q_{11}}$, $\mathbf{Q_{22}}$, and $\mathbf{Q_{33}}$ are gain components. The relationship of these gains with the matrices in Equation (3.4) is shown later in Equations (3.18) and (3.19). The term, $\bar{\mathrm{h}}(\boldsymbol{Y_1})$, is defined as:

$$\bar{h}(\mathbf{Y_1}) = \left(\mathbf{Y_1^T M Y_1}\right)\mathbf{Y_1^T M}.\,\widehat{\mathbf{A}}^{\mathbf{T}}_{\mathbf{state_{12}}}\mathbf{Q_{33}^{-1}}.\left(\mathbf{Y_1^T M Y_1}\right)\mathbf{M Y_1} \tag{3.9}$$

The virtual OPC force is derived as:

$$\boldsymbol{u'} = \mathbf{Y_2} = -\boldsymbol{Q_{22}^{-1}}\widehat{\mathbf{A}}^{\mathbf{T}}_{\mathbf{state_{12}}}\mathbf{P Y_1} + \mathbf{Q_{22}^{-1}}\widehat{\mathbf{A}}^{\mathbf{T}}_{\mathbf{state_{12}}}\left(\mathbf{Y_1^T M Y_1}\right)\mathbf{M Y_1} \tag{3.10}$$

in which the Ricatti matrix, $\mathbf{P}$, and $\mathbf{M}$ are determined as:

$$\mathbf{P}\widehat{\mathbf{A}}^{\mathbf{T}}_{\mathbf{state_{11}}} + \widehat{\mathbf{A}}^{\mathbf{T}}_{\mathbf{state_{11}}}\mathbf{P} - \mathbf{P}\widehat{\mathbf{A}}^{\mathbf{T}}_{\mathbf{state_{12}}}\mathbf{Q_2^{-1}}\widehat{\mathbf{A}}^{\mathbf{T}}_{\mathbf{state_{12}}}\mathbf{P} + \mathbf{Q_{11}} = \mathbf{0} \tag{3.11a}$$

$$0 = \mathbf{M}\left(\widehat{\mathbf{A}}_{\mathbf{state_{11}}} - \widehat{\mathbf{A}}^{\mathbf{T}}_{\mathbf{state_{12}}}\mathbf{Q}_{\mathbf{22}}^{-\mathbf{1}}\mathbf{A}_{\mathbf{12}}^{\mathbf{T}}\mathbf{P}\right) + \left(\widehat{\mathbf{A}}_{\mathbf{state_{11}}} - \widehat{\mathbf{A}}^{\mathbf{T}}_{\mathbf{state_{12}}}\mathbf{Q}_{\mathbf{22}}^{-\mathbf{1}}\mathbf{A}_{\mathbf{12}}^{\mathbf{T}}\mathbf{P}\right)^{\mathbf{T}}\mathbf{P} + \mathbf{Q_{33}} \tag{3.11b}$$

The condition in Equation (3.10) can be enforced through a sliding surface, **S**, that satisfies the stability condition ($\mathbf{S} = \mathbf{0}$; $\dot{\mathbf{S}} = \mathbf{0}$) according to the Utkin-Drazenovic method (Utkin, 1992). This surface can be defined by:

$$\mathbf{S} = \mathbf{Y_2} + \boldsymbol{Q}_{\mathbf{22}}^{-\mathbf{1}}\widehat{\mathbf{A}}^{\mathbf{T}}_{\mathbf{state_{12}}}\mathbf{P}\mathbf{Y_1} + \mathbf{Q}_{\mathbf{22}}^{-\mathbf{1}}\widehat{\mathbf{A}}^{\mathbf{T}}_{\mathbf{state_{12}}}\left(\mathbf{Y}_{\mathbf{1}}^{\mathbf{T}}\mathbf{M}\mathbf{Y_1}\right)\mathbf{M}\mathbf{Y_1} \tag{3.12}$$

Differentiating the sliding surface in Equation (12) with respect to time, $\dot{\mathbf{S}}$ is:

$$\dot{\mathbf{S}} = \dot{\mathbf{Y}}_{\mathbf{2}} + \boldsymbol{Q}_{\mathbf{22}}^{-\mathbf{1}}\widehat{\mathbf{A}}^{\mathbf{T}}_{\mathbf{state_{12}}}\mathbf{P}\dot{\mathbf{Y}}_{\mathbf{1}} + \dot{\boldsymbol{f}}(\mathbf{Y_1}) \tag{3.13}$$

where $\boldsymbol{f}(\mathbf{Y_1})$ equals $\mathbf{Q}_{\mathbf{22}}^{-\mathbf{1}}\widehat{\mathbf{A}}^{\mathbf{T}}_{\mathbf{state_{12}}}\left(\mathbf{Y}_{\mathbf{1}}^{\mathbf{T}}\mathbf{M}\mathbf{Y_1}\right)\mathbf{M}\mathbf{Y_1}$ and $\dot{\boldsymbol{f}}(\mathbf{Y_1})$ $\left(d\dot{\boldsymbol{f}}(\mathbf{Y_1})/dt\right)$ is the time differential. Substituting Equations (3.7a) and (3.7b) into Equation (3.13), $\dot{\mathbf{S}}$ can be derived as:

$$\dot{\mathbf{S}} = \left(\widehat{\mathbf{A}}_{\mathbf{state_{21}}}\mathbf{Y_1} + \mathbf{B_T}\mathbf{u} + \widehat{\mathbf{A}}_{\mathbf{state_2}}\mathbf{Y_2} + \widehat{\mathbf{F}}_{\mathbf{e_2}}\right) + \boldsymbol{Q}_{\mathbf{22}}^{-\mathbf{1}}\widehat{\mathbf{A}}^{\mathbf{T}}_{\mathbf{state_{12}}}\mathbf{P}\left(\widehat{\mathbf{A}}_{\mathbf{state_1}}\mathbf{Y_1} + \widehat{\mathbf{A}}_{\mathbf{state_{12}}}\mathbf{Y_2} + \widehat{\mathbf{F}}_{\mathbf{e_1}}\right) + \dot{\boldsymbol{f}}(\mathbf{Y_1}) \tag{3.14}$$

This equation can be rearranged as:

$$\dot{\mathbf{S}} = \begin{bmatrix}\boldsymbol{Q}_{\mathbf{22}}^{-\mathbf{1}}\widehat{\mathbf{A}}^{\mathbf{T}}_{\mathbf{state_{12}}}\mathbf{P} & \mathbf{1}\end{bmatrix}\begin{bmatrix}\widehat{\mathbf{A}}_{\mathbf{state_1}} & \widehat{\mathbf{A}}_{\mathbf{state_{12}}} \\ \widehat{\mathbf{A}}_{\mathbf{state_{21}}} & \widehat{\mathbf{A}}_{\mathbf{state_2}}\end{bmatrix}\begin{Bmatrix}\mathbf{Y_1} \\ \mathbf{Y_2}\end{Bmatrix} + \mathbf{B_T}\mathbf{u} + \begin{bmatrix}\boldsymbol{Q}_{\mathbf{22}}^{-\mathbf{1}}\widehat{\mathbf{A}}^{\mathbf{T}}_{\mathbf{state_{12}}}\mathbf{P} & \mathbf{1}\end{bmatrix}\begin{Bmatrix}\widehat{\mathbf{F}}_{\mathbf{e_1}} \\ \widehat{\mathbf{F}}_{\mathbf{e_2}}\end{Bmatrix} + \dot{\boldsymbol{f}}(\mathbf{Y_1}) \tag{3.15}$$

For the convergence of sliding surface, Equation (3.15) is equated to zero. Next, substituting $= \begin{Bmatrix} \mathbf{Y_1} \\ \mathbf{Y_2} \end{Bmatrix}$, $\hat{\mathbf{F}}_\mathbf{e} = \begin{Bmatrix} \hat{\mathbf{F}}_{\mathbf{e}_1} \\ \hat{\mathbf{F}}_{\mathbf{e}_2} \end{Bmatrix}$, $\boldsymbol{D_{00}} = \left[\boldsymbol{Q_{22}^{-1}}\widehat{\mathbf{A}}_{\mathbf{state_{12}}}^{\mathbf{T}}\mathbf{P} \quad \mathbf{1}\right]$, and $\widehat{\mathbf{A}}_{\mathbf{state}} = \begin{bmatrix} \widehat{\mathbf{A}}_{\mathbf{state_1}} & \widehat{\mathbf{A}}_{\mathbf{state_{12}}} \\ \widehat{\mathbf{A}}_{\mathbf{state_{21}}} & \widehat{\mathbf{A}}_{\mathbf{state_2}} \end{bmatrix}$, the control force, **u**, becomes

$$\mathbf{u} = -\mathbf{B}_\mathbf{T}^{-\mathbf{1}}\left(\boldsymbol{D_{00}}\widehat{\mathbf{A}}_{\mathbf{state}}\mathbf{Y} + \boldsymbol{D_{00}}\hat{\mathbf{F}}_\mathbf{e} + \dot{\boldsymbol{f}}(\mathbf{Y_1})\right) \tag{3.16}$$

The control force in Equation (3.15) works ideally for an external disturbance, $\hat{\mathbf{F}}_\mathbf{e}$, that is known a priori. However, for the case of seismic excitations, $\hat{\mathbf{F}}_\mathbf{e}$ is not known prior to the occurrence. Therefore, the term, $\hat{\mathbf{F}}_\mathbf{e}$, is dropped and is replaced by a properly selected parameter, μ (≥ 0), so that the reachability of the sliding mode is guaranteed with the condition of $\mathbf{S}\dot{\mathbf{S}} = 0$ (Adhikari and Yamaguchi, 1997). It is common that μ is considered to be a percentage of the inertial force ($\mu = \epsilon m\ddot{x}_g$, $0 \leq \epsilon \leq 1$). In this approach, the SMC-OPC control force is adjusted to:

$$\mathbf{u} = \boldsymbol{\sigma} - \mu\,\mathbf{sat}(\mathbf{S}) \tag{3.17}$$

where $\boldsymbol{\sigma}$ is defined as $-\boldsymbol{B_T^{-1}}\left(\boldsymbol{D_{00}}\widehat{\boldsymbol{A}}_{\boldsymbol{state}}\boldsymbol{Y} + \dot{\boldsymbol{f}}(\boldsymbol{Y_1})\right)$. In order to reduce chattering, the saturation function, $\mathbf{sat}(\cdot)$, can be replaced by a tangent hyperbolic function. Substituting $\mathbf{Y} = \begin{Bmatrix} \mathbf{Y_1} \\ \mathbf{Y_2} \end{Bmatrix} = \mathbf{DX}\left(= \begin{bmatrix} \mathbf{D_1} \\ \mathbf{D_2} \end{bmatrix}\mathbf{X}\right)$ and $\mathbf{Y_1} = \mathbf{D_1X}$ in Equation (3.8c), the performance index, L_{OPC}, is rearranged as:

$$L_{OPC} = \int_0^{\infty} \left(\mathbf{X^T D^T} \begin{bmatrix} \boldsymbol{Q_{11}} & \mathbf{0} \\ \mathbf{0} & \boldsymbol{Q_{22}} \end{bmatrix} \mathbf{DX} + \left(\mathbf{X^T D_1^T M D_1 X}\right)\left(\mathbf{X^T D_1^T Q_{33} D_1 X}\right) + \bar{h}(\mathbf{D_1 X}) \right) dt \tag{3.18}$$

which demonstrates the new optimization problem**.** Comparing Equation (3.18) to Equation (3.4), the matrix, $\mathbf{Q_1}$, and HOT are defined as:

$$\mathbf{Q_1} = \mathbf{D^T} \begin{bmatrix} \boldsymbol{Q_{11}} & \mathbf{0} \\ \mathbf{0} & \boldsymbol{Q_{22}} \end{bmatrix} \mathbf{D} \tag{3.19a}$$

$$\text{HOT} = \left(\mathbf{X^T D_1^T M D_1 X}\right)(\mathbf{X^T Q_2 X}) + \bar{h}(\mathbf{D_1 X}) \;\&\; \mathbf{Q_2} = \mathbf{D_1^T Q_{33} D_1} \tag{3.19b}$$

3.3 Case Study

The complex behavior of bridges during seismic events and the vulnerabilities of these assets have been widely studied with the purpose of enhancing the design and providing cost-effective mitigation options to reduce the potential of various types of damage and catastrophic failures. Primary types of damage that have been studied are shear and flexural failure of columns (Han et al., 2009; Kim et al., 2010), expansion joint failure (Zhang et al., 2008; Raheem, 2009), local failure of hinge bearings (Song and Kim, 2007; Johnson et al., 2008; Saiidi et al., 2012), and deck collapse (Pamuk et al., 2005; Han et al., 2009). In multi-span bridges, pounding between adjacent decks is particularly a type of damage that can impact the functionality of bridges following earthquakes and, therefore, has to be considered in the design of new or retrofit of existing bridges. Pounding is a complex phenomenon that induces plastic deformation, local cracking, and fracturing (DesRoches et al., 2011; Naserkhaki et al., 2012; Efraimiadou et al., 2013). Detrimental

implications has been detected due to pounding in adjacent structures e.g. multi-span highway bridges may experience minor (concrete crushing) to major (span unseating) damage as a result of pounding (Kawashima et al., 2009; Huo and Zhang, 2012; Won et al., 2015).

To investigate the effect of pounding on adjacent structures, the proposed control methodology in Section 3.2 is applied to a three span bridge equipped with two semi-active MR dampers attached between adjacent spans. The bridge model includes three reinforced concrete decks, each supported by four rubber bearings, as shown in Figure 1-2e. The dimensions of the bridge are given in the longitudinal and top views in Figure 3-1a. In this setting, the four supports of span A and the two left supports of span B are positioned on shaking table A, while the two right supports of span B and the supports of span C are placed on shaking table B. Considering the short distance between the supports, it is assumed that the ground motions are fully correlated meaning that the same ground motion records are applied to both shaking tables A and B as shown in Figure 3-4d. Since the structure is symmetric with respect to the longitudinal axis and ground motions are applied in the longitudinal direction, a one directional model will be able to predict the dynamic response of the decks.

In cases of large deformations, pounding in the bridge may occur between adjacent spans and between spans and abutments. Pounding can be detected by large acceleration spikes in the response of the spans. For seismic pounding mitigation, MR dampers manufactured by Lord Corporation, USA, are installed between adjacent spans for the passively and semi-actively controlled bridge, as shown in Figure 3-1a and Figure 3-1b. The input current to the MR dampers which control the forces applied to the system varies

from 0 to 2 Amp, the force capacity is ±2000 N, the maximum stroke is ±27.5 mm, the maximum velocity is 200 mm/sec, the extended length is 208 mm, and the weight is about 1 kg. During the shaking table test of the uncontrolled system, displacement and acceleration responses are measured in real-time using piezoelectric sensors and accelerometers, respectively, as shown in Figure 3-1. In the controlled system, the measured responses are used to estimate the state vector through an observer model. In the following subsections, the modeling approach of the bridge components including rubber and lead-rubber bearings, the semi-active device, and the pounding phenomenon is elaborated.

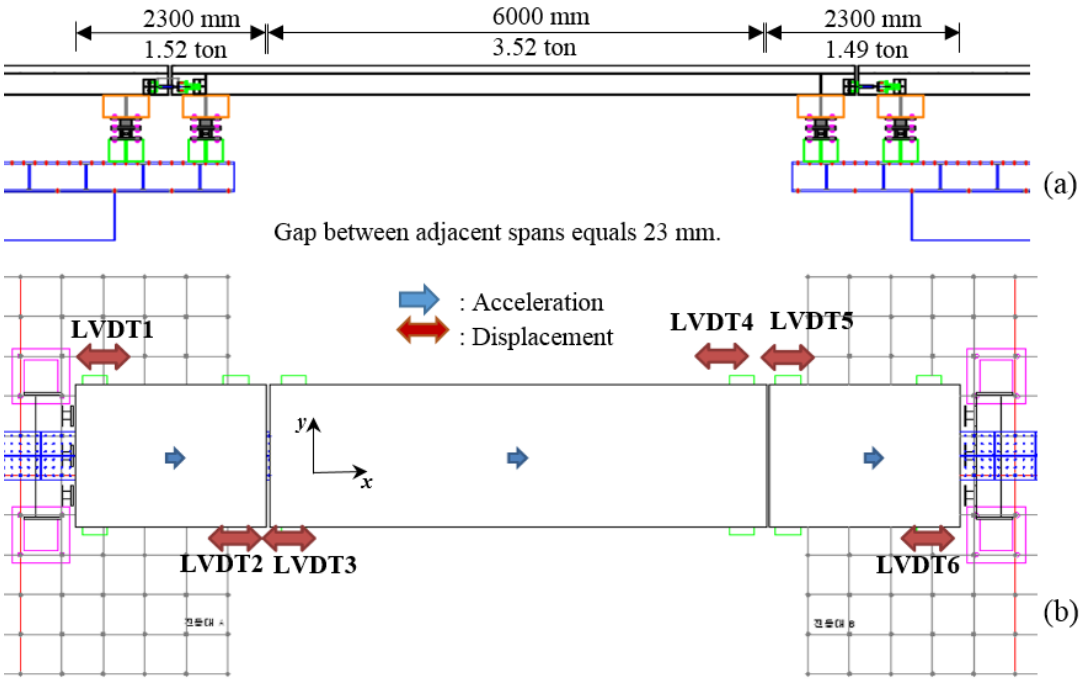

Figure 3-1 Three span bridge equipped with MR dampers between adjacent spans: (b) profile view of the three span bridge, and (c) top view of the three span bridge indicating the location and direction of linear variable differential transformers (LVDT) and accelerometers.

3.3.1 Models of Hysteretic Systems

Components such as bearings and MR dampers that dissipate energy can be characterized by their hysteretic behaviors (El-Khoury et al., 2015). In order to capture this type of nonlinearity, the Bouc-Wen model (Bouc, 1971; Wen, 1976) has been extensively used for different applications, e.g. system identification of MR dampers (Kwok et al., 2007; Ikhouane and Dyke, 2007), structural elements (Ikhouane et al., 2007), base-isolation devices (Marano et al., 2007), soil material (Gerolymos and Gazetas, 2007), and energy dissipation systems (Shih and Sung, 2005). The hysteresis is a form of nonlinearity where the restoring force depends on both the current deformation and the deformation history (Ikhouane and Rodellar, 2007). Here, the hysteretic force is modeled by a set of stiffness, damping, and hysteresis components, as shown in Figure 3-2a. This approach is implemented in this study to represent the nonlinear dynamic behavior of the uncontrolled and controlled bridge. In the uncontrolled state, each span is separated by a gap distance as defined in Figure 3-1. For the controlled state, the MR damper is added and modelled by a parallel system of damping, stiffness, and hysteresis, as depicted in Figure 3-2b.

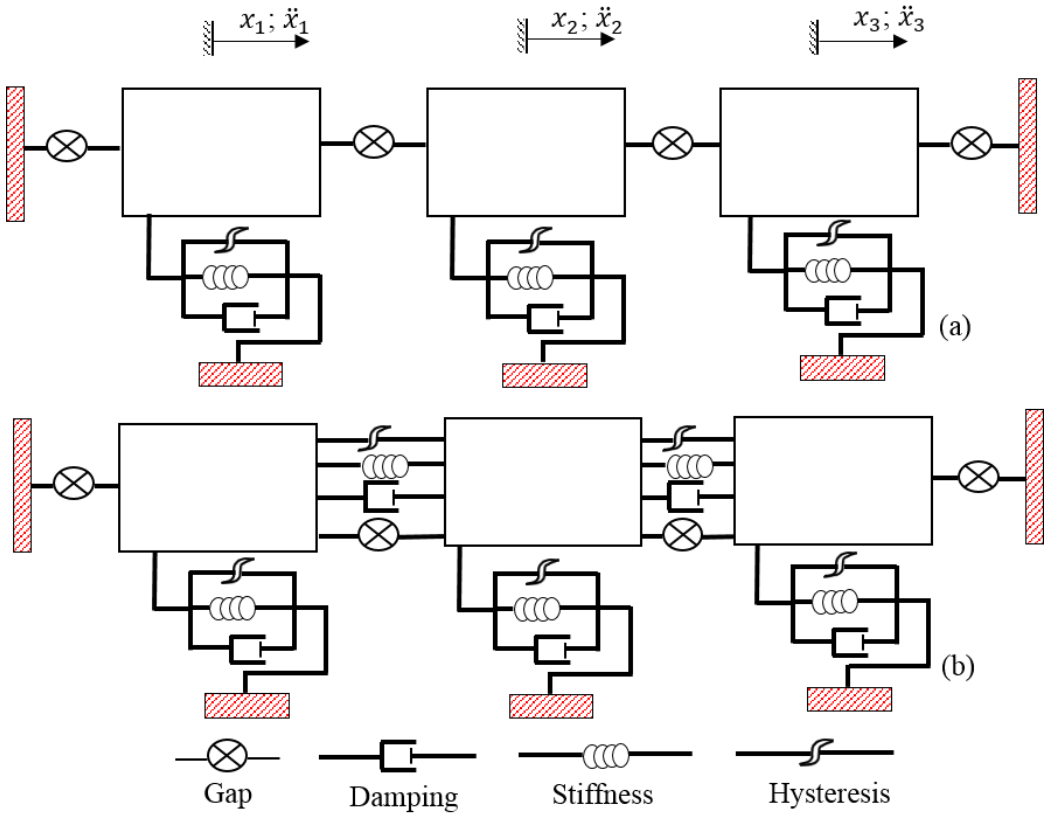

Figure 3-2 Components of the three span bridge model in (a) uncontrolled state and (b) controlled state equipped with MR dampers.

To capture the nonlinear behavior of the bearings and the MR damper, the restoring force for the rubber bearing, F_j, and the MR damper, F_{MR}, are modeled as:

$$F_j = \mathrm{k}_j\left(\alpha_j x_j + \left(1-\alpha_j\right)z_j\right) \ (j = 1, 2, 3) \tag{3.20}$$

$$F_{\mathrm{MR}} = \alpha_{\dot{\mathrm{x}}_{\mathrm{MR}}}\dot{x}_j + \alpha_{\mathrm{z}_{\mathrm{MR}}}z_j \ (j = 4, 5) \tag{3.21}$$

where x_j and $\dot{x}_j$ are the displacement and velocities of jth hysteretic component, respectively. The subscript j ranges from 1 to 5, referring to spans A, B, C, and the MR damper between spans A and B, and between spans B and C. The model parameters k_j, $\alpha_{\dot{\mathrm{x}}_{\mathrm{MR}}}$, and $\alpha_{\mathrm{z}_{\mathrm{MR}}}$ are the stiffness and pre-yield factor of rubber bearing, and the damping

and hysteretic component of the MR damper, respectively. In addition, the variable, z_j, is the *j*th evolutionary term governed by the Bouc-Wen differential equation defined as:

$$\dot{z}_j = A_{\mathrm{BW}_j}\dot{x}_j - \beta_{\mathrm{BW}_j}|\dot{x}_j|z_j - \gamma_{\mathrm{BW}_j}\dot{x}_j|z_j| \; (j = 1,..., 5) \tag{3.22}$$

where A_{BW_j}, γ_{BW_j}, and β_{BW_j} are parameters that control the shape of the loop. The general slope is controlled by $\left(\gamma_{\mathrm{BW}_j} + \beta_{\mathrm{BW}_j}\right)$. Parameters $\alpha_{\dot{x}_{\mathrm{MR}}}$ and $\alpha_{z_{\mathrm{MR}}}$ are decomposed into passive-off and passive-on components with respect to the current, i_c, as:

$$\alpha_{\dot{x}_{\mathrm{MR}}} = \alpha_{\dot{x}_{\mathrm{MR}_0}} + i_c\alpha_{\dot{x}_{\mathrm{MR}_1}} + i_c^2\alpha_{\dot{x}_{\mathrm{MR}_2}} \tag{3.23a}$$

$$\alpha_{z_{\mathrm{MR}}} = \alpha_{z_{\mathrm{MR}_0}} + i_c\alpha_{z_{\mathrm{MR}_1}} + i_c^2\alpha_{z_{\mathrm{MR}_2}} \tag{3.23b}$$

where $\alpha_{\dot{x}_{\mathrm{MR}_0}}$, $\alpha_{z_{\mathrm{MR}_0}}$, $\alpha_{\dot{x}_{\mathrm{MR}_1}}$, $\alpha_{z_{\mathrm{MR}_1}}$, $\alpha_{\dot{x}_{\mathrm{MR}_2}}$, and $\alpha_{z_{\mathrm{MR}_2}}$ characterize the impact of control current.

To determine the model parameters shown above, a global optimization method based on gradient descent for bearings and MR dampers is used to minimize an error cost function between the experimental data and simulation results (El-Khoury et al., 2015). For the bearings, the three span bridge is subjected to a scaled Kobe earthquake. The parameters of the nonlinear model for rubber bearings in spans A, B, and C are shown in Table 3-1. For the MR damper, data of cyclic tests with a frequency of 1 Hz for currents ranging between 0 and 2 Amp was provided by the manufacturing company. The Bouc-Wen parameters for MR damper are represented as a function of the input current ($\alpha_{\dot{x}_{\mathrm{MR}_2}}$ = -5.7 N.sec/mm.Amp^2 , $\alpha_{z_{\mathrm{MR}_2}}$ = -10.3 N /mm.Amp^2 , $\alpha_{\dot{x}_{\mathrm{MR}_1}}$ = 13.1 N.sec/mm.Amp , $\alpha_{z_{\mathrm{MR}_1}}$ = 51.9 N /mm.Amp , $\alpha_{\dot{x}_{\mathrm{MR}_0}}$ = 1.4 N.sec/mm , $\alpha_{z_{\mathrm{MR}_0}}$ = 7.0 N /mm , A_{BW_4} =45.48, γ_{BW_4} = 0.56, β_{BW_4} = 1.38, A_{BW_5} =45.48, γ_{BW_5} = 0.56, β_{BW_5} = 1.38) (Table 3-1). Calibration

results are shown in Figure 3-3 where a good agreement is observed between simulation and experiment results for the MR damper operating at different current levels (0 to 2 Amp). The force in the MR damper increases with current, from about 250 N at 0 Amp to around 2000 N at 2 Amp.

Rubber Bearings					
Parameters / Span	A_{BW_j}	γ_{BW_j}	β_{BW_j}	α_j	k_j (N/mm)
A (j = 1)	1.20	0.26	0.74	0.63	1548.0
B (j = 2)	1.99	0.89	0.11	0.68	945.2
C (j = 3)	8.29	0.36	0.64	0.94	1298.0

Table 3-1 Calibration results for Bouc-Wen model of rubber bearings.

3.3.2 Pounding Model

Pounding is a complex mechanism because of the inherent nonlinear nature of collision at the contact surfaces and the impacts on the vibrations of the structures. A variety of different collision models have been proposed. For instance, linear spring model is a straightforward approach that considers the contact force to be linearly related to the relative displacement when it is larger than the corresponding gap distance. This model is straightforward but does not consider the energy loss that occurs during impact (Maison and Kasai, 1992). To overcome this shortcoming, the Kelvin model includes a damping component. This model yields a uniform dissipation during the approach and restitution periods which is inconsistent with the actual mechanism of impact (Jankowski et al., 1998). Since the formulation of the Kelvin model is based on a static collision, it cannot properly present dissipation during contact (Chau and Wei, 2001). To better represent the dissipation during contact, Hertz model is suggested to model the impact force by a nonlinear spring

component. An extension of the Hertz model called Hertz Damped model incorporates nonlinear stiffness and damping, and considers the impact force, F_{impact}, as

$$F_{\text{impact}} = k_h(y_{12} - g_p)^o + c_h\dot{y}_{12} \tag{3.24}$$

where k_h is the impact stiffness, y_{12} is the relative displacement between two adjacent nodes, g_p is the gap distance, o is the Hertz coefficient that is typically taken as 3/2, and c_h is the nonlinear damping coefficient and is computed as follows:

$$c_h = \xi(y_{12} - g_p)^o \tag{3.25}$$

where ξ is the damping constant and is calculated by:

$$\xi = \frac{3}{4}\frac{(1 - ¥^2)k_h}{\Delta v_{12}} \tag{3.26}$$

where ¥ (= 0.6 for concrete) and Δv_{12} are the coefficient of restitution and relative velocity before impact, respectively (Muthukumar and DesRoches, 2006; Ye et al., 2009). From these equations, the pounding force can be computed as:

$$F_{\text{impact}} = k_h(\Delta y_{12} - g_p)^o \left[1 + \frac{3}{4}\frac{(1 - ¥^2)}{\Delta v_{12}}\,\dot{y}_{12}\right] \tag{3.27}$$

where $\dot{y}_{12}$ is the relative velocity of the adjacent nodes.

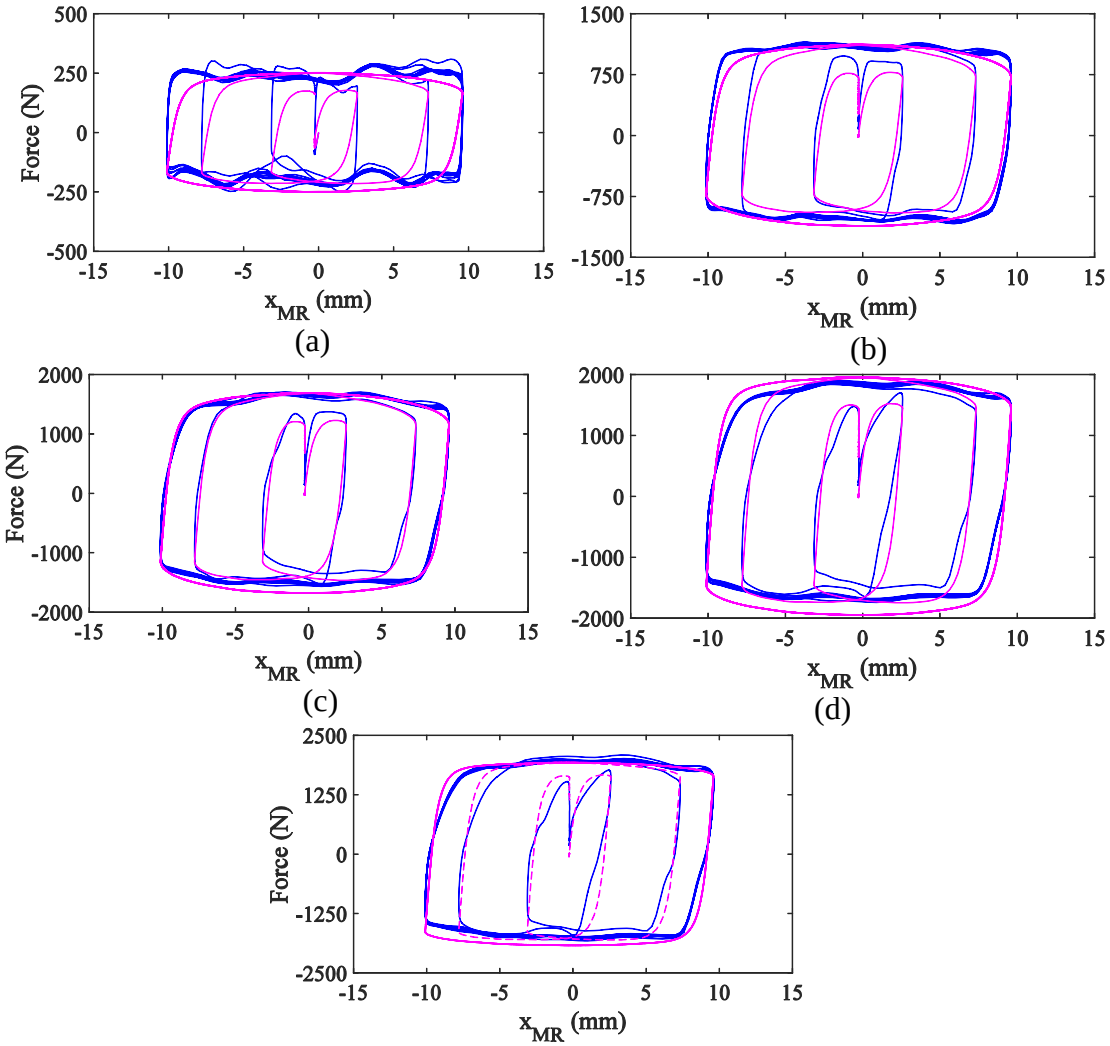

Figure 3-3 Calibration results based on harmonic tests of the MR damper set at different currents: (a) 0.0 Amp, (b) 0.5 Amp, (c) 1.0 Amp, (d) 1.5 Amp, and (e) 2.0 Amp (—— Experiment , ----- Simulation).

For experimental verification, pounding can be identified when large spikes in the absolute acceleration responses are observed. For instance, if opposite spikes at a given instant are observed in the absolute accelerations of adjacent spans, it indicates that pounding has occurred between those spans. Elsewhere, a large spike in the total span acceleration is an indication of the pounding between that span and the adjacent abutment.

The pounding model is tested for the uncontrolled three span bridge subjected to KB40 and the response is plotted in Figure 3-4. It can be observed that pounding occurred primarily between adjacent spans. In addition, the pounding model was able to capture the majority of acceleration spikes.

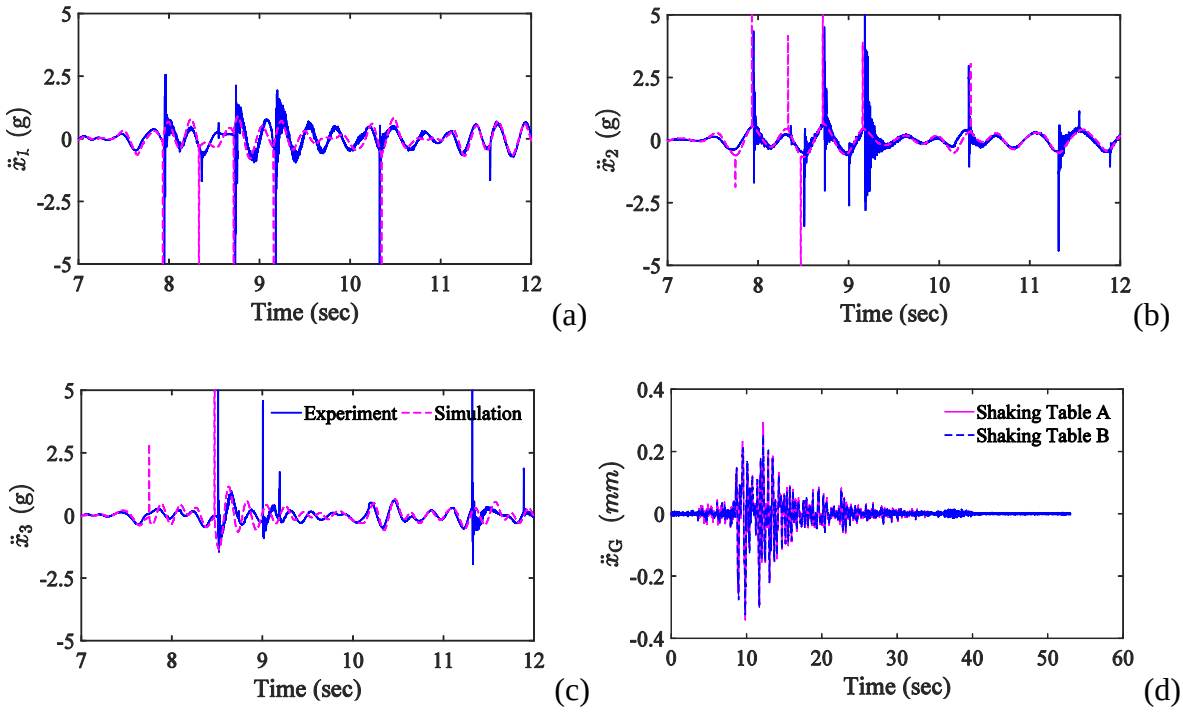

Figure 3-4 Acceleration response of the three span bridge subjected to KB40: (a) span A, (b) span B, and (c) span C and (d) ground motion accelerations of shaking tables.

3.4 Implementation of Control Algorithm

As mentioned earlier, this chapter investigates the semi-active control of a nonlinear partially observed system. In order to achieve an optimal control performance, a number

of additional steps are taken in the control design including linearization of the system, modeling constraints of the semi-active control force, and designing an observer for the partially observed system. First, the nonlinear passive-off bridge model is linearized stochastically. Next, a second level optimization is carried out in order to find the optimal gains of the SMC-OPC controller such that the performance of the MR damper is maximized based on a defined objective function. A clipped optimal strategy and a Kalman-based observer are designed to drive the MR damper forces into a feasible range based on current saturation and to estimate the state space given the measured responses, respectively.

3.4.1 Stochastic Linearization

In conventional linearization, the nonlinearity of the components is ignored and the system is calibrated and linearized based on initial or equivalent linear stiffness, which may yield inaccurate response predictions. Stochastic linearization replaces the hysteretic components by equivalent linear time invariant models through minimizing the residual errors arising from the linearization process (Basili and Angelis, 2007; Basili et al., 2013; El-Khoury et al., 2015). The stochastic linearization strategy is applied to the three span bridge equipped with MR dampers at zero current. The equation of motion of the dynamic system is presented as:

$$\mathbf{M\ddot{U} + C_d\dot{U} + K_U U + K_Z Z = M\ddot{U}_g} \tag{3.28}$$

where the matrices, $\mathbf{M}$, $\mathbf{C_d}$, $\mathbf{K_U}$, and $\mathbf{K_Z}$ are the mass, damping, linear stiffness, and nonlinear stiffness matrices, respectively. $\mathbf{U}$ is the linear displacement vector identified as $[x_1;\ x_2;\ x_3]$, and $\mathbf{Z}$ is the evolutionary vector presented as $[z_1;\ z_2; z_3; z_4; z_5]$. The variables

x_1, x_2, x_3 are displacements of spans A, B and C, and z_1, z_2, z_3, z_4, and z_5 are the hysteretic terms in the support models for spans A, B, and C, and the two MR dampers, respectively. $\mathbf{\ddot{U}_g}$ is the ground motion vector applied to the three span bridge. As mentioned in Section 3.1, the hysteretic behavior is characterized by the Bouc-Wen model, presented as:

$$\dot{z}_j = \mathrm{A}\dot{x}_j - \beta|\dot{x}_j|z_j - \gamma\dot{x}_j|z_j| \tag{3.29}$$

where the subscript, j (= 1, 2 … 5), refers to spans A, B, and C, and MR dampers, respectively. Since this equation depends only on the velocity and hysteretic term, the equivalent linearized equation is presented as:

$$\dot{z}_j = -\mathrm{C}_j\dot{x}_j - \mathrm{K}_j z_j \tag{3.30}$$

where C_j and K_j are the linearized parameters of the velocity and hysteretic term, respectively. Under the assumption that $\dot{x}_j$ and z_j are zero mean joint Gaussian processes, the linearized parameters, C_j and K_j, are obtained by partially differentiating Equation (3.33) with respect to $\dot{x}_j$ and z_j , respectively:

$$\mathrm{C}_j = -\frac{\partial(\dot{z}_j)}{\partial(\dot{x}_j)}, \mathrm{K}_j = -\frac{\partial(\dot{z}_j)}{\partial(z_j)} \tag{3.31}$$

Applying Equation (31) to Equation (30), the linearized parameters are presented as:

$$\mathrm{C}_j = \beta_j\,\mathrm{E}\left(\frac{z\,\partial(|\dot{x}_j|)}{\partial\dot{x}_j}\right) + \gamma_j\,\mathrm{E}(z_j) - \mathrm{A}_j \tag{3.32a}$$

$$\mathrm{K}_j = \beta_j\,\mathrm{E}[|\dot{x}_j|] + \gamma_j\,\mathrm{E}\left(\frac{\dot{x}_j\,\partial(|z_j|)}{\partial z_j}\right) \tag{3.32b}$$

Since the external excitation is assumed to be a Gaussian process and the variables are jointly Gaussian, the linearized parameters can be evaluated in terms of the second moments as follows:

$$C_j = \sqrt{\frac{2}{\pi}}\left[\beta_j \sigma_{z_j} + \frac{\gamma_j E\left(\dot{x}_j z_j\right)}{\sigma_{\dot{x}_j}}\right] - A_j \tag{3.33a}$$

$$K_j = \sqrt{\frac{2}{\pi}}\left[\frac{\beta_j E\left(\dot{x}_j z_j\right)}{\sigma_{z_j}} + \gamma_j \sigma_{\dot{x}_j}\right] \tag{3.33b}$$

where $E\left(\dot{x}_j z_j\right)$ is the expected value of $\dot{x}_j z_j$, and $\sigma_{\dot{x}_j}^2$ and $\sigma_{z_j}^2$ are the variances of $\dot{x}_j$ and z_j, respectively (Socha 2008; To, 2011). Using the initial values of the linearized parameters, a Lyapunov equation is used to compute the second moments which are then substituted in Equations (3.33a-b) until the difference in the results of the *p*th and (*p*+1)th iterations is within a prescribed margin of error. Next, the converged linearized parameters, C_j and K_j are substituted in Equation (3.28) and rearranged in the state space. Consequently, the linearized bridge model is derived as:

$$\dot{\mathbf{X}} = \mathbf{A_{state}}\mathbf{X} + \mathbf{F_e} \tag{3.34}$$

where the state vector, $\mathbf{X}$, is defined as:

$$\mathbf{X} = [\mathbf{U}; \dot{\mathbf{U}}; \mathbf{Z}] \tag{3.35}$$

The system matrix, $\mathbf{A_{state}}$, includes mass, damping, and nonlinear stiffness components of the three span bridge:

$$\mathbf{A_{state}} = \begin{bmatrix} \mathbf{0} & \mathbf{I} & \mathbf{0} \\ -\mathbf{M^{-1}K_U} & -\mathbf{M^{-1}C_d} & -\mathbf{M^{-1}K_Z} \\ \mathbf{0} & \mathbf{C_b} & \mathbf{K_b} \end{bmatrix} \tag{3.36}$$

where $\mathbf{C_b}$, $\mathbf{K_b}$, and $\mathbf{F_e}$ are the linearized parameters for velocity and hysteretic components in the system and the external excitation vector, respectively. This procedure is used to derive the stochastic linear model of the passive-controlled system, i.e. the bridge model combined with the passive component of the MR damper. The performance of this model

is compared to the nonlinear and linear elastic models of the bridge for the Kobe ground motion scaled at 40% (KB40), and the results are presented in Figure 3-5. It is seen that the stochastically linearized model predicts well the response of the nonlinear bridge compared to the deterministic linear elastic model. This performance is expected since stochastic linearization replaces the nonlinear differential equation of the system by a linear one that is derived based on statistical measures considering the hysteretic behavior of the bridge. This ensures more accurate representation of system responses compared to the conventional linear elastic approach which ignores the z component.

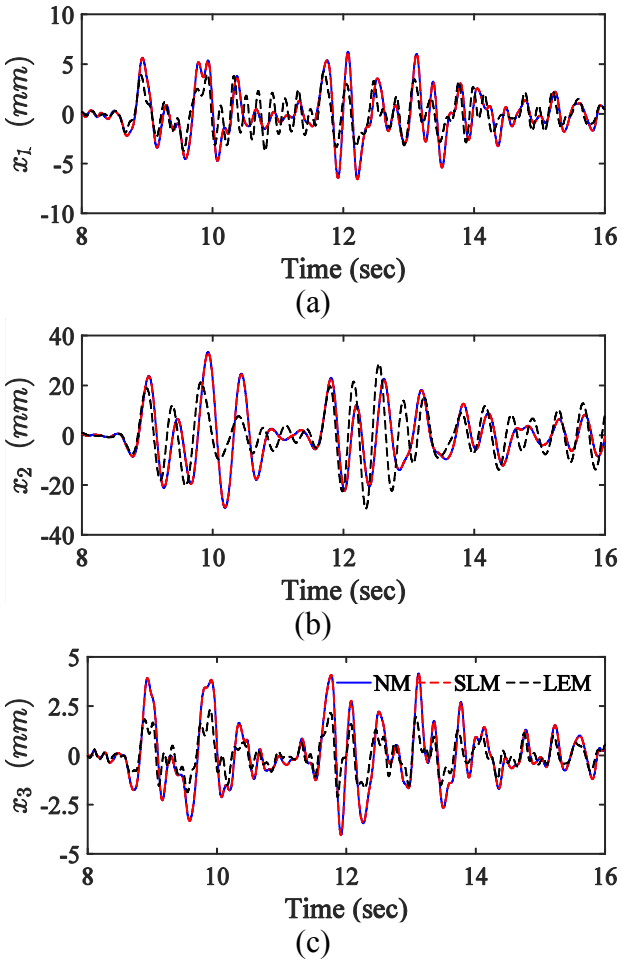

Figure 3-5 Time history of nonlinear model (NM) versus stochastic linearization (SLM) and linear elastic linearization (LEM) methods for (a) displacement of span A, (b) displacement of span B, and (c) displacement of span C under KB40.

3.4.2 Second Level Optimization

The weighting matrices in Equation (3.18) and Equation (3.19) are commonly determined based on the designer's prior knowledge or an iterative procedure. However, such methods may not yield optimal results in most cases and better solutions can be achieved through a well-defined second level optimization. In order to determine the optimal weighting matrices, $\mathbf{Q_1}$ and $\mathbf{Q_2}$, and the parameter, μ, in Equation (3.17), Equation (3.18), and

Equation (3.19), a second level optimization cost function can be defined based on the interest and the judgment of the designer. Here, the second level global optimization problem is defined by a cost function which includes a combination of different response variables. For the three span bridge, one of the primary objectives of the control strategy is to reduce the likelihood of pounding and acceleration. To consider a combination of the critical responses, an objective function, L_2, is considered to incorporate the critical displacements (pounding) and absolute span accelerations:

$$\mathbf{A_{state}} = \begin{bmatrix} \mathbf{0} & \mathbf{I} & \mathbf{0} \\ -\mathbf{M^{-1}K_U} & -\mathbf{M^{-1}C_d} & -\mathbf{M^{-1}K_Z} \\ \mathbf{0} & \mathbf{C_b} & \mathbf{K_b} \end{bmatrix} \tag{3.37}$$

where the subscripts $(\cdot)_C$ and $(\cdot)_P$ refers to the SMC-OPC and passive-on states, respectively. The critical displacements are relative displacements between two sides of a gap in the direction of gap closure. For example, $\max^{+}_{x_{12_C}}$ refers to the maximum of the positive relative displacement of span A with respect to span B, while $\max^{-}_{x_{1_C}}$ represents the maximum relative displacement of span C with respect to the adjacent abutment in the negative direction. If these displacements are equal to the corresponding gap sizes, pounding will occur. On the other hand, $\max_{x_{12_C}}$refers to the maximum absolute relative displacement of span A and span B irrespective of direction i.e. $\max(|x_1 - x_2|)$.The first four components consider the ratio of the max directional displacements, while the rest of the components take into account the ratio of the maximum absolute acceleration responses in the semi-actively controlled versus passively controlled bridge.

3.4.3 Clipped Semi-Active Control Forces

During simulation and shaking table tests, clipped optimal rules are considered in order to apply the control force constraints of the semi-active device. These constraints include the dependency of the applied control force on the direction of the dynamic response of the MR damper and the force capacity of the device. To incorporate these limitations in the control model, the feasible range of 0 and 2 Amp for the input current to the MR damper is considered and the following force saturation model is applied:

$$\mathbf{u}_{\text{constrained}} = \left[\begin{cases} 0 & \Delta_j < 0 \text{ Amp} \\ u_{\text{unconstrained}_j} & 0 \text{ Amp} \leq \Delta_j \leq 2 \text{ Amp} \\ -\left(\Delta_j \alpha_{\dot{x}_{MR_1}} + \Delta_j^2 \alpha_{\dot{x}_{MR_2}}\right) \dot{x}_j & \\ \quad + \left(\Delta_j \alpha_{z_{MR_1}} + \Delta_j^2 \alpha_{z_{MR_2}}\right) z_j & \Delta_j > 2 \text{ Amp} \end{cases}_j \right] \tag{3.38}$$

where Δ_j (j = 4, 5) is the root of

$$u_{\text{unconstrained}_j} - \left(\Delta_j \alpha_{\dot{x}_{MR_1}} + \Delta_j^2 \alpha_{\dot{x}_{MR_2}}\right) \dot{x}_j + \left(\Delta_j \alpha_{z_{MR_1}} + \Delta_j^2 \alpha_{z_{MR_2}}\right) z_j = 0 \tag{3.39}$$

and the unconstrained control force vector, $\mathbf{u}_{\text{unconstrained}}$, is the active control force from Equation (3.17).

3.5 Results

In order to evaluate the control performance of the three span bridge subjected to seismic excitations, four cases are considered for shaking table experiments:

1- Uncontrolled, where no MR damper is installed on the bridge.

2- Passive-off, where two MR dampers are installed between adjacent spans and are set to minimum current of 0 Amp.

3- Passive-on, where both dampers are set to maximum current of 2 Amp.

4- SMC-OPC control, where a current value is determined from the control algorithm and fed into the MR damper instantaneously.

In this study, Kobe earthquake is considered which is a near-field event with high amplitude long period velocity pulses and a peak ground acceleration (PGA) of 0.821g. This ground motion exported from NGA database (Chiou et al., 2008) was recorded at the KJMA Observatory station, with a distance to fault rupture of 0.6 km.

The results, here, are analyzed for Kobe ground motion scaled at 20% (KB20) and 40% (KB40). For KB20, no pounding is observed in any of the cases; however, the critical displacement responses, x_{12}^{+} and x_{23}^{+}, are reduced to 23% and 48% at passive-on state and 28% and 61% at semi-active state, respectively, in comparison to the uncontrolled case. As for the acceleration responses, the passive-off case has the smallest absolute accelerations, in which $\ddot{x}_1$, $\ddot{x}_2$, and $\ddot{x}_3$ are reduced by 10%, 13%, and 1%, respectively, compared to the uncontrolled case (Table 3-2).

State	Critical/Peak displacements (mm) and peak accelerations (g)						
	x_1	x_{12}	x_{23}	x_3	$\ddot{x}_1$	$\ddot{x}_2$	$\ddot{x}_3$
Uncont.	2.40/2.80	16.61/17.05	16.86/17.10	1.32/1.64	0.33	0.38	0.27
Passive-off	2.75/2.65	12.34/12.34	11.56/12.61	1.41/1.83	0.30	0.33	0.27
Passive-on	4.93/6.01	3.89/6.01	8.04/8.04	3.20/3.36	0.36	0.35	0.30
SMC-OPC	4.76/6.3	4.64/7.15	10.01/10.11	2.92/3.08	0.33	0.35	0.36
State	**RMS of displacements (mm) and accelerations (g)**						
	x_1	x_{12}	x_{23}	x_3	$\ddot{x}_1$	$\ddot{x}_2$	$\ddot{x}_3$
Uncont.	0.32	2.42	2.43	0.23	0.05	0.06	0.04
Passive-off	0.37	1.78	1.79	0.26	0.05	0.05	0.04
Passive-on	0.65	0.50	0.70	0.78	0.05	0.05	0.05
SMC-OPC	0.69	0.66	0.82	0.87	0.05	0.05	0.05

Current Ratio = $\frac{\bar{\imath}_{\mathrm{SMC-OPC}}}{\bar{\imath}_{\mathrm{Passive-on}}}$ / Energy Ratio = $\frac{\bar{E}_{\mathrm{SMC-OPC}}}{\bar{E}_{\mathrm{Passive-on}}}$

State	MR-AB	MR-BC
SMC-OPC	0.61 / 0.31	0.62 / 0.31

Table 3-2 Results for three span bridge subjected to KB 20.

For KB40, the performance of passive and semi-active control strategies are more pronounced as compared to the uncontrolled bridge (Table 3-3). For this scaled ground motion, significant pounding is observed between adjacent spans in both the uncontrolled and passive-off states. Nevertheless, the number of acceleration spikes for passive-off are reduced by at least 25% compared to the uncontrolled state; four spikes for $\ddot{x}_1$, eight spikes for $\ddot{x}_2$, and four spikes for $\ddot{x}_3$. As for the semi-actively controlled system, a significant improvement is shown compared to the uncontrolled state especially where 41% and 32%

reductions in the relative displacements, x_{12} and x_{23} are observed. For the same response measures, these reductions are 46% and 37% for the passive-on control case. For further illustration, the time history of displacement and acceleration responses are shown in Figures 3-6 and 3-7. In addition, the bearing forces applied on span B are plotted in Figure 3-8 where a pronounced improvement is observed in terms of the peak forces compared to the uncontrolled case: 32% reduction for both passive-on and SMC-OPC, and 13% reduction for passive-off. Similar behaviors are seen for bearings of spans A and C.

State	**Critical/Peak displacements (mm) and peak accelerations (g)**						
	x_1	x_{12}	x_{23}	x_3	$\ddot{x}_1$	$\ddot{x}_2$	$\ddot{x}_3$
Uncontrolled	13.62/18.56	28.88/28.88	30.31/30.31	8.24/15.95	7.32	7.60	16.79
Passive-off	10.73/11.79	25.99/25.99	29.00/29.00	4.38/12.66	1.41	1.71	1.50
Passive-on	8.72/11.22	15.70/18.94	19.43/19.43	4.65/4.76	0.56	0.51	0.49
SMC-OPC	9.37/11.99	16.97/19.97	20.35/20.35	4.98/5.52	0.57	0.53	0.49
State	**RMS of displacements (mm) and accelerations (g)**						
	x_1	x_{12}	x_{23}	x_3	$\ddot{x}_1$	$\ddot{x}_2$	$\ddot{x}_3$
Uncontrolled	1.82	4.23	4.64	1.26	0.17	0.15	0.23
Passive-off	1.42	4.11	4.42	0.80	0.10	0.11	0.10
Passive-on	1.45	1.97	2.35	0.78	0.08	0.08	0.07
SMC-OPC	1.54	2.02	2.38	0.87	0.08	0.09	0.07

Current Ratio = $\frac{\bar{\imath}_{\text{SMC-OPC}}}{\bar{\imath}_{\text{Passive-on}}}$ / Energy Ratio = $\frac{\bar{E}_{\text{SMC-OPC}}}{\bar{E}_{\text{Passive-on}}}$

State	MR-AB	MR-BC
SMC-OPC	0.74 / 0.37	0.53 / 0.26

Table 3-3 Results for three span bridge subjected to KB 40.

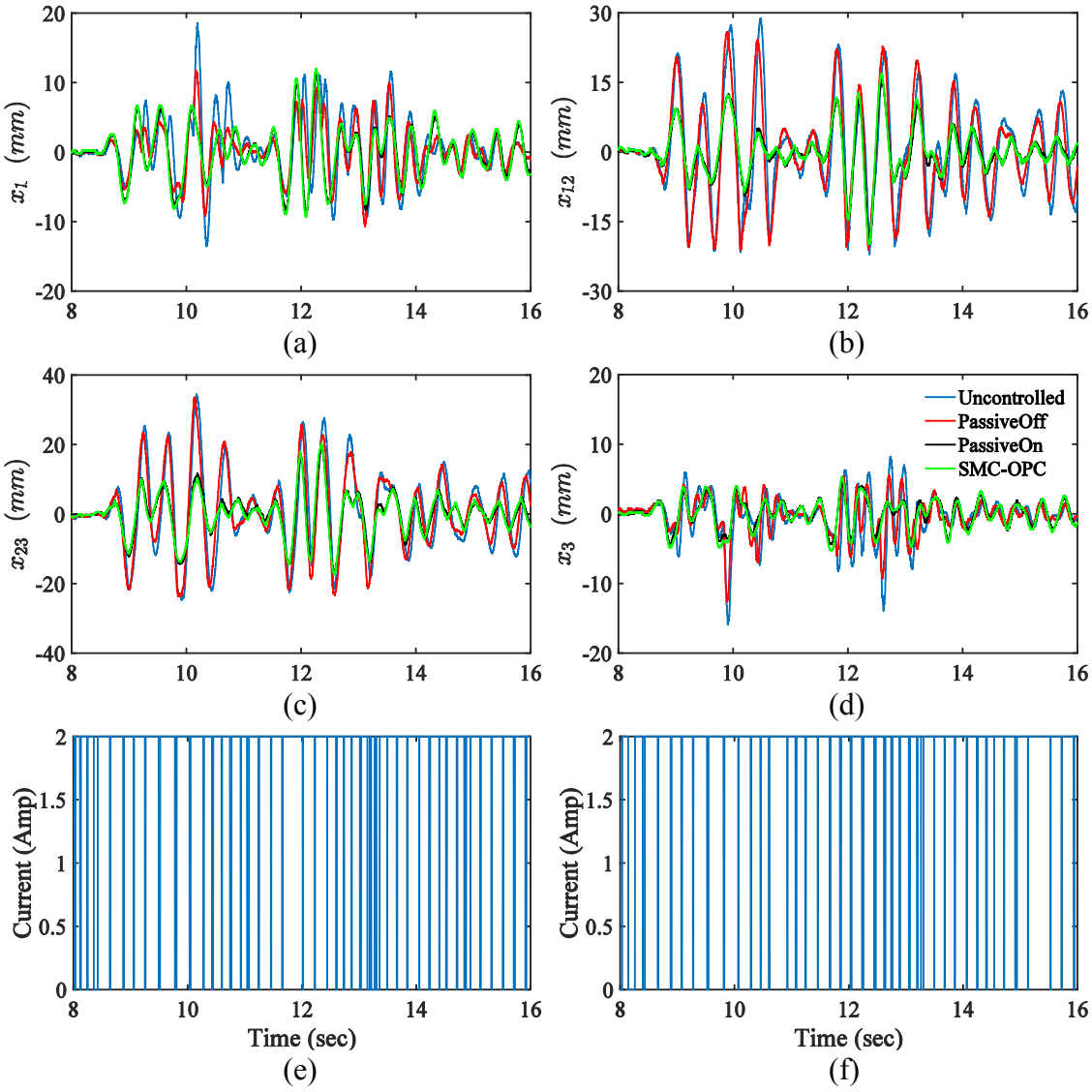

Figure 3-6 Time history response of the three span bridge with various control states subjected to KB40 for displacements of (a) span A, (b) AB, (c) BC, and (d) span C and current of MR dampers (e) AB and (f) BC.

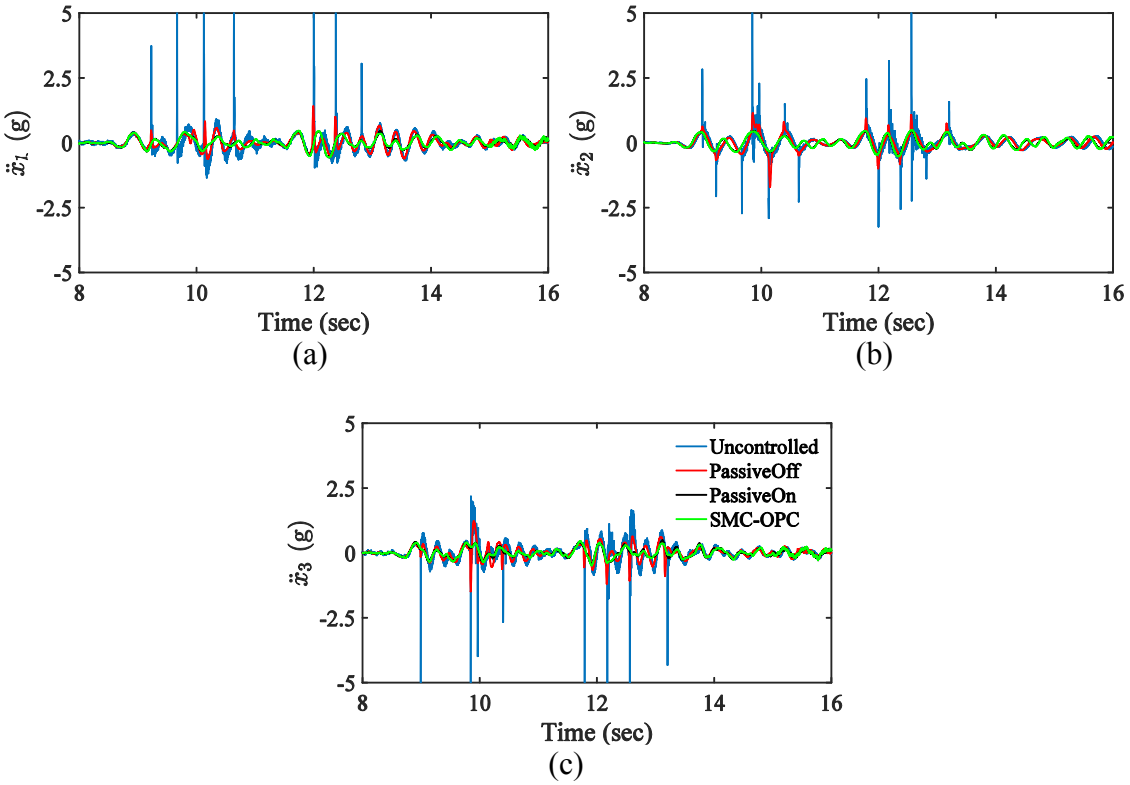

Figure 3-7 Absolute acceleration time history of three span bridge for different control states subjected to KB40 for (a) span A, (b) span B, and (c) span C.

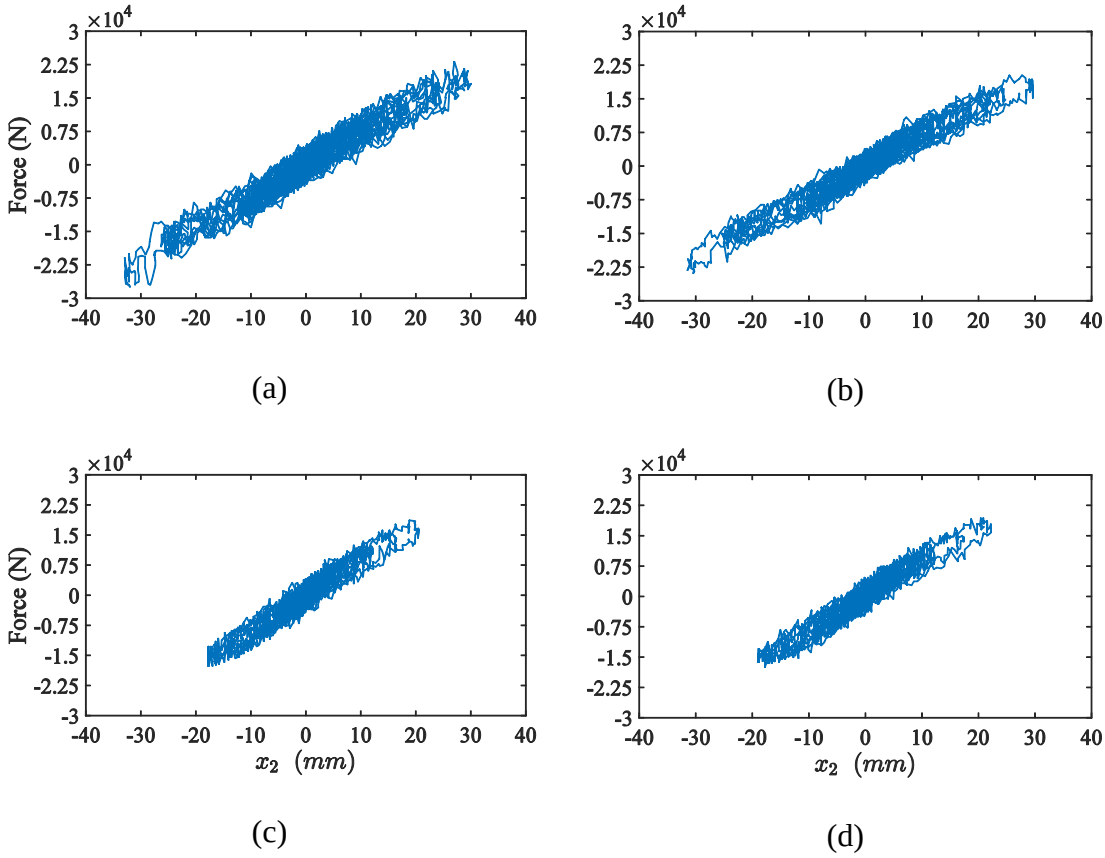

Figure 3-8 Force-deformation behavior of bearing forces applied to span B under KB40 for (a) uncontrolled, (b) passive-off, (c) passive-on, and (d) SMC-OPC.

One of the main advantages of the control algorithm is its performance convergence to that of passive-on but at a lower cost by minimizing current and energy consumptions, as recorded in Tables 3-2 and 3-3. The control energy, E, of an MR damper is a more accurate measure than current to indicate the power consumption of the system. The control energy is defined as

$$E = i_c^2 R_{coil} \tag{3.40}$$

where R_{coil} is the resistance of the coil wire (Nguyen et al., 2008). The results can be summarized as follows: the mean current values for semi-active MR-AB and MR-BC at

KB40 are reduced to 74% and 53% of passive-on case, and the energy consumptions for both MR dampers are reduced further to 37% and 26% of passive-on state. Similar results are observed for KB20, where the power consumption is reduced by 69% for both MR dampers compared to passive-on case.

From the experiment results especially for the high intensity earthquake, it appears that reducing critical displacements helps in avoiding pounding and hence the acceleration values stay within moderate levels. Adding MR dampers enhances the energy dissipation capabilities of the system especially for ground motions with large PGA. Using these strategies, the likelihood of failure, collapse, and pounding can be noticeably reduced. For semi-active control, the performance of the system converges to that of the passive-on state with a considerable reduction in the energy consumption, as shown earlier. However, if the damper cannot operate semi-actively or at a constant nonzero current value, the passive-off state can still reduce the impact of pounding as observed with fewer and less severe acceleration spikes compared to uncontrolled state (Figures 3-6 and 3-7). As a result, both passive and semi-active strategies have noticeable impacts on the seismic performance of the bridge and can be adopted as alternative solutions for seismic risk reduction of critical structures.

3.6 Closure

The effectiveness of MR dampers controlled using passive and semi-active strategies are examined for response reduction and in particular pounding mitigation of adjacent structures. The damper is set at zero current, maximum current, and a current value that is determined through a semi-active control strategy. In that respect, a new state space based control algorithm, named SMC-OPC is introduced and derived. SMC-OPC is based on a

nonlinear sliding mode control, in which the linear sliding surface is expanded to a higher order trajectory. The higher order surface provides more flexibility to optimize the performance and maximize the robustness of the controller compared to linear sliding surfaces. Alongside the passive states, SMC-OPC is designed and tested using shaking table experiments for a three span bridge supported by nonlinear bearings. For this system, the control objectives are to reduce excessive deformations that may lead to collapse and the potential of pounding, depicted by spikes of absolute accelerations, since it may pose considerable damage to adjacent structures.

To suppress the extreme effects of seismic-induced vibrations, two MR dampers are installed between adjacent spans. For semi-active technology, the clipped semi-active control strategy is adopted to optimize the performance of the MR damper as compared to the three conditions: uncontrolled, passive-off where the input current is zero, and passive-on which has the maximum input current of 2 Amp. The control design process starts with developing numerical models for the characterization of nonlinear components of the system. The hysteresis in both the MR damper and rubber bearings is simulated using the Bouc-Wen model, while the nonlinear pounding phenomenon between spans and abutments is captured using Damped Hertz model.

To design the state space control strategy, the nonlinear system is stochastically linearized where the nonlinear behavior of the passive MR damper is incorporated. Next, a clipped optimal strategy is utilized to account for MR damper constraints in the SMC-OPC algorithm. To provide an optimal performance of the control device, the selection of the weighting matrices is made based on a global second level optimization of a prescribed cost function. Shaking table experiments are conducted for the bridge models for scaled

near-field ground motion records. The results show that passive-on at the stronger earthquake provides the best control performance with respect to reducing structural responses. The proposed SMC-OPC semi-active control method provides a balance between the performance of the controlled system with respect to its reliability, and the power consumption of the controller which affects the performance of the control device during the event. This strategy yields very close performance to the passive-on case but with a significantly reduced energy consumption during the large ground motion. Although the passive-off state is not as efficient as SMC-OPC and passive-on, it is able to noticeably reduce displacement and acceleration responses compared to the uncontrolled state during moderate and large earthquakes. This observation is important as passive-off state can represent the case where the power supply to the MR damper is failed. Considering these factors, it can be concluded that installation of MR dampers between adjacent structures has the potential to reduce damage due to pounding and excessive gap openings in adjacent structures in addition to mitigating other critical structural responses. Such passive and semi-active strategies can keep bridges operational following moderate and large seismic events.

Chapter 4: Enhanced Stochastic Averaging of Non-integrable Nonlinear Systems

4.1 Introduction

Stochastic systems may exhibit nonlinear behavior in their dynamic response; these responses are often uncertain due to the stochasticity in input excitations and other sources as discussed in Section 2.2.1. To generate simplified models for such systems, stochastic linearization techniques were developed (Anh et al., 2015) to determine parameters of an equivalent linear model by minimizing the error between the responses of the nonlinear and linear systems (Socha, 2005). Stochastic linearization was used in Chapter 3 to linearize the nonlinear behavior in both rubber bearings of the bridge and semi-active control device; furthermore, the state space control algorithms (nonlinear sliding mode control based on optimal polynomial control) were designed based on the stochastic linearized system. This linearization method is an adequate approximation scheme, but the accuracy of these methods reduces as the nonlinearity in the system and the number of the degrees of freedom (DOF) increase (Socha, 2005).

Alternatively, stochastic averaging is a solution that is proven to provide higher accuracy, since it retains the intrinsic nature of nonlinearity in the system behavior as well as effects of stochasticity in input excitations (Bellizzi et al., 2001). Stochastic averaging has been used for system identification and control design in different domains such as

structural engineering (Zhu et al., 2004; Cheng et al., 2006; El-Khoury and Shafieezadeh, 2015), earth and environmental sciences (Cai, 2009), and physics (Deng et al., 2011). As described in 2.2.2, stochastic averaging of energy envelope, one of the three stochastic averaging methods, is chosen here to transform the dynamic system into the Hamiltonian domain. This method can be applied to lightly damped systems subjected to weak excitations (Zhu, 2006). In addition, this method reduces the dimension of dynamic systems, while preserving the nonlinearity in system behavior and its stochasticity arising from input excitations. In stochastic averaging of energy envelope, the total energy of the system is known as the Hamiltonian. Common response variables of dynamic systems e.g. displacements and velocities are often rapidly varying quantities, while energy envelopes of systems are slowly varying quantities. This method exploits this feature to average the rapidly varying processes to yield the averaged Itô equations for slowly varying processes.

Generally, real-world systems are non-integrable. By definition, non-integrable systems include dependent potential energies, where the entire system can only be represented by a single Hamiltonian (Huang and Zhu, 2009) for all DOFs. Conventional stochastic averaging methods for such general systems neglect effects of off-diagonal damping terms and consider a collective contribution of the diagonal entries rather than their individual effects. They also treat external stochastic excitations on applied DOFs as independent processes (Gu and Zhu, 2014). These factors may limit the application of stochastic averaging for nonlinear systems given that these systems often do not comply with those conditions. To address these limitations, this chapter proposes an equivalent nonlinear models for hysteretic non-integrable multi-DOF systems subjected to stochastic excitations. In that respect, parameters of the equivalent nonlinear model including

modified damping parameters and equivalent excitation intensity are derived through the application of the method of weighted residuals to the drift and diffusion components in the Itô equation for actual and modified systems. The proposed methodology, called the enhanced stochastic averaging method, uses high order moments of velocity response variables to derive equivalent damping and intensity parameters; this improves the accuracy of the stochastic averaging method when applied to nonlinear non-integrable systems with coupled damping terms.

The application of the new strategy is demonstrated for stochastic averaging of a nonlinear foundation-structure system subjected to stochastic excitations. It is noteworthy that SSI considerably influences the dynamic characteristics of seismically excited structures; the flexibility of the soil beneath the structure affects the response of the structure and therefore the extent of damage sustained by the structure following the earthquake. The challenge of modeling SSI arises from the induced material and geometric nonlinearities (Amini and Shadllou, 2011). As a result, past stochastic analyses of structures have generally neglected contributions from soil and foundation behaviors by assuming fixed support conditions, or oversimplified behaviors of foundations. Due to these complexities, capturing the nonlinear behavior of foundations and the interaction with the structure during earthquakes can yield more accurate estimates of the seismic performance of structures; this is essential for making proper design and retrofit decisions for structures (Kausel, 2010). This study considers a one-story building on a nonlinear raft foundation in loose sand subjected to Gaussian white noise excitations. The probability density function of the Hamiltonian and its moments are derived using the proposed method and are compared to those computed using conventional stochastic averaging and

Monte Carlo simulations (MCS). It should be noted that the proposed method is general and can be applied to multi-DOF non-integrable hysteretic systems. The rest of the chapter is structured as follows. Section 4.2 presents a comprehensive derivation of the proposed methodology. Next, results of the numerical study are presented in Section 4.3, and conclusions of the research are summarized in Section 4.4.

4.2 Enhanced Stochastic Averaging of Energy Envelope

Natural and engineered dynamic systems are often nonlinear and non-integrable. A multi-story building supported by a nonlinear foundation subjected to lateral excitations is among such systems. A representative model for these structures is shown in Figure 4-1a where the DOFs of the system are coupled through damping and stiffness over the entire building. In conventional stochastic averaging methods, the effects of the off-diagonal damping terms vanish and a collective contribution rather than individual effects of diagonal terms is considered. In addition, these methods treat external excitations on DOFs of systems as independent processes, while in many cases such as the structure in Figure 4-1a, these disturbances are perfectly correlated, or have high degrees of correlation. These limitations may result in unacceptable response predictions of realistic systems using conventional methods of stochastic averaging of energy envelope. These conventional strategies are extended to provide more accurate representation of system behavior. The derivations of the proposed method for a general nonlinear hysteretic system subjected to Gaussian white noise excitation are presented in this section. The equations of motion of a *p*-DOF hysteretic system subjected to a single white noise excitation (Figure 4-1a) are as follows.

$$m_i\ddot{x}_i = (g_i(x_{i-1}, x_i, x_{i+1}) + \tau_i(z_{i-1}, z_i, z_{i+1}) + c_{i-1}\dot{x}_{i-1} - c_{i-1}\dot{x}_i + c_i\dot{x}_{i+1} - c_i\dot{x}_i) + m_i\sigma_0\frac{\mathrm{d}B}{\mathrm{d}t} \quad (4.1a)$$

$$\tau_{x_i}(x_{i-1}, x_i, x_{i+1}) = \left(-\left(\alpha_{z_i}k_i + \alpha_{z_{i-1}}k_{i-1}\right)x_i + \alpha_{z_{i-1}}k_{i-1}x_{i-1} + \alpha_{z_i}k_i x_{i+1}\right) \quad (4.1b)$$

$$\tau_{z_i}(z_{i-1}, z_i, z_{i+1}) = \left(-\left(\left(1-\alpha_{z_i}\right)k_i + \left(1-\alpha_{z_{i-1}}\right)k_{i-1}\right)z_i + \left(1-\alpha_{z_{i-1}}\right)k_{i-1}z_{i-1} + \left(1-\alpha_{z_i}\right)k_i z_{i+1}\right) \quad (4.1c)$$

where m_i, x_i, $\dot{x}_i$, z_i, and $\ddot{x}_i (i = 1, \ldots, p)$ are the mass, displacement, velocity, evolutionary variable, and acceleration of the ith DOF, respectively. The coupled functions, $\tau_{x_i}(x_{i-1}, x_i, x_{i+1})$ and$\tau_{z_i}(z_{i-1}, z_i, z_{i+1})$, are dependent on the displacements and evolutionary variables, respectively. c_i is the damping coefficient of the ith DOF $\left(c_0 = c_{p+1} = 0\right)$. The parameters k_i and α_{z_i} represent the stiffness component and the level of nonlinearity, respectively. In Equation (4.1a), B is the Brownian motion, also known as Weiner process, and its derivative with respect to time, dB/dt, yields the Gaussian white noise excitation. In this case, the term, $\mathrm{d}B/dt$, represents the input acceleration that is applied to the system. The standard deviation of the excitation is represented by σ_0.

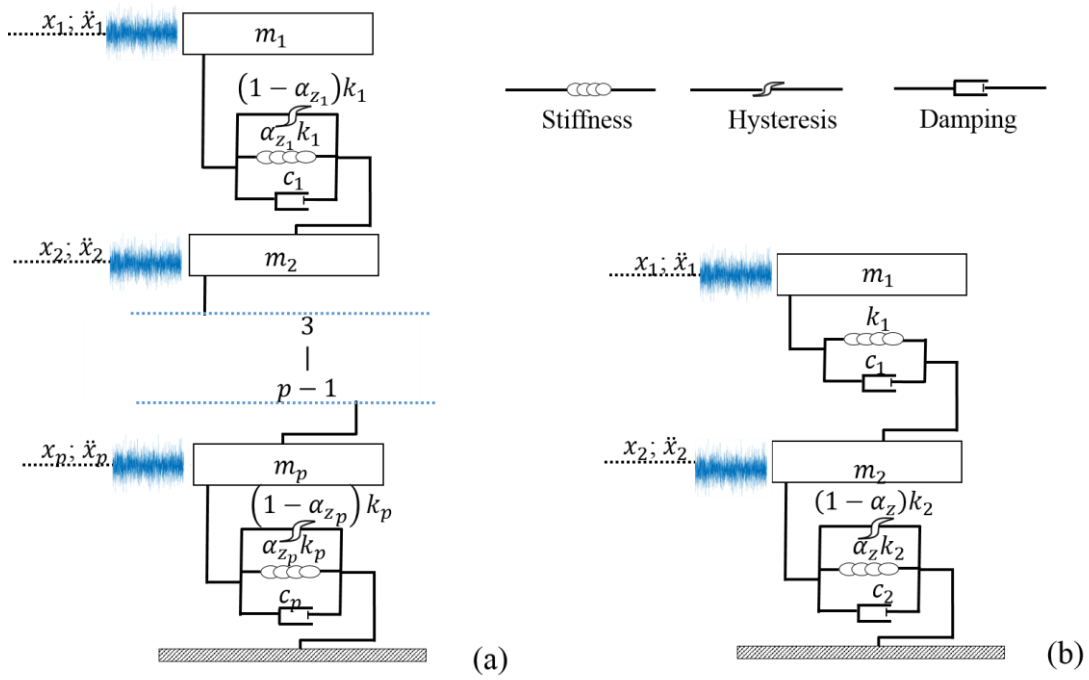

Figure 4-1 Hysteretic systems: (a) multi-DOF hysteretic system and (b) 2-DOF hysteretic system in study.

The component $\pounds_E(x_1, x_2, \dots, x_p, z_1, z_2, \dots, z_p)$ represents the potential energy and depends on the displacements, $x_1, x_2, \dots, x_p$, and evolutionary variables, $z_1, z_2, \dots, z_p$. The potential energy of the p-DOF hysteretic system is:

$$\pounds_E(x_1, x_2, \dots, x_p, z_1, z_2, \dots, z_p)$$

$$= \int \tau_{x_i}(x_{i-1}, x_i, x_{i+1})dx_i + \int \tau_{z_i}(z_{i-1}, z_i, z_{i+1})dz_i$$

$$+ \text{IND}(x_1, x_2, \dots, x_{i-1}, x_{i+1}, \dots, x_p, z_1, z_2, \dots, z_{i-1}, z_{i+1}, \dots, z_p)$$

$$= \sum_{i=1}^{p} (\alpha_{z_i}k_i + \alpha_{z_{i-1}}k_{i-1})\frac{x_i^2}{2} + \sum_{i=1}^{p} ((1-\alpha_{z_i})k_i + (1-\alpha_{z_{i-1}})k_{i-1})\frac{z_i^2}{2}$$

$$-\sum_{i=1}^{p-1}\alpha_{z_i}k_i x_i x_{i+1}-\sum_{i=1}^{p-1}(1-\alpha_{z_i})k_i z_i z_{i+1} \tag{4.2}$$

The function $\mathrm{IND}(x_1, x_2, \dots, x_{i-1}, x_{i+1}, \dots, x_p, z_1, z_2, \dots, z_{i-1}, z_{i+1}, \dots, z_p)$ is the component of energy that is independent of the variables z_i and x_i. The energy, E, of the system in Equation (4.1a) is divided into potential and kinetic energies as follows:

$$E(x_1, x_2, \dots, x_p, \dot{x}_1, \dot{x}_2, \dots, \dot{x}_p, z_1, z_2, \dots, z_p) = \sum_{i=1}^{p} m_i \frac{\dot{x}_i^2}{2} + £_E(x_1, x_2, \dots, x_p, z_1, z_2, \dots, z_p) \tag{4.3}$$

For detailed derivations, a 2-DOF nonlinear hysteretic system with equal masses ($m_1 = m_2 = m$) is considered here; however, the presented methodology is general and can be applied to larger DOF systems. The damping and stiffness components of the first DOF are linear ($\alpha_{z_1} = 1$), while the second DOF has damping, stiffness, and nonlinear hysteresis components ($\alpha_{z_2} = \alpha_z < 1$). This case can represent a single story building on a nonlinear foundation as shown in Figure 4-1b. To simplify the derivations without loss of accuracy, the energy of the system is derived for unit mass. This measure of energy is represented by *e* and is composed of kinetic energy per unit mass, $v(\dot{x}_1, \dot{x}_2)$, and potential energy per unit mass, $£_e(x_1, x_2, z_2) = £_1(x_1, x_2) + £_2(z_2)$:

$$e = v(\dot{x}_1, \dot{x}_2) + £_e(x_1, x_2, z_2) \tag{4.4a}$$

$$v(\dot{x}_1, \dot{x}_2) = \frac{\dot{x}_1^2}{2} + \frac{\dot{x}_2^2}{2} \tag{4.4b}$$

$$£_1(x_1, x_2) = \frac{k_1}{m}\frac{x_1^2}{2} - \frac{k_1}{m}x_1 x_2 + \frac{(k_1 + \alpha_z k_2)}{m}\frac{x_2^2}{2} \tag{4.4c}$$

$$£_2(z_2) = (1 - \alpha_z)\frac{k_2}{m}\frac{z_2^2}{2} \tag{4.4d}$$

The equations of motion of the 2-DOF system can be described as:

$$\begin{aligned}\ddot{x}_1 &= \left(-\frac{\partial £_1(x_1, x_2)}{\partial x_1} - \frac{c_1}{m}\dot{x}_1 + \frac{c_1}{m}\dot{x}_2\right) + \sigma_0\frac{\mathrm{d}B}{\mathrm{d}t} \\ \ddot{x}_2 &= \left(-\frac{\partial £_1(x_1, x_2)}{\partial x_2} - \frac{\partial £_2(z_2)}{\partial z_2} - \frac{{c_2}''}{m}\dot{x}_2 + \frac{c_1}{m}\dot{x}_1\right) + \sigma_0\frac{\mathrm{d}B}{\mathrm{d}t}\end{aligned} \tag{4.5}$$

where ${c_2}''$ equals $(c_1 + c_2)$ and σ_0 is the standard deviation of the white noise excitation.

The derivatives of the displacement and velocity are denoted by:

$$\mathrm{d}\dot{x}_i = \ddot{x}_i\mathrm{d}t \;\&\; \mathrm{d}x_i = \dot{x}_i\mathrm{d}t \;\; (i = 1, 2) \tag{4.6}$$

Applying Equation (4.6) to Equation (4.5) yields:

$$\begin{aligned}\mathrm{d}\dot{x}_1 &= \left(-\frac{\partial £_1(x_1, x_2)}{\partial x_1} - \frac{c_1}{m}\dot{x}_1 + \frac{c_1}{m}\dot{x}_2\right)\mathrm{d}t + \sigma_0\mathrm{d}B \\ \mathrm{d}\dot{x}_2 &= \left(-\frac{\partial £_1(x_1, x_2)}{\partial x_2} - \frac{\partial £_2(z_2)}{\partial z_2} - \frac{{c_2}''}{m}\dot{x}_2 + \frac{c_1}{m}\dot{x}_1\right)\mathrm{d}t + \sigma_0\mathrm{d}B\end{aligned} \tag{4.7}$$

The total energy of the system, e, in Equation (4.4) is alternatively known as the Hamiltonian of the non-integrable system in Equation (4.7). Differentiating the Hamiltonian by applying Itô's stochastic calculus (Calin, 2012), the differential equation for energy is derived as follows:

$$\mathrm{d}e = \dot{x}_1\mathrm{d}\dot{x}_1 + \frac{1}{2}\mathrm{d}\dot{x}_1\mathrm{d}\dot{x}_1 + \dot{x}_2\mathrm{d}\dot{x}_2 + \frac{1}{2}\mathrm{d}\dot{x}_2\mathrm{d}\dot{x}_2 + \mathrm{d}£_1(x_1, x_2) + \mathrm{d}£_2(z_2) \tag{4.8}$$

Substituting Equation (4.7) into Equation (4.8), the differential equation for the Hamiltonian is

$$\mathrm{d}e = \dot{x}_1\left(\left(-\frac{\partial £_1(x_1,x_2)}{\partial x_1} - \frac{c_1}{m}\dot{x}_1 + \frac{c_1}{m}\dot{x}_2\right)\mathrm{d}t + \sigma_0\mathrm{d}B\right) + \frac{1}{2}{\sigma_0}^2\mathrm{d}t$$

$$+ \dot{x}_2\left(\left(-\frac{\partial £_1(x_1,x_2)}{\partial x_2} - \frac{\partial £_2(z_2)}{\partial z_2} - \frac{{c_2}''}{m}\dot{x}_2 + \frac{c_1}{m}\dot{x}_1\right)\mathrm{d}t \right. \tag{4.9}$$

$$\left. + \sigma_0\mathrm{d}B\right) + \frac{1}{2}{\sigma_0}^2\mathrm{d}t + \mathrm{d}£_1(x_1,x_2) + \mathrm{d}£_2(z_2)$$

Rearranging this equation to separate drift $\left((\dots)\mathrm{d}t\right)$ and diffusion$\left((\dots)\mathrm{d}B\right)$ components, the stochastic differential equation is represented as:

$$\mathrm{d}e = \left(-\frac{\partial £_1(x_1,x_2)}{\partial x_1}\dot{x}_1 - \frac{c_1}{m}\dot{x}_1^2 + \frac{c_1}{m}\dot{x}_1\dot{x}_2 - \frac{\partial £_1(x_1,x_2)}{\partial x_2}\dot{x}_2\right.$$

$$\left. - \frac{\partial £_2(z_2)}{\partial z_2}\dot{x}_2 - \frac{{c_2}''}{m}\dot{x}_2^2 + \frac{c_1}{m}\dot{x}_1\dot{x}_2 + {\sigma_0}^2\right)\mathrm{d}t \tag{4.10}$$

$$+ \sigma_0(\dot{x}_1 + \dot{x}_2)\mathrm{d}B + \mathrm{d}£_1(x_1,x_2) + \mathrm{d}£_2(z_2)$$

The terms $\mathrm{d}u_2(z_2)$ and $\mathrm{d}u_1(x_1,x_2)$are expanded using the chain rule of total derivatives, as follows:

$$\mathrm{d}£_2(z_2) = \frac{d£_2(z_2)}{dz_2}\,\mathrm{d}z_2 = (1-\alpha_z)k_2z_2\frac{dz_2}{dx_2}\dot{x}_2\mathrm{d}t \tag{4.11a}$$

$$d£_1(x_1,x_2) = \frac{\partial £_1(x_1,x_2)}{\partial x_1}\dot{x}_1\mathrm{d}t + \frac{\partial u_1(x_1,x_2)}{\partial x_2}\dot{x}_2\mathrm{d}t \tag{4.11b}$$

Applying Equations (4.11a-b) to Equation (8), the following equation is derived:

$$\mathrm{d}e = \left(-\frac{\alpha_1}{m}\dot{x}_1^2 + \frac{\alpha_1}{m}\dot{x}_1\dot{x}_2 - (1-\alpha_z)k_2z_2\dot{x}_2 - \frac{c_1}{m}\dot{x}_1^2 - \frac{{c_2}''}{m}\dot{x}_2^2 + 2\frac{c_1}{m}\dot{x}_1\dot{x}_2\right.$$

$$\left. + {\sigma_0}^2 + (1-\alpha_z)k_2z_2\frac{dz_2}{dx_2}\dot{x}_2\right)\mathrm{d}t + \sigma_0(\dot{x}_1 + \dot{x}_2)\mathrm{d}B \tag{4.12}$$

The stochastic differential equation is represented by the drift and diffusion components:

$$\mathrm{d}e = M_{\mathrm{drift}}\mathrm{d}t + \sigma_{\mathrm{diffusion}}\mathrm{d}B \tag{4.13a}$$

$$M_{\mathrm{drift}} = \left(-(1-\alpha_z)k_2 z_2 \dot{x}_2 - \frac{c_1}{m}\dot{x}_1^2 - \frac{{c_2}''}{m}\dot{x}_2^2 + 2\frac{c_1}{m}\dot{x}_1\dot{x}_2 + \sigma_0^2 + (1-\alpha_z)k_2 z_2 \frac{dz_2}{dx_2}\dot{x}_2\right) \tag{4.13b}$$

$$\sigma^2_{\mathrm{diffusion}} = (\sigma_0^2\dot{x}_1^2 + \sigma_0^2\dot{x}_2^2 + 2\sigma_0^2\dot{x}_1\dot{x}_2) \tag{4.13c}$$

The Hamiltonian of the system, e, is a slowly varying process, while the response variables $(x_1, x_2, \dot{x}_1, \dot{x}_2)$ are rapidly varying processes. The stochastic averaging should be performed across the negative and positive velocities. From Equation (4.4a), the negative velocity, $\dot{x}_2^-$, and positive velocity, $\dot{x}_2^+$, are equal to $\mp\sqrt{2(e-u(x_1,x_2,z_2)-\dot{x}_1^2)}$, respectively. In general, the stochastic averaging of a function $f(x_1, x_2, \dot{x}_1, \dot{x}_2)$ depends on the response variables of the system in Equation (4.5), and can be derived using the weighted measure, $\mathrm{d}x_1\mathrm{d}x_2\mathrm{d}\dot{x}_1/\dot{x}_2$, as follows:

$$\bar{f}(e) = \overline{f(x_1, x_2, \dot{x}_1, \dot{x}_2)} = \iiint_{\Upsilon} f(x_1, x_2, \dot{x}_1, \dot{x}_2)\frac{\mathrm{d}x_1\mathrm{d}x_2\mathrm{d}\dot{x}_1}{\dot{x}_2} \Big/ \iiint_{\Upsilon}\frac{\mathrm{d}x_1\mathrm{d}x_2\mathrm{d}\dot{x}_1}{\dot{x}_2} \tag{4.14a}$$

Υ

$$= \left\{(x_1, x_2, \dot{x}_1, \dot{x}_2)\middle| \begin{array}{c} \frac{\dot{x}_1^2}{2} + \frac{k_1}{m}\frac{x_1^2}{2} - \frac{k_1}{m}x_1x_2 + \\ \frac{(k_1+\alpha_z k_2)}{m}\frac{x_2^2}{2} + (1-\alpha_z)\frac{k_2}{m}\frac{z_2^2}{2} \le e \end{array}\right\} \tag{4.14b}$$

where Υ is the domain of integration and e ranges from 0 to $+\infty$. Applying Equations (4.14a-b) to Equation (4.13), the averaged drift and diffusion components are derived as:

$$\bar{M}_{\text{drift}}$$

$$= \frac{\iiint_{\Upsilon} \left(-\frac{c_1}{m}\dot{x}_1^2 - \frac{c_2''}{m}\dot{x}_2^2 + 2\frac{c_1}{m}\dot{x}_1\dot{x}_2\right)\frac{\mathrm{d}x_1\mathrm{d}x_2\mathrm{d}\dot{x}_1}{\dot{x}_2}}{\iiint_{\Upsilon} \frac{\mathrm{d}x_1\mathrm{d}x_2\mathrm{d}\dot{x}_1}{\dot{x}_2}}$$

$$+ \frac{\iiint_{\Upsilon} \left(\sigma_0^2 - (1-\alpha_z)k_2 z_2 \dot{x}_2 + (1-\alpha_z)k_2 z_2 \frac{dz_2}{dx_2}\dot{x}_2\right)\frac{\mathrm{d}x_1\mathrm{d}x_2\mathrm{d}\dot{x}_1}{\dot{x}_2}}{\iiint_{\Upsilon} \frac{\mathrm{d}x_1\mathrm{d}x_2\mathrm{d}\dot{x}_1}{\dot{x}_2}} \tag{4.15a}$$

$$\bar{\sigma}^2_{\text{diffusion}}$$

$$= \iiint_{\Upsilon} (\sigma_0^2\dot{x}_1^2 + \sigma_0^2\dot{x}_2^2 + \sigma_0^2\dot{x}_1\dot{x}_2)\frac{\mathrm{d}x_1\mathrm{d}x_2\mathrm{d}\dot{x}_1}{\dot{x}_2} \Big/ \iiint_{\Upsilon} \frac{\mathrm{d}x_1\mathrm{d}x_2\mathrm{d}\dot{x}_1}{\dot{x}_2} \tag{4.15b}$$

In Equations (4.15a-b), the stochastic averaging is applied to all terms as follows:

$$\emptyset_1 = \iiint_{\Upsilon} \frac{\dot{x}_1\dot{x}_2}{\dot{x}_2}\mathrm{d}x_1\mathrm{d}x_2\mathrm{d}\dot{x}_1 = \tag{4.16a}$$

$$\emptyset_2 = \iiint_{\Upsilon} \frac{(1-\alpha_z)k_2 z_2 \frac{dz_2}{dx_2}\dot{x}_2}{\dot{x}_2}\,\mathrm{d}x_1\mathrm{d}x_2\mathrm{d}\dot{x}_1 = 0 \tag{4.16b}$$

Other terms in Equations (4.15a-b) are:

$$\emptyset_3 = \iiint_{\Upsilon} \frac{\dot{x}_1^2}{\dot{x}_2}\mathrm{d}x_1\mathrm{d}x_2\mathrm{d}\dot{x}_1 = \iint \pi\big(2e - 2u(x_1,x_2) - 2u_2(z_2)\big)\,\mathrm{d}x_1\mathrm{d}x_2 \tag{4.17a}$$

$$\emptyset_4 = \iiint_{\Upsilon} \frac{\dot{x}_2^2}{\dot{x}_2}\mathrm{d}x_1\mathrm{d}x_2\mathrm{d}\dot{x}_1 = \iint \pi\big(2e - 2u(x_1,x_2) - 2u_2(z_2)\big)\,\mathrm{d}x_1\mathrm{d}x_2 \tag{4.17b}$$

Equation (4.16) and Equations (4.17a-b) are fully derived in Appendix A. Substituting these equations into Equation (4.15), the drift and diffusion components are ($\emptyset_3 = \emptyset_4 = \emptyset_0$):

$$\bar{M}_{\text{drift}} = -\left(\frac{c_1}{m}+\frac{c_2''}{m}\right)\emptyset_0 \Big/ \iiint_{\Upsilon} \frac{\mathrm{d}x_1\mathrm{d}x_2\mathrm{d}\dot{x}_1}{\dot{x}_2} + \iiint_{\Upsilon} (\sigma_0^2-(1-\alpha_z)k_2z_2\dot{x}_2)\frac{\mathrm{d}x_1\mathrm{d}x_2\mathrm{d}\dot{x}_1}{\dot{x}_2} \Big/ \iiint_{\Upsilon} \frac{\mathrm{d}x_1\mathrm{d}x_2\mathrm{d}\dot{x}_1}{\dot{x}_2} \tag{4.18a}$$

$$\bar{\sigma}^2_{\text{diffusion}} = \iiint_{\Upsilon} 2\sigma_0^2\emptyset_0\frac{\mathrm{d}x_1\mathrm{d}x_2\mathrm{d}\dot{x}_1}{\dot{x}_2} \Big/ \iiint_{\Upsilon} \frac{\mathrm{d}x_1\mathrm{d}x_2\mathrm{d}\dot{x}_1}{\dot{x}_2} \tag{4.18b}$$

Since $\emptyset_1 = 0$, the off-diagonal damping term, $c_{12} = c_{21} = -c_1$,vanishes from the formulation of the stochastically averaged system. However, in real systems, this component may have a noticeable effect on the covariance matrix of the system response, among other measures. In addition, the diagonal damping terms, c_1 and c_2, have a collective impact in the stochastic averaging. This limitation results in two identical systems but with different c_1 and c_2'' to yield the same stochastic averaging results as long as they have identical $c_1 + c_2''$. Since the component $\emptyset_1$ is equal to zero, stochastically averaging the term $\sigma_0^2\overline{\dot{x}_1\dot{x}_2} = \sigma_0^2\emptyset_1$ yields zero as well. To overcome these shortcomings, Equation (4.13) is transformed to an equivalent nonlinear system as follows:

$$\mathrm{d}e = M'_{\text{drift}}\mathrm{d}t + \sigma'_{\text{diffusion}}\mathrm{d}B \tag{4.19a}$$

$$M'_{\text{drift}} = \left(-(1-\alpha_z)k_2z_2\dot{x}_2 - \frac{c'}{m}\dot{x}_1^2 - \frac{c'}{m}\dot{x}_2^2 + \sigma'^2_0 + (1-\alpha_z)k_2z_2\frac{dz_2}{dx_2}\dot{x}_2\right) \tag{4.19b}$$

$$\sigma'^2_{\text{diffusion}} = (\sigma'^2_0\dot{x}_1^2 + \sigma'^2_0\dot{x}_2^2) \tag{4.19c}$$

where c' and σ'^2_0 are the equivalent damping and excitation variance terms, respectively. To determine these parameters, the method of weighted residuals (Lin and Cai, 2004) is utilized. In that respect, a weighting polynomial function is applied to both original and

equivalent nonlinear systems and the integration of the residue over the entire domain is derived to zero. Here, residues are defined for drift and diffusion components by comparing Equation (4.13) and Equation (4.19).The mean of the weighted residues are equated to zero and the equivalent parameters, c' and σ'^2_0, are computed subsequently:

$$\Delta_{\text{drift}} = \int\int\int\int W(\dot{x}_1, \dot{x}_2) \times \delta_{\text{drift}}(\dot{x}_1, \dot{x}_2) \times p_{\text{f}}(x_1, x_2, \dot{x}_1, \dot{x}_2) dx_1 \, \mathrm{d}x_2 \, \mathrm{d}\dot{x}_1 \, \mathrm{d}\dot{x}_2 \tag{4.20a}$$

$$\Delta_{\text{diffusion}} = \int\int\int\int W(\dot{x}_1, \dot{x}_2) \times \delta_{\text{diffusion}}(\dot{x}_1, \dot{x}_2) \times p_{\text{f}}(x_1, x_2, \dot{x}_1, \dot{x}_2) dx_1 dx_2 \, d\dot{x}_1 d\dot{x}_2 \tag{4.20b}$$

where $p_{\text{f}}(x_1, x_2, \dot{x}_1, \dot{x}_2)$ is the joint stationary probability density function for of the rapidly varying processes i.e. displacements and velocities of the system. The parameters δ_{drift} and $\delta_{\text{diffusion}}$ are the error measures defined as:

$$\delta_{\text{drift}} = M'_{\text{drift}} - M_{\text{drift}} \tag{4.21a}$$

$$\delta_{\text{diffusion}} = \sigma'^2_{\text{diffusion}} - \sigma^2_{\text{diffusion}} \tag{4.21b}$$

In addition, the weighting function, $W(\dot{x}_1, \dot{x}_2)$, has the following polynomial form:

$$W(\dot{x}_1, \dot{x}_2) = \dot{x}_1^2 + \dot{x}_2^2 + K_w \dot{x}_1 \dot{x}_2 \tag{4.22}$$

where K_w equals 1. Substituting Equation (13), Equation (19), Equation (20), Equation (21), and Equation (22) into Equations (20a-b), the integrands are derived as:

$$W(\dot{x}_1, \dot{x}_2) \times \delta_{\text{drift}}$$

$$= \left(\frac{(c_1 - c')}{m} \dot{x}_1^2 + \frac{(c_2{}'' - c')}{m} \dot{x}_2^2 - 2\frac{c_1}{m} \dot{x}_1 \dot{x}_2 \right. \tag{4.23a}$$

$$\left. + \left(\sigma'^2_0 - \sigma_0^2 \right) \right) \times (\dot{x}_1^2 + \dot{x}_2^2 + K_w \dot{x}_1 \dot{x}_2)$$

$$W(\dot{x}_1, \dot{x}_2) \times \delta_{\text{diffusion}}$$

$$= \left(\left(\sigma_0^2 - \sigma'^2_0 \right) \dot{x}_1^2 + \left(\sigma_0^2 - \sigma'^2_0 \right) \dot{x}_2^2 + 2\sigma_0^2 \dot{x}_1 \dot{x}_2 \right) \tag{4.23b}$$

$$\times (\dot{x}_1^2 + \dot{x}_2^2 + K_w \dot{x}_1 \dot{x}_2)$$

Expanding the integrands in Equations (4.23a-b) and applying the integral in Equations (20a-b), the equivalent parameters are computed using higher order moments as:

$$c' = \frac{c_1 \left(\mathrm{E}(\dot{x}_1^4) + \mathrm{E}(\dot{x}_1^2 \dot{x}_2^2) + K_w \mathrm{E}(\dot{x}_1^3 \dot{x}_2) \right)}{\left(\mathrm{E}(\dot{x}_1^4) + \mathrm{E}(\dot{x}_2^4) + 2\mathrm{E}(\dot{x}_1^2 \dot{x}_2^2) + K_w \mathrm{E}(\dot{x}_1 \dot{x}_2^3) + K_w \mathrm{E}(\dot{x}_1^3 \dot{x}_2) \right)}$$

$$+ \frac{c_2'' \left(\mathrm{E}(\dot{x}_2^4) + \mathrm{E}(\dot{x}_1^2 \dot{x}_2^2) + K_w \mathrm{E}(\dot{x}_1 \dot{x}_2^3) \right)}{\left(\mathrm{E}(\dot{x}_1^4) + \mathrm{E}(\dot{x}_2^4) + 2\mathrm{E}(\dot{x}_1^2 \dot{x}_2^2) + K_w \mathrm{E}(\dot{x}_1 \dot{x}_2^3) + K_w \mathrm{E}(\dot{x}_1^3 \dot{x}_2) \right)}$$

$$- \frac{2c_1 \left(\mathrm{E}(\dot{x}_1 \dot{x}_2^3) + \mathrm{E}(\dot{x}_1^3 \dot{x}_2) + K_w \mathrm{E}(\dot{x}_1^2 \dot{x}_2^2) \right)}{\left(\mathrm{E}(\dot{x}_1^4) + \mathrm{E}(\dot{x}_2^4) + 2\mathrm{E}(\dot{x}_1^2 \dot{x}_2^2) + K_w \mathrm{E}(\dot{x}_1 \dot{x}_2^3) + K_w \mathrm{E}(\dot{x}_1^3 \dot{x}_2) \right)}$$

$$+ \frac{m \left(\sigma'^2_0 - \sigma_0^2 \right) \times \left(\mathrm{E}(\dot{x}_1^2) + \mathrm{E}(\dot{x}_2^2) + K_w \mathrm{E}(\dot{x}_1 \dot{x}_2) \right)}{\left(\mathrm{E}(\dot{x}_1^4) + \mathrm{E}(\dot{x}_2^4) + 2\mathrm{E}(\dot{x}_1^2 \dot{x}_2^2) + K_w \mathrm{E}(\dot{x}_1 \dot{x}_2^3) + K_w \mathrm{E}(\dot{x}_1^3 \dot{x}_2) \right)} \tag{4.24a}$$

$$\sigma'^2_0$$

$$= \sigma_0^2 \left(\frac{\mathrm{E}(\dot{x}_1^4) + \mathrm{E}(\dot{x}_2^4) + (2 + 2K_w)\mathrm{E}(\dot{x}_1^2 \dot{x}_2^2)}{\mathrm{E}(\dot{x}_1^4) + \mathrm{E}(\dot{x}_2^4) + 2\mathrm{E}(\dot{x}_1^2 \dot{x}_2^2) + K_w \mathrm{E}(\dot{x}_1 \dot{x}_2^3) + K_w \mathrm{E}(\dot{x}_1^3 \dot{x}_2)} \right. \tag{4.24b}$$

$$\left. + \frac{(2 + K_w)\mathrm{E}(\dot{x}_1 \dot{x}_2^3) + (2 + K_w)\mathrm{E}(\dot{x}_1^3 \dot{x}_2)}{\mathrm{E}(\dot{x}_1^4) + \mathrm{E}(\dot{x}_2^4) + 2\mathrm{E}(\dot{x}_1^2 \dot{x}_2^2) + K_w \mathrm{E}(\dot{x}_1 \dot{x}_2^3) + K_w \mathrm{E}(\dot{x}_1^3 \dot{x}_2)} \right)$$

In these equations, the second order moments are determined according to Lyapunov equation for stochastically linearized systems (El-Khoury et al., 2016). In addition, the even order moments can be expressed in terms of second order moments since the system is subjected to a Gaussian white noise and the response variables are considered Gaussian (Muravyov et al., 1999):

$$\mathrm{E}\left(\dot{x}_q\dot{x}_r\dot{x}_s\dot{x}_t\right) = \mathrm{E}\left(\dot{x}_q\dot{x}_r\right) \times \mathrm{E}(\dot{x}_s\dot{x}_t) + \mathrm{E}\left(\dot{x}_q\dot{x}_s\right) \times \mathrm{E}(\dot{x}_r\dot{x}_t) + \mathrm{E}\left(\dot{x}_q\dot{x}_t\right) \times \mathrm{E}(\dot{x}_r\dot{x}_s) \tag{4.25}$$

Applying stochastic averaging to the derived equivalent nonlinear system results in:

$$\overline{M'}_{\mathrm{drift}} = \frac{-2\frac{c'}{m}\emptyset_0}{\iiint_Y \frac{\mathrm{d}x_1\mathrm{d}x_2\mathrm{d}\dot{x}_1}{\dot{x}_2}} + \frac{\iiint_Y (\sigma'^2_0 - (1-\alpha_z)k_2z_2\dot{x}_2)\frac{\mathrm{d}\dot{x}_1\mathrm{d}x_1\mathrm{d}x_2}{\dot{x}_2}}{\iiint_Y \frac{\mathrm{d}x_1\mathrm{d}x_2\mathrm{d}\dot{x}_1}{\dot{x}_2}} \tag{4.26a}$$

$$\bar{\sigma}'^2_{\mathrm{diffusion}} = \frac{2\sigma'^2_0\emptyset_0}{\iiint_Y \frac{\mathrm{d}x_1\mathrm{d}x_2\mathrm{d}\dot{x}_1}{\dot{x}_2}} \tag{4.26b}$$

Consequently, the stationary Fokker-Planck-Kolmogorov equation of the stochastically averaged differential equation in Equation (4.26) is defined as:

$$\frac{\mathrm{d}p_{\mathrm{s}}(e)}{\mathrm{d}t} = -\frac{\mathrm{d}}{\mathrm{d}e}\left[\overline{M'}_{\mathrm{drift}}(e) \times p_{\mathrm{s}}(e)\right] + \frac{1}{2}\frac{\mathrm{d}^2}{\mathrm{d}e^2}\left[\bar{\sigma}'^2_{\mathrm{diffusion}}(e) \times p_{\mathrm{s}}(e)\right] \tag{4.27}$$

where $p_{\mathrm{s}}(e)$ represents the stationary PDF of energy that is derived by considering $(\mathrm{d}p_{\mathrm{s}}(e)/dt = 0)$ and solving the FPK equation:

$$p_{\mathrm{s}}(e) = \frac{\lambda_{\mathrm{e}}}{\bar{\sigma}'^2_{\mathrm{diffusion}}}\exp\left\{\int_0^e \frac{2\overline{M'}_{\mathrm{drift}}(y)}{\bar{\sigma}'^2_{\mathrm{diffusion}}(y)}\mathrm{d}y\right\} \tag{4.28}$$

where λ_e is a constant to ensure that the integration of the PDF function over the entire domain yields one:

$$\lambda_e = \frac{1}{\int_0^{+\infty} \frac{1}{\bar{\sigma}'^2_{\text{diffusion}}(e)} \exp\left\{\int_0^e \frac{2\bar{M}'_{\text{drift}}(y)}{\bar{\sigma}'^2_{\text{diffusion}}(y)} \mathrm{d}y\right\} \mathrm{d}e} \tag{4.29}$$

Having found $p_s(e)$, the mean of the Hamiltonian, $\mathrm{E}(e)$, and second order moment, $\mathrm{E}(e^2)$, can be determined as

$$\mathrm{E}(e) = \int_0^{+\infty} y p_s(y)\, \mathrm{d}y \tag{4.30a}$$

$$\mathrm{E}(e^2) = \int_0^{+\infty} y^2 p_s(y)\, \mathrm{d}y \tag{4.30b}$$

4.3 Numerical Example

During seismic excitations, structural systems interact with surrounding soil at the foundation level; these interactions alter the seismic behavior of structures. Such effects can be in the form of elongation of the natural vibration period of structures, an increase in the damping and energy dissipation of the system, and a reduction in the overall stiffness. In design and analysis of structures especially controlled systems, buildings are commonly assumed to have rigid foundation. This assumption is realistic only when the structure is built on solid rock; for other cases, it may lead to inaccurate predictions of system responses such as displacements, induced forces and moments, and generally the state of the structure (Isbiliroglu et al., 2015). During medium to large intensity seismic excitations, the induced nonlinear hysteretic behavior of soil-foundation can have even more prominent impact on the performance of structures (Mason et al., 2013). Consequently, incorporating nonlinear

hysteresis behavior of soil-foundation in the control design is necessary since the soil is likely to behave nonlinearly even when the structure is equipped with control systems.

A single story structure supported on a nonlinear raft foundation in loose sand is considered here to demonstrate the application of the proposed reliability-based controllers. The structure is assumed to be linear with a natural period of 0.25 sec and a damping ratio of 1.0%, while the foundation is considered to have a nonlinear hysteretic behavior. The dimensions, the mass of the structure, and the embedment depth of the shallow foundation are given in Figure 4-1a. The nonlinear hysteretic behavior of the foundation is simulated using the Bouc-Wen model (El-Khoury et al., 2015; El-Khoury et al., 2016). This model that is presented in Equations (3a-b) consists of linear stiffness, damping, and hysteresis as shown in Figure 4.2. In order to obtain the model parameters, a foundation model consisting of an array of independent nonlinear springs, dashpots, and gap elements (Gajan et al., 2010) is developed in the finite eslement platform of OpenSEES (McKenna, 2011). The implemented nonlinear horizontal springs are able to capture sliding and passive pressure effects on the sides and the base of the foundation. This model takes as input a set of soil properties including shear modulus (G = 5 MPa), poisons ratio ($v_p = 0.25$), angle of friction ($\emptyset_a = 25^o$), soil density ($\rho_s = 2000$ kg/m^3), and soil type. The natural period of the structure is 0.25 sec and the damping ratio is 1%. The entire system is subjected to a lateral Gaussian white noise with three levels of standard deviation to represent low, moderate, and high levels of excitation intensity. The reference point for the standard deviation of the excitation is 0.2 g (Spencer et al., 1998; Rofooei et al., 2001) and the two additional intensity levels correspond to $\pm$60% [0.12g, 0.32g] of the reference intensity.

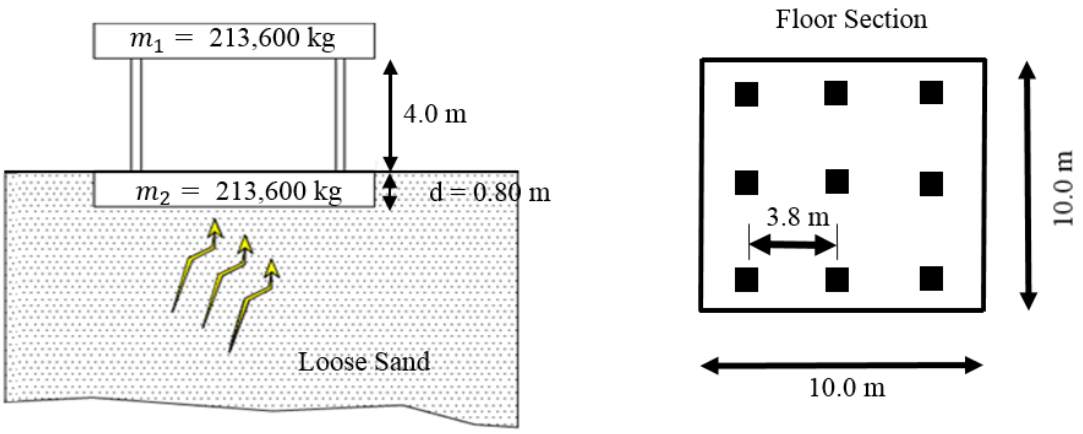

Properties of Structure, Soil and Foundation
$T_{structure}$ = 0.25 sec; $\xi_{structure}$ = 0.01
Soil Properties: Loose Sand; $\upsilon = 0.25$; $\emptyset = 25^{o}$; $G = E_s/2(1+\upsilon) =$ 5 MPa; $\rho = 2000$ kg/m^3

Figure 4-2 A single story building on a raft foundation with loose sand properties – structural period ($T_{structure}$), damping ratio ($\xi_{structure}$), Young's modulus (E_s), shear modulus (G), poisons ratio (υ), angle of friction ($\emptyset$), and soil density (ρ) are provided.

4.3.1 Discussion

The nonlinear foundation-structure system is modeled in OpenSEES McKenna (2011) which is an object oriented Finite Element platform for earthquake engineering simulations. The horizontal force versus lateral displacement and velocity responses of the foundation model when the system is subjected to excitation realizations for three levels of intensity are presented in Figure 4-3. The area enclosed by the force-deformation loops represents hysteresis or alternatively energy dissipation. It is seen that the foundation behavior is nonlinear and therefore a nonlinear analysis is required (Pecker et al., 2014). As expected, higher intensities of input excitation yield larger hysteresis area. In order to apply stochastic averaging, the model representing the behavior of the foundation should comply with the general form of system model given in Equation (4.5). Bouc-Wen models (Ismail et al., 2009) can properly capture nonlinear hysteretic responses (El-Khoury et al.,

2015), and are used in this study to represent foundation behavior. The overall foundation force is decomposed into stiffness, damping, and hysteretic components, which are connected in parallel as shown in Figure 4-3b. The differential equation for the hysteretic component of the Bouc-Wen model is presented in Appendix A. Parameters of the Bouc-Wen model are determined by deriving the error of model outputs with respect to OpenSEES results to zero using a constrained numerical optimization approach based on gradient descent (Rao and Rao, 2009). The objective function, J, is defined based on the peaks of the lateral forces (PLF) as follows:

$$J_{@\ 0.20\mathrm{g}} = \sum_{\text{all peaks}} \left| \mathrm{PLF}_{\text{Bouc–Wen Model}} - \mathrm{PLF}_{\text{OpenSees}} \right|_{\alpha_z,\, \mathrm{A_{BW}},\, \gamma_{\mathrm{BW}},\, c_2,\, k_2} \tag{4.31}$$

where $\mathrm{A_{BW}}$ and γ_{BW} are parameters that control the shape of the loop. Parameters of the Bouc-Wen model are derived for the medium intensity level of 0.20 g; these parameters are used for the other two intensity levels. Comparison of the horizontal force-deformation behavior from Bouc-Wen model and OpenSEES simulations in Figure 4-3 indicates that a good agreement is achieved for all excitation intensity levels using the parameters derived for 0.20 g intensity level.

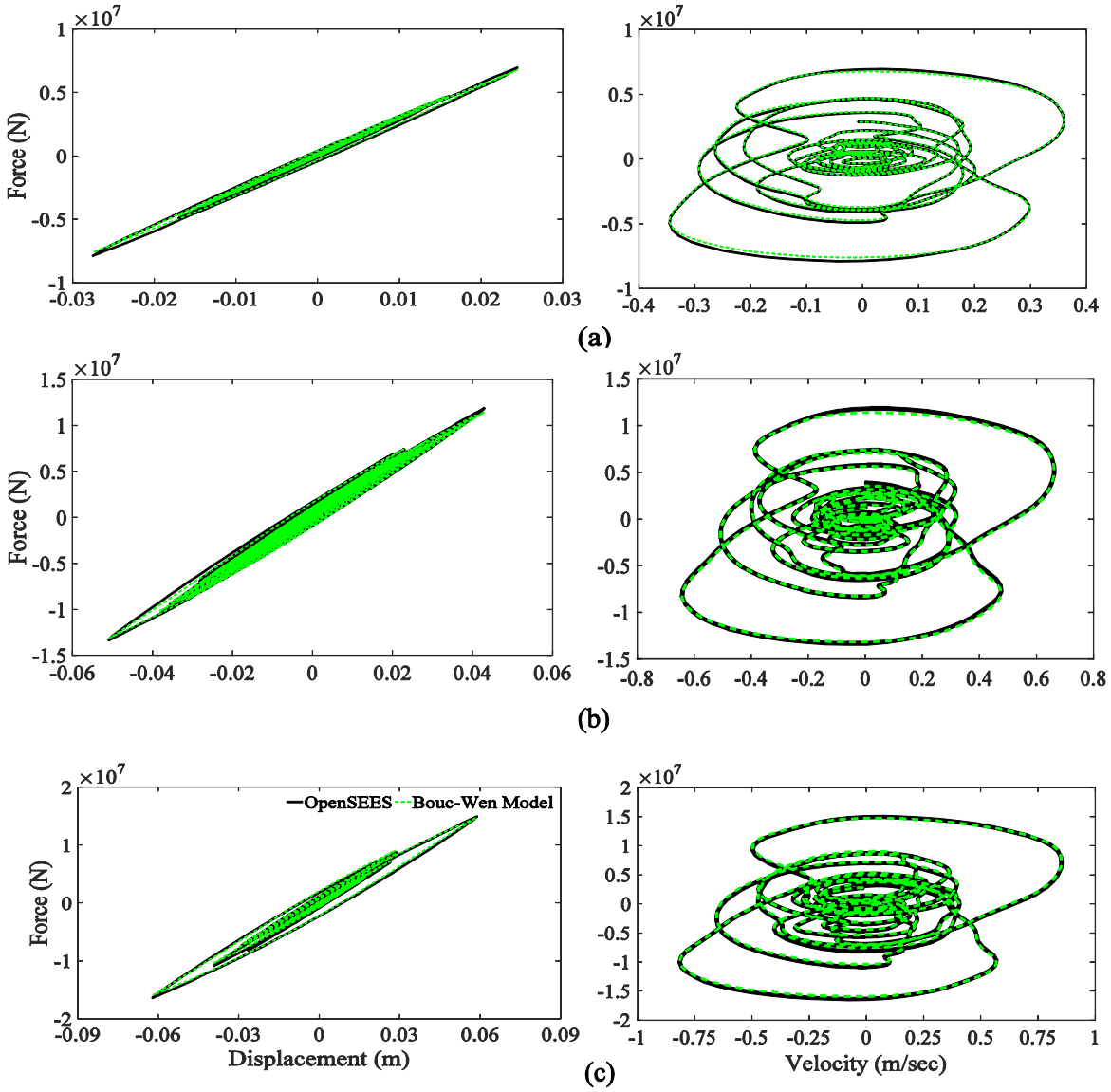

Figure 4-3 Characterization of the nonlinear foundation based on Bouc-Wen model for white noise excitations at different standard deviations: (a) 0.12 g, (b) 0.24 g, and (c) 0.32 g (α_z= 0.30; A_{BW}= 0.77; γ_{BW}= 5.82 m^{-1}; k_1= 1.35 × 10^8 N/m; k_2= 3.50 × 10^8 N/m; c_1 = 1.07 × 10^5 N.sec/m; c_2" = 2.18 × 10^5 N.sec/m).

As the benchmark to assess the accuracy of the conventional and proposed enhanced stochastic averaging methods, Monte Carlo simulations are conducted on the nonlinear system subjected to a set of white Gaussian noise. The structure-foundation system with a

Bouc-Wen model representing the nonlinear foundation behavior complies with the form of the equations of motion in Equation (4.5). In order to apply the proposed enhanced stochastic averaging method, the stochastic differential equation of the Hamiltonian is first derived as presented in Equations (4.13a-b). Subsequently the system is converted to an equivalent model in Equations (20a-b) and the equivalent damping, c', and equivalent intensity, σ_0', are derived using Equations (4.24a-b). Following this process for each of the three considered intensity levels yields c'/c_1 of 1.40, 1.44, and 1.48 for low, medium, and high intensity levels, while the ratio σ_0'/σ_0 remained nearly the same and equal to 1.67 for all three intensity levels. The very small variation of the derived equivalent parameters against the intensity shows the robustness of the proposed strategy to changes in excitation intensity. In this study, equivalent parameters derived for the moderate intensity level of 0.20 g (i.e. $c' = 1.44\ c_1$ and $\sigma_0' = 1.67\ \sigma_0$) is used to evaluate the proposed enhanced stochastic averaging for all intensity levels. Subsequently, the stationary PDF and the first and second order moments of energy, $\mathrm{E}(e)$ and $\mathrm{E}(e^2)$, are determined according to Equation (4.28) and Equation (4.30). Figure 4-4 shows stationary PDF of total energy per unit mass derived using MCS, enhanced stochastic averaging (ESA), and conventional stochastic averaging (CSA) methods for three levels of excitation intensity. It appears that the PDF of the Hamiltonian of the system derived using ESA method has a very good agreement with the PDF derived using Monte Carlo simulations. On the other hand, results produced using CSA are inaccurate. This is due to the fact that the conventional stochastic averaging neglects the effects of off-diagonal damping terms, accounts for a collective rather than individual effects of diagonal damping terms, and assumes independent stochastic excitations for the foundation and the roof of the structure. The estimated

expected values of the energy for 0.12 g intensity level are 0.046 J/kg, 0.051 J/kg, and 0.031 J/kg, for 0.20 g intensity level are 0.121 J/kg, 0.125 J/kg, and 0.077 J/kg, and for 0.32 g intensity level are 0.262 J/kg, 0.281 J/kg, and 0.175 J/kg, using MCS, ESA, and CSA methods, respectively. The errors for the mean estimate of energy for ESA range from 3% to 10%, while these errors for the case of CSA are 33% to 36%. In terms of the second order moment of energy, the estimates of $E(e^2)$ at 0.20 g intensity level are 0.025 J^2/kg^2, 0.022 J^2/kg^2, and 0.009 J^2/kg^2 based on MCS, ESA, and CSA methods, respectively. The estimated quantities for 0.12 g intensity level are 0.0040 J^2/kg^2, 0.0037 J^2/kg^2, and 0.0014 J^2/kg^2, and for 0.32 g intensity level are 0.122 J^2/kg^2, 0.110 J^2/kg^2, and 0.044 J^2/kg^2, for MCS, ESA, and CSA methods, respectively. It appears that the proposed ESA method outperforms the conventional approach for the estimation of $E(e^2)$ where the error for ESA varies from 8% to 10%, while the corresponding errors for CSA is between 64% and 66%.

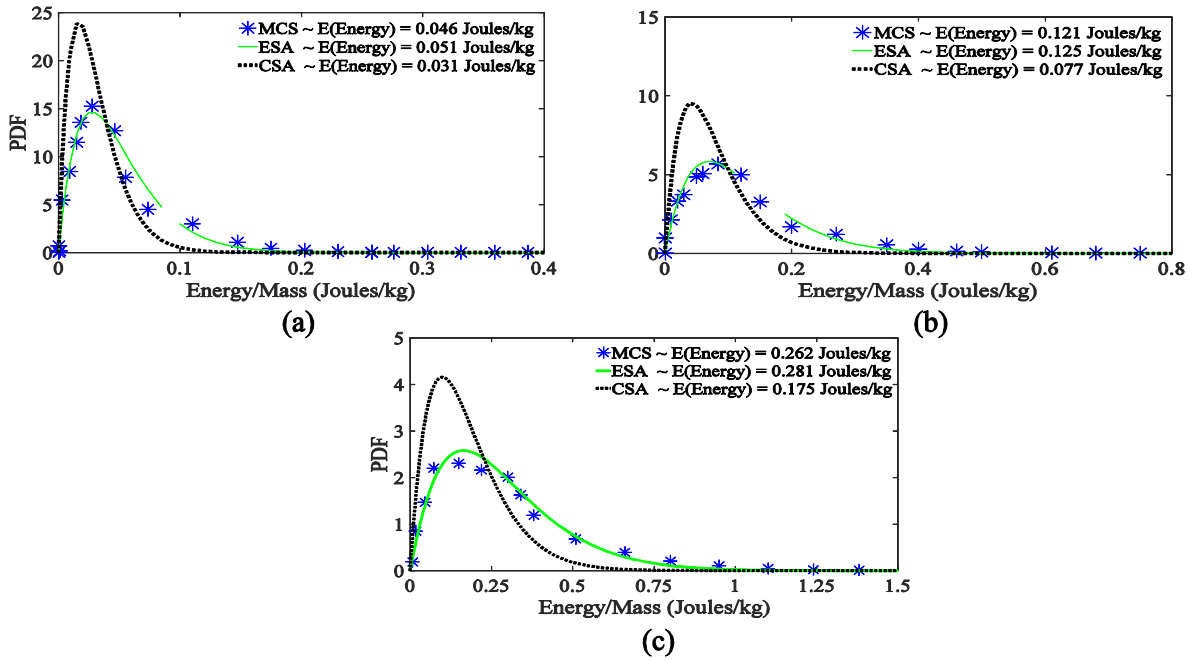

Figure 4-4 Probability density function of the energy of the system subjected to single white Gaussian noise at different standard deviations; (a) 0.12 g, (b) 0.20 g , and (c) 0.32 g.

4.4 Closure

Non-integrable systems such as buildings and bridges have a general form of damping matrix which is coupled, sparse, symmetric, and positive definite. Such systems are often subjected to a single or a set of correlated excitations. The conventional stochastic averaging approach does not account for the off-diagonal damping terms as well as for individual effects of the diagonal components. In addition, this method assumes independent stochastic excitations for involved degrees of freedom of the system. Herein, a methodology is presented to extend the conventional stochastic averaging method to non-integrable systems with general form of damping matrices subjected to perfectly correlated excitations. The proposed method called enhanced stochastic averaging applies method of weighted residuals to the drift and diffusion components of the original and equivalent

stochastic nonlinear systems to derive modified lumped damping and excitation intensity parameters. Subsequently, stochastic averaging of energy envelope is applied in this approach to obtain the probability density function (PDF) of the Hamiltonian.

The application of the proposed method is demonstrated for a one-story building on a nonlinear raft foundation. The foundation is modelled using finite elements and its force-deformation responses under stochastic excitations are used to derive and calibrate a Bouc-Wen hysteresis model. The stationary PDF of the Hamiltonian of the building and foundation system is derived analytically using enhanced as well as conventional stochastic averaging methods; the results are compared to that of Monte Carlo simulations. The accuracy of both analytical methods is evaluated in terms of PDF and the mean and second order moment of the Hamiltonian of the system at different excitation levels. While errors in the estimated mean of energy using the conventional method ranges from 33% to 36%, this error is found to be less than 10% for the proposed method. In addition, enhanced stochastic averaging approach provides more accurate estimates of the tails of the stationary PDF compared to the conventional method. The proposed enhanced stochastic averaging method can be applied to multi-DOF systems and can be used in different fields such as reliability analysis and robust control of dynamic systems subjected to stochastic excitations.

Chapter 5: A Stochastic Averaging-Based Optimal Control for Nonlinear Systems: Application to a Structure with Soil-Structure Interaction

5.1 Introduction

The design of control algorithms in optimal control strategies is commonly an optimization problem with the objective of minimizing a cost function. This function is usually composed of components representing the response of the system and the applied control forces. In feedback control designs, the set of control forces to be applied to the system is derived as functions of some measured responses. The parameters of such functions are determined via optimization techniques considering system dynamics. Since actual systems behave in a nonlinear manner especially in response to moderate to large disturbances and the fact that the nature of such excitations is often stochastic, incorporation of system dynamics in optimization problems becomes very challenging. As discussed in Chapter 2, conventional optimal control designs provide a solution as they require simplified models of nonlinear dynamic systems often based on their initial linear elastic behavior. For instance, Linear Quadratic Regulators (LQR) can be viewed as a solution of a simplified Hamilton-Jacobi-Bellman (HJB) equation that are limited to linear systems and second order convex objective functions of response variables and control forces (Todorov, 2006; Shafieezadeh et al., 2008; El-Khoury et al., 2015; El-Khoury et al.,

2016). Although these approaches are simple to implement, they neglect the nonlinear behavior of the system in response to stochastic excitations; therefore, the derived control forces will not be optimal for the actual nonlinear system. This issue has been partially addressed through stochastic linearization where the nonlinear system is replaced with an equivalent linearized system such that the root mean square (RMS) of the error of the nonlinear term is minimized. However, the accuracy of this approach for predicting high order moments and peaks of system responses, among other measures, decreases as the number of DOFs of the system and the extent of nonlinearity in system behavior increase (Crandall, 2001; Socha, 2005). A class of nonlinear controllers known as nonlinear stochastic control algorithms based on stochastic averaging of energy envelope can overcome these limitations (Gu and Zhu, 2014). These methods can offer the following features: conservation of the nonlinearity of the system and the nature of the excitation, incorporation of high order convex objective functions, and reduction in the dimension of the problem.

The above class of nonlinear stochastic control methods are based on stochastic averaging of energy envelope which suffers from the limitations explained in Chapter 4. This chapter introduces a stochastic controller based on the proposed enhanced stochastic averaging method presented in Chapter 4 in order to control the lateral deformations and story drift of the structure with nonlinear soil-structure-interactions (elaborate in the previous chapter) subjected to white Gaussian noise and seismic ground motions. Section 5.2 presents the proposed algorithm for the controlled system. Section 5.3 discusses the results for the uncontrolled case, controlled state using LQR algorithm, and controlled state

based on the proposed method using enhanced stochastic averaging. Conclusions of the study are provided in Section 5.4.

5.2 Methodology

This section presents the proposed control method which employs a new stochastic averaging method based on energy envelope for representation of system dynamics in energy domain. The control strategy is derived for a two degree of freedom (DOF) nonlinear system; however, the method is general and can be applied to systems with higher DOFs. This section focuses on the control design, and the formulations are expanded for a fully observed system. However, the presented methods are general, and observer systems including sensor layout and observer algorithm can be designed and implemented separately. The design of the observer system is out of scope of this research.

5.2.1 Optimal Control Design

Adding the control force to the system in Equation (4.5), the equations of motion of the controlled system (Figure 5-1) can be presented as:

$$\begin{aligned} \ddot{x}_1 &= \left(-\frac{\partial \pounds_1(x_1,x_2)}{\partial x_1} - \frac{c_1}{m}\dot{x}_1 + \frac{c_1}{m}\dot{x}_2 - u\right) + \sigma_0 \frac{\mathrm{d}B}{\mathrm{d}t} \\ \ddot{x}_2 &= \left(-\frac{\partial \pounds_1(x_1,x_2)}{\partial x_2} - \frac{\partial \pounds_2(z_2)}{\partial z_2} - \frac{{c_2}''}{m}\dot{x}_2 + \frac{c_1}{m}\dot{x}_1 + u\right) + \sigma_0 \frac{\mathrm{d}B}{\mathrm{d}t} \end{aligned} \tag{5.1}$$

The variable, u, represents the control force of the actuator shown in Figure 5-1. Adding the effect of the control force, Itô's formulation in Equations (4.19a-c) is modified to:

$$\mathrm{d}e = M'_{\text{drift}}\mathrm{d}t + \sigma'_{\text{diffusion}}\mathrm{d}B \tag{5.2a}$$

$$M'_{\text{drift}} = \left(-(1-\alpha_z)k_2 z_2 \dot{x}_2 - \frac{c'}{m}\dot{x}_1^2 - \frac{c'}{m}\dot{x}_2^2 + \sigma'^2_0 \right.$$

$$\left. + (1-\alpha_z)k_2 z_2 \frac{dz_2}{dx_2}\dot{x}_2 \right) + u(\dot{x}_2 - \dot{x}_1) \tag{5.2b}$$

$$\sigma'^2_{\text{diffusion}} = (\sigma'^2_0 \dot{x}_1^2 + \sigma'^2_0 \dot{x}_2^2) \tag{5.2c}$$

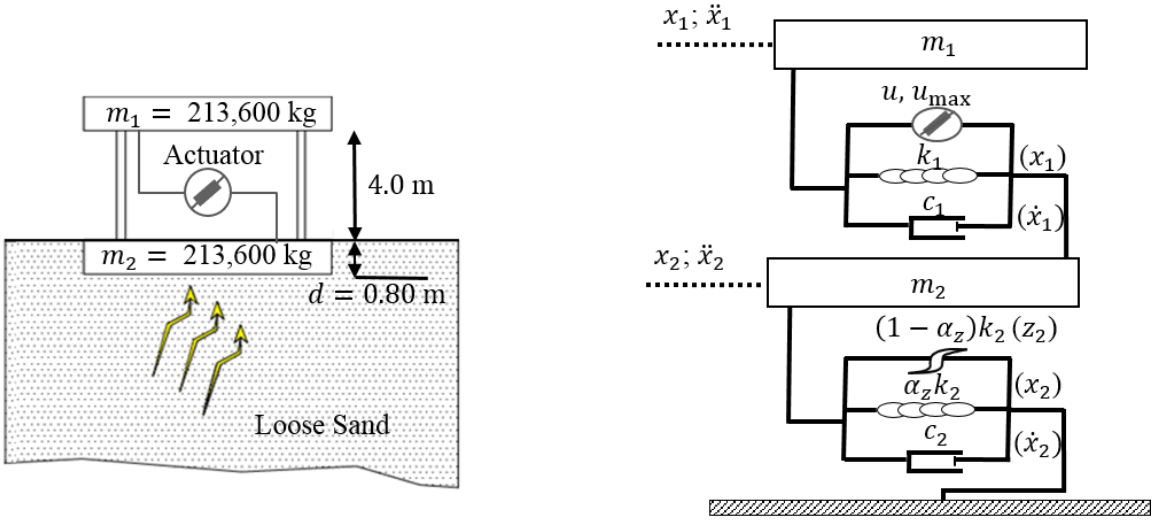

Figure 5-1 Building model (a) schematic of the soil-foundation-structure system and (b) the representative lumped.

Applying stochastic averaging to Equations (5.2a-c) using Equations (4.16a-b), (4.17a-b), and (4.18a-b), the drift and diffusion components are

$$\mathrm{d}e = \overline{M'}_{\text{drift}}\mathrm{d}t + \overline{\sigma'}_{\text{diffusion}}\mathrm{d}B \tag{5.3a}$$

$$\overline{M'}_{\text{drift}} = -2\frac{c'}{m}\emptyset_0 - ((1-\alpha_z)k_2\overline{z_2\dot{x}_2}) + \sigma'^2_0 + \bar{u}(\dot{x}_2 - \dot{x}_1) \tag{5.3b}$$

$$\overline{\sigma'^2}_{\text{diffusion}} = 2\sigma'^2_0\emptyset_0 \tag{5.3c}$$

The design of the control strategy is treated as an optimization problem where a functional representing the cost objective function is minimized while satisfying a constraint that is the nonlinear dynamic behavior of the system. This optimization problem can be presented as the dynamic programming equation, also known as HJB equation. The functional or alternatively the value function, $V(t,e)$, is initially introduced and defined in terms of the performance index, $L(t,e,\bar{u})$, as (Fleming and Soner, 2006; Sun, 2006):

$$\begin{aligned} V(t,e) &= \min\left(\int_t^T L(\tau,e,\bar{u})\,\mathrm{d}\tau\right) = \min\left(\int_t^{t+dt} L(\tau,e,\bar{u})\,\mathrm{d}\tau + \int_{t+dt}^T L(\tau,e,\bar{u})\,d\tau\right) \\ &= \min\left(\int_t^{t+dt} L(\tau,e,\bar{u})\,d\tau + V(t+\mathrm{d}t, e+\mathrm{d}e)\right) \\ &= \min\big(L(t,e,\bar{u})\mathrm{d}t + V(t+\mathrm{d}t, e+\mathrm{d}e)\big) \end{aligned} \tag{5.4}$$

where T is the final time. Applying the second order Taylor approximation, Equation (5.4) can be written as:

$$V(t,e) = L(t,e,\bar{u})\mathrm{d}t + V(t,e) + \frac{\partial V}{\partial t}\mathrm{d}t + \frac{\partial V}{\partial e}\mathrm{d}e + \frac{1}{2}\frac{\partial^2 V}{\partial e^2}(\mathrm{d}e)^2 \tag{5.5}$$

Substituting Equations (5.3a-c) in Equation (5.5), the HJB equation is derived as:

$$\begin{aligned} 0 = {} & \frac{\partial V(t,e)}{\partial t}\mathrm{d}t + L(t,e,\bar{u})dt + \bar{M}'_{\text{drift}}\frac{\partial V(t,e)}{\partial e}\mathrm{d}t + \bar{\sigma}'_{\text{diffusion}}\frac{\partial V(t,e)}{\partial e}\frac{\mathrm{d}B\times\mathrm{d}t}{\mathrm{d}t} \\ & + \frac{\overline{M'^2}_{\text{drift}}}{2}\frac{\partial^2 V(t,e)}{\partial e^2}\mathrm{d}t\times\mathrm{d}t + \frac{\overline{\sigma'^2}_{\text{diffusion}}}{2}\frac{\partial^2 V(t,e)}{\partial e^2}\mathrm{d}B\times\mathrm{d}B \end{aligned} \tag{5.6}$$

Applying Itô's calculus ($\mathrm{d}t \neq 0$; $\mathrm{d}t\times\mathrm{d}t = 0$; $\mathrm{d}t\times\mathrm{d}B = 0$; $\mathrm{d}B\times\mathrm{d}B = \mathrm{d}t$), the above equation can be simplified to:

$$\frac{\partial V(t,e)}{\partial t} = -L(t,e,\bar{u}) - \bar{M}'_{\text{drift}}\frac{\partial V(t,e)}{\partial e} - \frac{\overline{\sigma'^2}_{\text{diffusion}}}{2}\frac{\partial^2 V(t,e)}{\partial e^2} \tag{5.7}$$

For optimal control design, the system in Equation (5.1) is subjected to stationary Gaussian white noise and infinite time horizon for control is considered i.e. $T = \infty$. To ensure boundedness of the solution, the value function, $V(t, e)$, and the objective function, $L(t, e, \bar{u})$, can be decomposed into products of two independent functions: one solely dependent on time and the other on energy (Fleming and Soner, 2006):

$$V(t, e) = \exp(-\rho t) \times V'(e) \tag{5.8a}$$

$$L(t, e, \bar{u}) = \exp(-\rho t) \times L'(e, \bar{u}) \tag{5.8b}$$

where ρ (> 0) known as the discount factor represents the rate of convergence of the value function, $V'(e)$. The cost function, $L'(e, u)$, is defined as

$$L'(e, \bar{u}) = \theta(e) + R\bar{u}^2 \tag{5.9}$$

where $\theta(e)$ is a convex polynomial function that depends on the energy of the system and R is a positive gain factor that represents the gain for the control force in the objective function. Substituting Equations (5.7a-b) into Equation (5.6), the modified HJB equation is derived as:

$$\rho V'(e) = L'(e, \bar{u}) + \bar{M}'_{\text{drift}} \frac{\mathrm{d}V'(e)}{de} + \frac{\sigma^{2\prime}_{\text{diffusion}}}{2} \frac{\mathrm{d}^2 V'(e)}{de^2} \tag{5.10}$$

By partially differentiating Equation (5.10) with respect to $\bar{u}$, the expression for averaged control force is obtained as:

$$\bar{u} = -\frac{1}{2R} \frac{\mathrm{d}V'(e)}{de} \overline{(\dot{x}_2 - \dot{x}_1)} \tag{5.11}$$

Substituting Equation (5.11) into Equations (5.3a-c), the Itô equation for the energy of the system can be derived as:

$$\mathrm{d}e = \overline{M'}_{\text{drift}} \mathrm{d}t + \overline{\sigma'}_{\text{diffusion}} \mathrm{d}B \tag{5.12a}$$

$$\overline{M'}_{\text{drift}} = -2\frac{c'}{m}\emptyset_0 - ((1-\alpha_z)k_2\overline{z_2\dot{x}_2}) + {\sigma'}_0^2 - \frac{1}{2R}\frac{\mathrm{d}V'}{de}\overline{(\dot{x}_2 - \dot{x}_1)^2} \tag{5.12b}$$

$$\overline{\sigma'^2}_{\text{diffusion}} = 2{\sigma'}_0^2\emptyset_0 \tag{5.12c}$$

The stochastic averaging of the term $(\dot{x}_2 - \dot{x}_1)^2$, yields:

$$\overline{(\dot{x}_2 - \dot{x}_1)^2} = \overline{\dot{x}_1^2} + \overline{\dot{x}_2^2} - 2\overline{\dot{x}_1\dot{x}_2} = 2\emptyset_0 \tag{5.12d}$$

Replacing Equation (5.12d) into Equation (5.12b), the Itô equation is:

$$\mathrm{d}e = \overline{M'}_{\text{drift}}\mathrm{d}t + \overline{\sigma'}_{\text{diffusion}}\mathrm{d}B \tag{5.13a}$$

$$\overline{M'}_{\text{drift}} = -2\frac{c'}{m}\emptyset_0 - ((1-\alpha_z)k_2\overline{z_2\dot{x}_2}) + {\sigma'}_0^2 - \frac{1}{R}\frac{\mathrm{d}V'}{de}\emptyset_0 \tag{5.13b}$$

$$\overline{\sigma'^2}_{\text{diffusion}} = 2{\sigma'}_0^2\emptyset_0 \tag{5.13c}$$

Substituting Equations (5.13a-b) into Equation (5.10), the resulting dynamic equation becomes solely a function of energy. This nonlinear differential equation can be solved iteratively using collocation method (Miranda and Fackler, 2002). In this approach, V', is discretized to

$$V' = \sum_{j=1}^{n} h_j\varphi_j(e) \tag{5.14}$$

where $\varphi_1,\ldots,\varphi_n$ are known independent basis functions and $h_1,\ldots,h_n$ are unknown coefficients. Substituting Equation (5.14) into Equation (5.10) yields:

$$\rho\sum_{j=1}^{n} h_j\varphi_j(e) = L'(e,\bar{u}) + \bar{M}'_{\text{drift}}\sum_{j=1}^{n} h_j\frac{\mathrm{d}\varphi_j(e)}{\mathrm{d}e}$$

$$+\frac{{\sigma'^2}_{\text{diffusion}}}{2}\sum_{j=1}^{n} h_j\frac{\mathrm{d}^2\varphi_j(e)}{\mathrm{d}e^2} \tag{5.15}$$

To solve this nonlinear equation at *n* collocation nodes, an iterative rule is used to update the coefficients until convergence is achieved. The convergence within the domain is measured by low residue values at the collocation nodes. The implemented basis functions are Chebyshev basis polynomials which provide computationally efficient and accurate solution. This procedure ensures minimizing the residue and determining a well-defined solution for the value function (Miranda and Fackler, 2002). Increasing the number of the nodes, basis functions, and the domain of interest can improve the quality of the solutions. Using the collocation method, $V'(e)$ in Equation (5.15) can be obtained and replaced in the control force equation to derive:

$$u = -\frac{1}{2R}\frac{\mathrm{d}V'(e)}{de}(\dot{x}_2 - \dot{x}_1) \tag{5.16}$$

For multi-DOF non-integrable systems, the nonlinear HJB formulation can be derived in a form similar to Equation (5.10). In this case, one Hamiltonian representing the total energy of the system is defined, a single nonlinear HJB equation is derived, and a value function is determined, accordingly. It should be noted that the computational demand to apply enhanced stochastic averaging method based on energy envelope increases with the size (or DOFs) of the system. This issue will be addressed in future research via methods such as advanced multi-dimensional integration techniques.

5.3 Discussion

The system in Figure 5-1a is subjected to a series of white noise excitations with various intensity levels (σ_0 = 0.12 g, 0.20 g, 0.32 g) as well as ground motions from historic earthquakes including 1994 Northridge (peak ground motion (PGA) = 1.33 g recorded at the Sepulveda Veterans Hospital station), 1940 El-Centro (PGA = 0.35 g recorded at the

Imperial Valley Irrigation District station), and 1995 Kobe (PGA = 1.28 g recorded at the Kobe University station); Northridge and Kobe ground motions are considered near-field earthquakes, while El-Centro ground motion is considered a far-field earthquake. The ground motions were extracted from the PEER Strong Motion Database (http://peer.berkeley.edu/smcat). Figure 5-2 presents the power spectral density of the selected ground motions and highlights the differences in the amplitude and frequency domain characteristics of these records. The lateral force-displacement response of the foundation under Northridge earthquake is shown in Figure 5-3a. It is seen that the response is nonlinear but the extent of nonlinearity is limited. In order to assess the performance of considered controllers for highly nonlinear systems, the Bouc-Wen model parameter, γ_{BW}, that controls the shape of the hysteresis loops is increased by five times. The new structure model is called the modified system, and the lateral force-displacement response of its foundation under Northridge earthquake is shown in Figure 5-3b where higher extent of nonlinearity is observed.

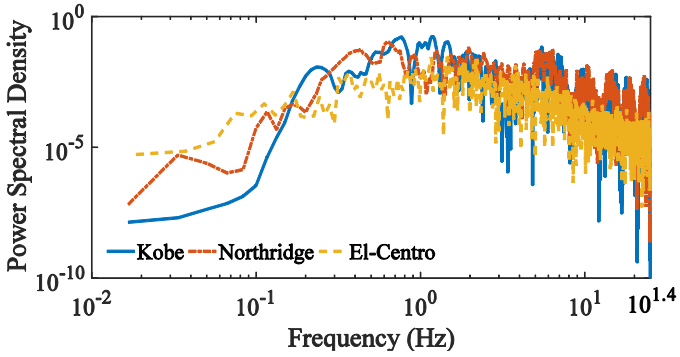

Figure 5-2 Power spectral density versus frequency.

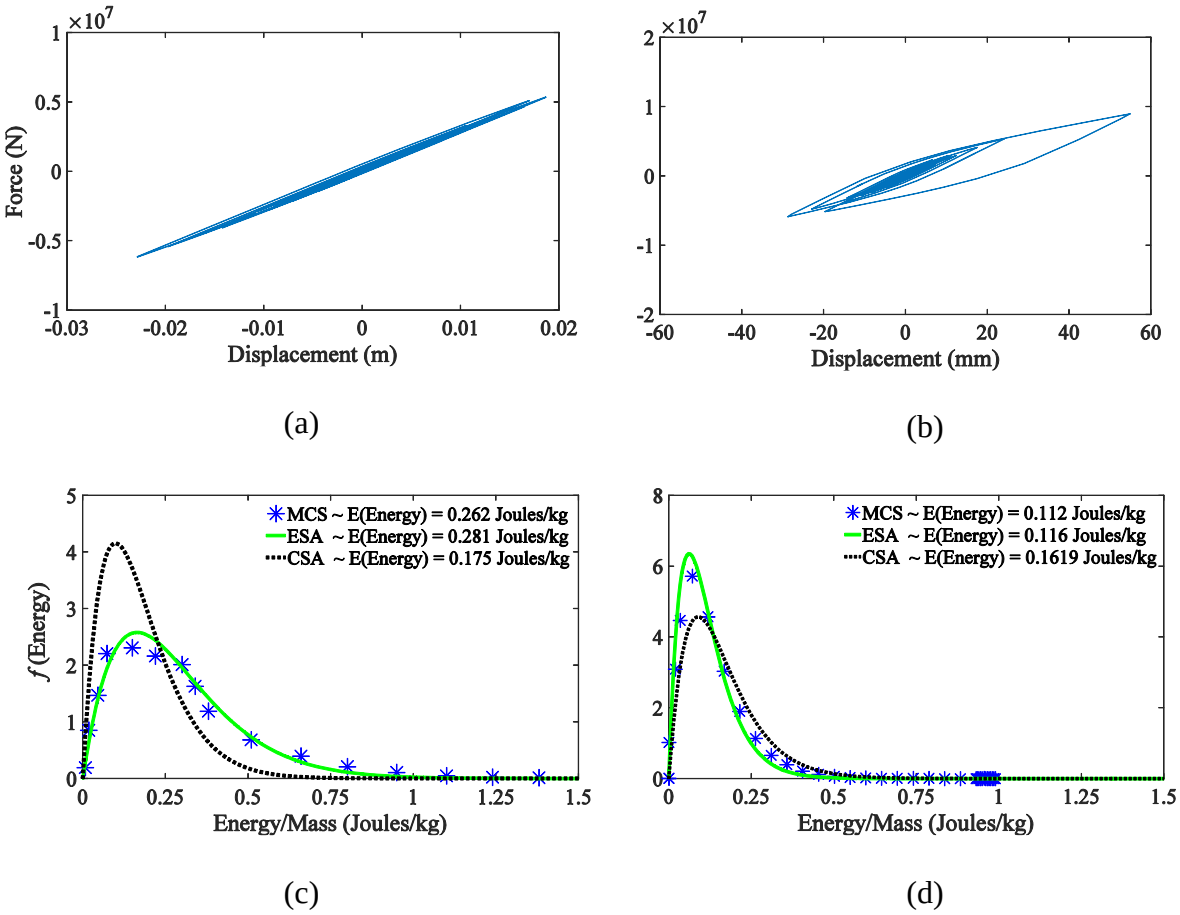

Figure 5-3 The nonlinear foundation response under Northridge earthquake for (a) the uncontrolled original system ($\gamma_{BW} = 5.82 m^{-1}$) and (b) the uncontrolled modified system ($\gamma_{BW} = 29.1 m^{-1}$), and the PDF of the energy of (c) the original uncontrolled system ($\gamma_{BW} = 5.82\ m^{-1}$, $K_w = 1$, $c' = 1.44\ c_1$, $\sigma_0' = 1.67\ \sigma_0$) and (d) the modified uncontrolled system ($\gamma_{BW} = 29.1\ m^{-1}$, $K_w = -2$, $c' = 4.12\ c_1$, $\sigma_0' = 1.41\ \sigma_0$) derived using Monte Carlo simulations (MCS), enhanced stochastic averaging (ESA), and conventional stochastic averaging (CSA) (K_w is defined in Equation (4.22) and the parameters c' and σ_0' are defined in Equations (4.24a-b)).

In order to evaluate the performance of the proposed controller, additional cases are considered including the uncontrolled structure and the building controlled using the LQR strategy. In conventional linear feedback control, nonlinearity is ignored and the LQR algorithm is designed based on the initial linear behavior of the system (Todorov, 2006).

To further optimize the performance of the conventional controller and have a fair comparison with the proposed control strategy, stochastic LQR (SLQR) method is adopted. In this approach, the system model used for control design is derived using stochastic linearization, where the hysteresis component is linearized and considered as part of the response variables of the system (Basili and Angelis, 2007; El-Khoury et al., 2015; El-Khoury et al., 2016). In addition, the LQR control design requires considering positive definite weighting matrices, Q_{SLQR} and R_{SLQR}, to indicate the importance of system response variables and applied control forces in the optimization process, respectively. In this case, R_{SLQR} is considered 1 and Q_{SLQR} for the vector of five state variables $(x_1, x_2, \dot{x}_1, \dot{x}_2, z_2)$ is considered to have the following form:

$$Q_{\mathrm{SLQR}} = \mathrm{diag}\left(\mathrm{v}_{\mathrm{SLQR}}, \mathrm{v}_{\mathrm{SLQR}}, 0,0,0\right) \tag{5.17}$$

where $\mathrm{v}_{\mathrm{SLQR}}$ is a positive number that is chosen such that the applied control forces in SLQR are at the same level of control forces in ESA-Control strategy.

The two controlled systems together with the uncontrolled structure are subjected to a white Gaussian noise excitation with the intensity of 0.32 g and Kobe ground motion. The relative displacement results and the applied control forces are presented in Figure 5-4 (the drift $(x_2 - x_1)$ foundation displacements (x_2) and the absolute acceleration of the roof, $\ddot{x}_{1\mathrm{A}}$ ($\mathrm{R}_1 = \frac{\mathrm{ESA-Control}}{\mathrm{SLQR}}$)). Under the white noise disturbance, the reduction in the relative displacement achieved via the ESA-control method is 8% more than that gained using SLQR at a comparable control force level: this can be observed in the time history of the applied control force of the actuator in Figure 5-4 f. Similar performance is observed for the case of 0.2 g intensity for the white noise in Table 5-1 where 7% further reduction is

gained using ESA-control method with respect to SLQR for the relative displacement response of the structure. When the uncontrolled system is subjected to white noise with $\sigma_0 = 0.32$ g, the drift ratio is found as 1.19% resulting in an irreparable damage in the structure. Both considered controllers reduce the drift ratio to fall within the repairable range: the drift ratios for ESA-control and SLQR are found 0.53% and 0.56%, respectively. Compared to SLQR, noticeable improvements in the response variables are also observed under Kobe ground motion where 16%, 12%, and 14% reductions are achieved for the maximum relative displacement of the structure with respect to the foundation, the foundation displacement, and the absolute acceleration of the roof, as presented in Table 5-1. For Northridge earthquake, the SLQR performs slightly better than the ESA-control method, but both strategies reduce the drift ratio to within the safe and repairable damage state ($DR < 1.00\%$). For the El-Centro ground motion, the proposed control algorithm reduces the peak relative displacement of the structure and foundation displacement by 7% compared to SLQR as seen in Table 5-1.

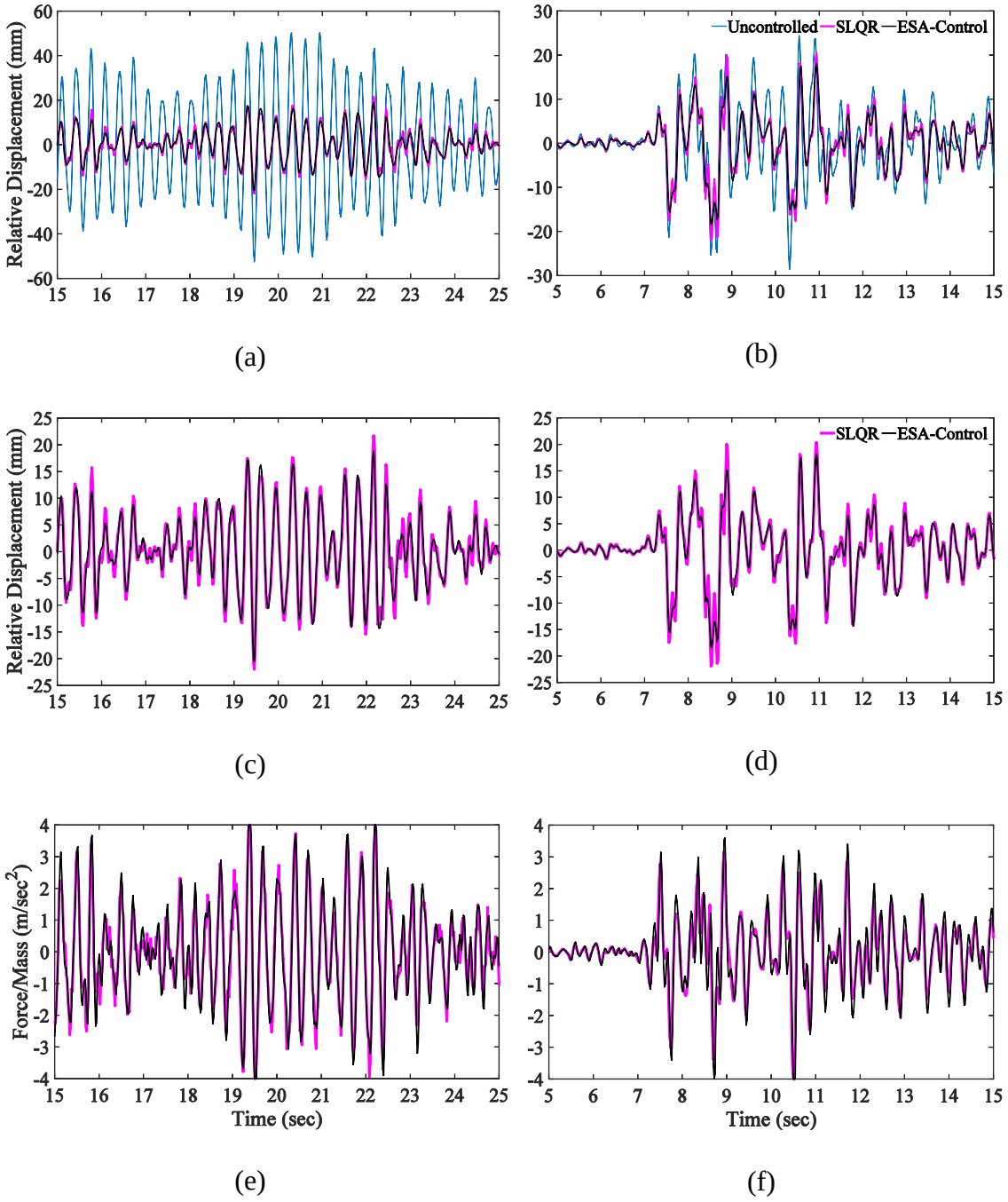

Figure 5-4 The relative displacement of the structure with respect to foundation for the two control cases and the uncontrolled structure subjected to (a) white noise with intensity of 0.32 g and (b) Kobe ground motion. The relative displacement results for the two control cases under (c) white noise with intensity of 0.32 g and (d) Kobe ground motion. Time-history of applied control forces for the two control strategy under (e) white noise with intensity of 0.32 g and (f) Kobe ground motion.

$\gamma_{BW} = 5.82 m^{-1}$							
White Noise (0.12 g)	Peak/RMS			**White Noise (0.2 g)**	Peak/RMS		
State	$(x_2 - x_1)$ (mm)	x_2 (mm)	$\ddot{x}_{1A}$ (m/sec^2)	State	$(x_2 - x_1)$ (mm)	x_2 (mm)	$\ddot{x}_{1A}$ (m/sec^2)
Uncont.	21.0/6.5	14.1/4.2	13.3/4.1	Uncont.	32.5/10.1	22.3/6.6	20.5/6.4
ESA-Cont.	7.8/2.1	6.0/1.6	5.4/1.5	ESA-Cont.	13.1/3.6	10.1/2.7	8.9/2.4
SLQR	8.5/2.3	6.2/1.6	5.4/1.5	SLQR	14.1/3.8	10.3/2.7	9.0/2.5
R_1	0.92/0.92	0.98/0.99	0.98/0.99	R_1	0.93/0.93	0.98/0.99	0.99/0.99
White Noise (0.32 g)	Peak/RMS			**Northridge**	Peak/RMS		
State	$(x_2 - x_1)$ (mm)	x_2 (mm)	$\ddot{x}_{1A}$ (m/sec^2)	State	$(x_2 - x_1)$ (mm)	x_2 (mm)	$\ddot{x}_{1A}$ (m/sec^2)
Uncontrolled	47.7/14.8	33.8/9.9	30.2/9.3	Uncont.	54.9/10.7	44.3/7.3	34.8/6.8
ESA-Control	21.3/5.7	16.5/4.4	14.5/3.9	ESA-Cont.	38.4/4.7	33.6/3.6	25.9/3.1
SLQR	22.4/6.1	16.7/4.4	14.5/3.9	SLQR	36.3/4.6	34.7/3.5	26.3/2.9
R_1	0.95/0.94	0.99/1.00	1.00/0.99	R_1	1.06/1.03	0.97/1.01	0.98/1.04
El-Centro	Peak/RMS			**Kobe**	Peak/RMS		
State	$(x_2 - x_1)$ (mm)	x_2 (mm)	$\ddot{x}_{1A}$ (m/sec^2)	State	$(x_2 - x_1)$ (mm)	x_2 (mm)	$\ddot{x}_{1A}$ (m/sec^2)
Uncont.	23.4/3.6	15.9/3.6	14.8/3.5	Uncont.	28.6/5.0	22.9/3.7	18.1/3.2
ESA-Cont.	9.8/1.5	7.0/1.5	6.7/1.3	ESA-Cont.	18.4/3.6	17.8/3	12.4/2.4
SLQR	10.5/1.5	7.5/1.5	6.9/1.3	SLQR	21.9/3.7	20.3/3.1	14.4/2.4
R_1	0.93/1.02	0.93/1.01	0.98/1.01	R_1	0.84/0.95	0.88/0.98	0.86/0.98

Table 5-1 Simulation results for various control cases for the original system.

To investigate the effectiveness of the considered control algorithms for higher levels of nonlinearity in the system, the parameter, γ_{BW}, is increased by five times. This modification results in a decrease of the equivalent stiffness of about 50% with an increase in the dissipative energy as shown in Figure 5-5b. As seen in Table 5-2, with the increase of the extent of hysteretic nonlinearity, the foundation displacement increases and the inter-story drift decreases; this trend has also been observed in general multi-story buildings (Raychowdhury, 2011; Nateghi-A and Rezaei-Tabrizi, 2013). Similar to the case of the original system, the enhanced stochastic averaging is applied to the modified structure and

the PDF of energy is derived and compared to that from Monte Carlo simulations and the conventional stochastic averaging approach in Figure 5-3d. It is observed that ESA provides a considerably better estimation of the PDF of energy of the system compared to the conventional method. Simulation results for the uncontrolled structure and the two control systems under white noise and recorded ground motions are shown in Table 5-2. The most pronounced improvement achieved using ESA-control approach versus SLQR is under Kobe ground motion where 14%, 21%, and 15% reductions are gained respectively for peak relative story displacement, foundation displacement, and roof acceleration. Under white noise excitation, the largest improvement is 8% for the RMS of the relative displacement for the intensity of $\sigma_0 = 0.12$ g. Unlike the case in the original system, the ESA-control method performed better than SLQR under Northridge ground motion where the proposed control approach further reduced the relative story displacement and foundation displacement 2% and 3%, respectively, compared to SLQR. In addition, the uncontrolled system under Northridge earthquake does not sustain damage as the drift ratio is 0.93%. The likelihood of damage is reduced using both controllers: the drift ratio is 0.77% and 0.79% for ESA-control method and SLQR, respectively. Time histories of the relative story displacement of the modified uncontrolled structure and the modified system equipped with SLQR and ESA-control methods together with the applied control forces for a white noise excitation with intensity of 0.32 g and Kobe ground motion are shown in Figures 5.5a-f.

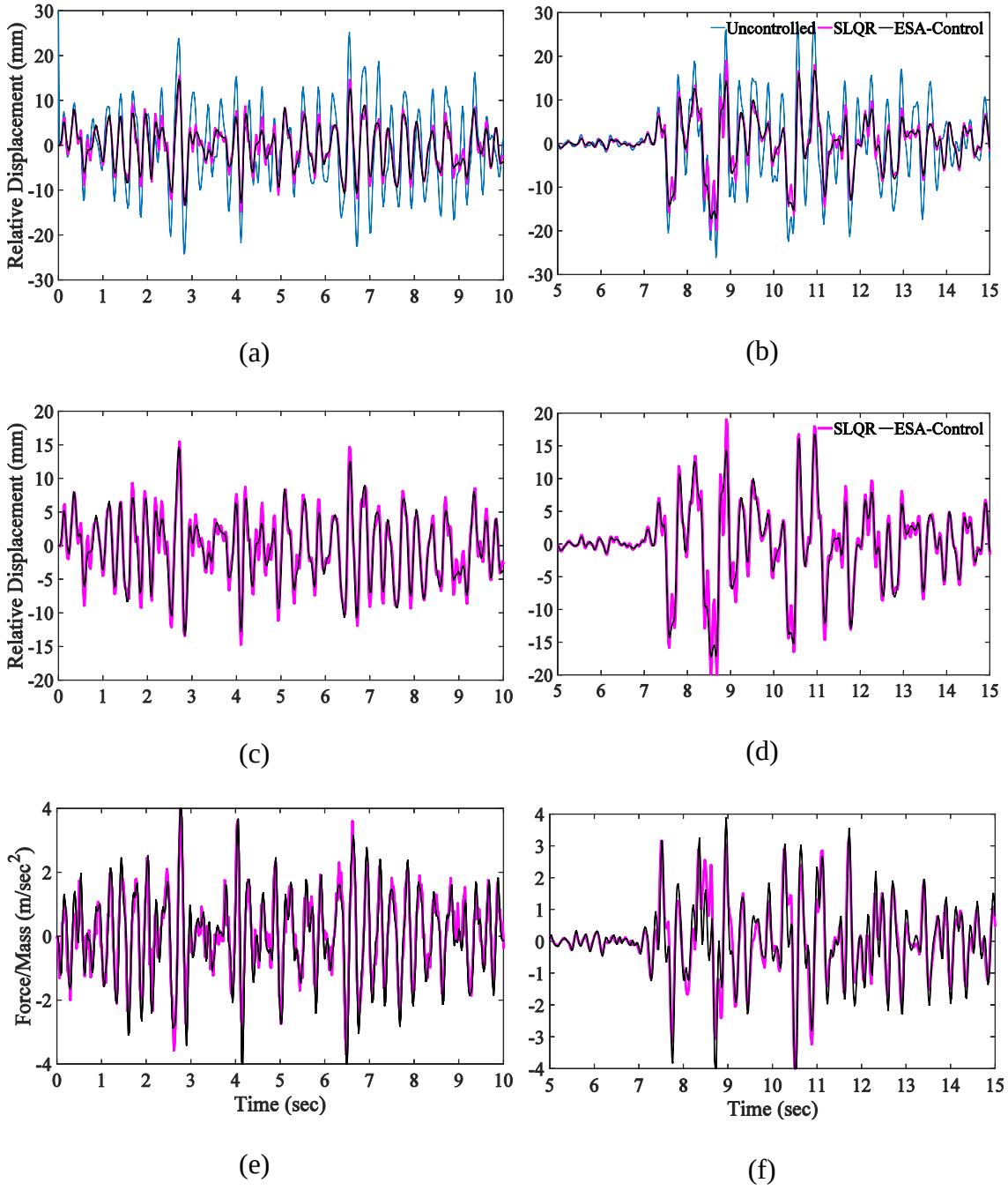

Figure 5-5 The relative displacement of the modified structure with respect to foundation for the two control cases and the uncontrolled modified structure subjected to (a) white noise with intensity of 0.32 g and (b) Kobe ground motion. The relative displacement results for the two control cases under (c) white noise with intensity of 0.32 g and (d) Kobe ground motion. Time-history of applied control forces for the two control strategy under (e) white noise with intensity of 0.32 g and (f) Kobe ground motion.

γ_{BW} = 29.1 m^{-1}							
White Noise (0.12 g)	Peak/RMS			**White Noise (0.2 g)**	Peak/RMS		
State	$(x_2 - x_1)$ (mm)	x_2 (mm)	$\ddot{x}_{1A}$ (m/sec^2)	State	$(x_2 - x_1)$ (mm)	x_2 (mm)	$\ddot{x}_{1A}$ (m/sec^2)
Uncont.	15.2/4.8	11.6/3.3	9.6/3.00	Uncont.	21.8/6.9	18.3/5	13.8/4.40
ESA-Cont.	6.9/2.0	6.0/1.6	4.80/1.40	ESA-Cont.	11.2/3.2	10.5/2.7	7.70/2.20
SLQR	7.4/2.1	6.2/1.6	4.90/1.40	SLQR	11.8/3.4	10.7/2.7	7.90/2.20
R_1	0.93/0.92	0.98/0.99	0.98/0.99	R_1	0.94/0.93	0.98/1.00	0.98/0.99
White Noise (0.32 g)	Peak/RMS			**Northridge**	Peak/RMS		
State	$(x_2 - x_1)$ (mm)	x_2 (mm)	$\ddot{x}_{1A}$ (m/sec^2)	State	$(x_2 - x_1)$ (mm)	x_2 (mm)	$\ddot{x}_{1A}$ (m/sec^2)
Uncontrolled	29.7/9.5	28.6/7.3	18.70/6.00	Uncont.	37.0/5.9	54.9/5.2	23.5/3.70
ESA-Control	17.3/5	17.9/4.4	11.90/3.50	ESA-Cont.	30.8/4.0	46.1/4.1	21.90/2.70
SLQR	17.7/5.3	17.9/4.4	12.10/3.50	SLQR	31.4/3.8	47.7/4.1	22.5/2.60
R_1	0.98/0.95	1.00/1.00	0.98/1.00	R_1	0.98/1.04	0.97/1.00	0.98/1.03
El-Centro	Peak/RMS			**Kobe**	Peak/RMS		
State	$(x_2 - x_1)$ (mm)	x_2 (mm)	$\ddot{x}_{1A}$ (m/sec^2)	State	$(x_2 - x_1)$ (mm)	x_2 (mm)	$\ddot{x}_{1A}$ (m/sec^2)
Uncont.	16.1/3	14/2.8	10.20/2.70	Uncont.	27.9/5.5	29.9/5	17.60/3.50
ESA-Cont.	8.9/1.5	7.3/1.4	6.30/1.20	ESA-Cont.	17.2/3.5	23.4/3.5	11.60/2.30
SLQR	9.6/1.5	7.0/1.4	6.50/1.20	SLQR	20.0/3.5	29.6/3.6	13.70/2.40
R_1	0.93/1.02	1.04/1.01	0.97/1.01	R_1	0.86/0.99	0.79/0.95	0.85/0.99

Table 5-2 Simulation results for various control cases for the modified system.

5.4 Closure

This study proposes a stochastic control algorithm based on an enhanced stochastic averaging method of the energy envelope. The developed enhanced stochastic averaging method addresses current limitations in conventional techniques with respect to damping effects and applied stochastic excitations in nonlinear non-integrable systems. The improvement is achieved by deriving an equivalent nonlinear stochastic system with an equivalent excitation intensity and modified damping parameters by equating drift and diffusion components of the modified and the original system using method of weighted residuals and employing high order moments of system velocities. The optimization

process to derive the optimal control force model is formulated according to the nonlinear Hamilton-Jacobi-Bellman equation where the objective is to reduce the excitation-induced energy of the system.

The performance of the proposed control model is assessed for response mitigation of a one-story building on a shallow nonlinear hysteretic foundation in loose sand. The system is subjected to various excitations including white noise of different intensity levels and historic ground motions with different peak ground accelerations. In addition, the proposed control strategy is compared to the uncontrolled system and the structure controlled with an LQR design based on a stochastically linearized system model (SLQR) with similar maximum applied control forces. To investigate the sensitivity of the system to external excitation, the system is subjected to three artificial excitations of different intensity levels and three ground motions with different peak ground acceleration (El-Centro, Northridge and Kobe) and the analysis is performed accordingly. Simulation results for both synthetic and recorded excitations indicate significant improvements for the suggested control algorithm versus SLQR. For instance, the proposed method reduced drift ratio and foundation displacement responses by 16% and 12%, respectively compared to SLQR method using equivalent level of forces under Kobe ground motion. To evaluate the effectiveness of the considered control methods for higher levels of nonlinearity, the system model parameter that control the shape of hysteresis loop of the foundation is increased resulting in a decrease in the equivalent stiffness and increase in the dissipation energy in the foundation. Simulations results indicate higher levels of improvement in the system response with respect to SLQR compared to the case of the original system: under Kobe ground motion, reductions of 14% and 21% are achieved for the maximum relative

displacement and foundation displacement respectively using the proposed method compared to SLQR.

Similarly for multi-story buildings with nonlinear SSI, the proposed framework can be generalized to determine the equivalent damping and excitation parameters using the method of Weighted Residuals and conduct stochastic averaging of energy envelope. For the considered historic ground motions, Gaussian white noise excitations, and the structural system, it can be concluded that the proposed control strategy based on enhanced stochastic averaging of energy envelope is more efficient than SLQR algorithm. This superior performance is due to ability of the proposed control strategy to explicitly incorporate the nonlinearity of the system through the averaging method and implement more complex and higher order objective functions in the HJB equation compared to conventional optimal control techniques. The conclusions of this study can be further expanded by evaluating the seismic performance of the proposed control system for various structures and other ground motion records. This strategy can be adopted in various engineering fields and applied to improve robustness and reliability of different systems. In addition to buildings, the proposed control strategy can be used to suppress vertical vibrations of cars, mitigate the dynamic response and enhance the efficiency of wind turbines, and reduce the potential of pounding in multi-span bridges, among other applications.

Chapter 6: Reliability-based Control Algorithms Using Enhanced Stochastic Averaging

6.1 Introduction

As discussed in Section 2.4, current reliability-based control techniques have been successfully applied to linear systems; however, incorporation of stochastic nonlinear behavior of systems in such control designs remains a challenge (Yuen and Beck, 2003; Scruggs et al., 2006; Taflanidis et al., 2008a; Taflanidis et al., 2008b; Taflanidis and Scruggs, 2010).

The primary contribution here is the development of reliability-based control algorithms for nonlinear hysteretic systems. Compared to other approaches including the work presented in Chapter 5 and in El-Khoury and Shafieezadeh (2016) that aimed at minimizing structure responses without considering the implications of the response levels for the performance of the systems, the proposed algorithms here explicitly optimize reliability of structures; hence, the primary objective function in the optimization algorithms is the probability of failure. This chapter presents two reliability-based control algorithms that minimize failure probabilities of nonlinear hysteretic systems subjected to stochastic excitations. The proposed methods include constrained reliability-based control (CRC) and unconstrained reliability-based control (URC) algorithms. Accurate probabilistic estimates of nonlinear system responses to stochastic excitations are derived

analytically using enhanced stochastic averaging of energy envelope proposed previously by the authors. Convolving these demand estimates with capacity models yields the reliability of nonlinear systems in the control design process. In the CRC approach, first- and second-level optimizations are implemented. The first-level optimization entails obtaining the value function of the Hamilton-Jacobi-Bellman (HJB) equation (Fleming and Soner, 2006) through enhanced stochastic averaging of energy envelope. The second-level optimization considers minimizing the probability of failure subjected to force constraints by searching for gain parameters in the objective function. Here, the probability of failure is defined as the likelihood of exceeding a predefined limit. In the URC approach, a single optimization process is utilized to minimize the probability of failure by directly searching for the optimal control gain. To ensure that applied control forces are dissipative, they are enforced to follow a particular form. The performance of the reliability-based algorithms is evaluated on the system introduced in Chapter 4.

The rest of the chapter is organized as follows. Section 6.2 presents the detailed formulation of the proposed reliability-based control algorithms. Section 6.3 implements the design for the system with soil structure interaction (SSI) discussed in Chapter 3. Section 6.3.1 presents optimization procedures for the reliability-based algorithms. Section 6.3.2 discusses the results of the proposed algorithms in comparison to the uncontrolled case and the system controlled using LQR algorithm applied to a stochastically linearized model of the system. Finally, conclusions of the study are presented in Section 6.4.

6.2 Methodology

The reliability-based control algorithms for non-integrable nonlinear systems are developed using enhanced stochastic averaging (refer to Section 4.2) (El-Khoury and Shafieezadeh, 2016) of energy envelope. This process and the integration of reliability concepts into stochastic control design for nonlinear hysteretic systems subjected to stochastic excitations are explained in detail in Sections 6.2.1 and 6.2.2. Two approaches are derived: constrained reliability-based control (CRC) and unconstrained reliability-based control (URC). In CRC approach (Section 6.2.1), an analytical optimization method solves the Hamilton-Jacobi-Bellman equation and then a numerical optimization technique minimizes the probability of failure by searching for optimal gains. In URC approach (Section 6.2.2), a numerical optimization method is employed to directly minimize the probability of failure.

6.2.1 Constrained Reliability-Based Control Algorithm

In order to develop CRC design, first, the dynamic equilibrium equation of the controlled system is translated into the Itô equation of energy envelope using enhanced stochastic averaging. The active controller added here could be a system of electric or hydraulic actuators; this controller installed in the first story connecting the foundation to the roof as shown Figures 5-1a-b. Next, the HJB equation is derived for the first-level optimization, the probability of failure is defined as the objective in the second-level optimization, and a numerical minimization technique is applied to find optimal control gain parameters such that the probability of failure is minimized while constraining the magnitude of control forces to an upper bound that represents the capacity of actuators. The equations of motion of the controlled system can be presented as:

$$\ddot{x}_1 = \left(-\frac{\partial \pounds_1(x_1, x_2)}{\partial x_1} - \frac{c_1}{m}\dot{x}_1 + \frac{c_1}{m}\dot{x}_2 - u\right) + \sigma_0 \frac{\mathrm{d}B}{\mathrm{d}t}$$
$$\ddot{x}_2 = \left(-\frac{\partial \pounds_1(x_1, x_2)}{\partial x_2} - \frac{\partial \pounds_2(z_2)}{\partial z_2} - \frac{{c_2}''}{m}\dot{x}_2 + \frac{c_1}{m}\dot{x}_1 + u\right) + \sigma_0 \frac{\mathrm{d}B}{\mathrm{d}t} \quad (6.1)$$

Applying stochastic averaging of energy envelope to Equation (6.1), the drift and diffusion components are:

$$\mathrm{d}e = \overline{M'}_{\text{drift}}\mathrm{d}t + \overline{\sigma'}_{\text{diffusion}}\mathrm{d}B \quad (6.2a)$$

$$\overline{M'}_{\text{drift}} = -2\frac{c'}{m}\emptyset_0 - ((1-\alpha_z)k_2\overline{z_2\dot{x}_2}) + {\sigma'}_0^2 + \bar{u}(\dot{x}_2 - \dot{x}_1) \quad (6.2b)$$

$$\overline{\sigma'^2}_{\text{diffusion}} = 2{\sigma'}_0^2\emptyset_0 \quad (6.2c)$$

Next, the control force is determined based on constrained reliability-based control design. As mentioned earlier, the constrained reliability-based design incorporates first-level and second-level optimizations that are implemented as follows.

6.2.1.1 First Level Optimization

In the first-level optimization, the HJB formulation for the system model in Equations (6.2-a-c) is derived in Equation (5.10) and Equation (5.11):

$$\rho V'(e) = L'(e, \bar{u}) + \bar{M}'_{\text{drift}}\frac{\mathrm{d}V'(e)}{de} + \frac{{\sigma^2}'_{\text{diffusion}}}{2}\frac{\mathrm{d}^2V'(e)}{de^2} \quad (6.3a)$$

$$\bar{u} = -\frac{1}{2R}\frac{\mathrm{d}V'(e)}{de}\overline{(\dot{x}_2 - \dot{x}_1)} \quad (6.3b)$$

$$L_1 = L'(e, \bar{u}) = \theta(e) + R\bar{u}^2 \quad (6.3c)$$

where $\theta(e)$ (e.g. $s_1 e + s_2 e^2$; $s_i \geq 0$; $i = 1, 2$) is a convex polynomial function that depends on the energy of the system and R is a positive gain factor that represents the gain for the control force in the objective function. As discussed in Section 5.2, Equations (6.3a-b) are solved using the collocation method (Miranda and Fackler, 2002). In the process of solving

the HJB equation, the number of nodes, basis functions, and the domain of interest can be increased to improve the quality of the solutions (Miranda and Fackler, 2002).

6.2.1.2 Second Level Optimization

A numerical optimization is employed to find optimal gain parameters s_1 and s_2 in Equation (6.3c) such that the probability of failure L_2 is minimized:

$$L_2 = P(e \geq e_c) = \int_{e_c}^{\infty} p_{\mathrm{s}}(e)de \tag{6.4}$$

Restrictions are applied to ensure the convexity of the cost function L_1. Herein, the objective is to reduce the(likelihood of exceeding a critical threshold e_c. The probability distribution function (PDF) of energy, $p(e)$, can be derived as:

$$p(e) = \frac{\lambda_{\mathrm{e}}}{\bar{\sigma}'^2_{\mathrm{diffusion}}} \exp\left\{\int_0^e \frac{2\overline{M'}_{\mathrm{drift}}(y)}{\bar{\sigma}'^2_{\mathrm{diffusion}}(y)} \mathrm{d}y\right\} \tag{6.5}$$

where for controlled and uncontrolled states, $\overline{M'}_{\mathrm{drift}}$ are derived as shown in Equation (6.2b), respectively:

$$\overline{M'}_{\mathrm{drift}} = -2\frac{c'}{m}\emptyset_0 - ((1-\alpha_z)k_2\overline{z_2\dot{x}_2}) + \sigma'^2_0 + \frac{1}{2R}\frac{\mathrm{d}V'}{de}\overline{(\dot{x}_2 - \dot{x}_1)^2} \tag{6.6}$$

In the above equations, λ_{e} is a constant to ensure that the integration of the PDF function over the entire domain yields one:

$$\lambda_{\mathrm{e}} = \frac{1}{\int_0^{+\infty} \frac{1}{\bar{\sigma}'^2_{\mathrm{diffusion}}(e)} \exp\left\{\int_0^e \frac{2\bar{M}'_{\mathrm{drift}}(y)}{\bar{\sigma}'^2_{\mathrm{diffusion}}(y)} \mathrm{d}y\right\} \mathrm{d}e} \tag{6.7}$$

6.2.2 Unconstrained Reliability-Based Control Algorithm

To provide more flexibility for the form of the control force, the unconstrained reliability-based control approach is proposed. This algorithm does not rely on the HJB equation to

define the structure of the control force. Rather, it considers a similar but more flexible form for the control force represented as:

$$\bar{u} = -\frac{1}{2R}\mathrm{g}(e)\overline{(\dot{x}_2 - \dot{x}_1)} \tag{6.8}$$

where $g(e)$ is a second order polynomial function in terms of energy and is defined as:

$$g(e) = j_0 + j_1 e + j_2 e^2 \tag{6.9}$$

A numerical optimization similar to the constrained reliability-based control algorithm is applied to find optimal values for parameters j_0, j_1, and j_2 such that the following objective function that estimates the probability of failure is minimized.

$$L_0 = P(e \geq e_c) = \int_{e_c}^{\infty} p(e)de \tag{6.10}$$

Restrictions are appropriately enforced on the space of admissible controllers to yield a bounded dissipative control force. In this case, the constants j_i (i = 0, 1, 2) are chosen such that $g(e)$ remains positive across the domain $(0, e_{\max})$. This condition ensures a negative gain in Equation (6.8) and hence ensures response reduction and dissipation of energy. In addition, the limit $u_{\max}$ is applied to the control force to account for the capacity of the control device.

6.3 Implementation

The reliability-based algorithms are implemented in the same system with SSI discussed in Chapters 3 and 4. the control design is aimed at mitigating the probability of failure due to large story drifts. Next, the constrained reliability-based control (CRC) and unconstrained reliability-based control (URC) algorithms are applied, and their

performance is compared to stochastic LQR (SLQR) and uncontrolled cases. The controlled and uncontrolled systems are subjected to artificial and historic ground motions similar to Chapter 5.

6.3.1 Control Designs

Initially, the Itô formulation of the uncontrolled system is derived based on the enhanced stochastic averaging (ESA) method of energy envelope in Section 4.2. After modeling the uncontrolled system, the Itô equation of the controlled system is derived by adding the effect of the control force in Equation (6.1). Then, the control algorithms are designed following the procedures explained in Section 6.2. In the CRC design, first- and second-level optimizations are sequentially implemented in order to minimize the cost function, L_1, in Equation (6.3c) and the probability of failure, L_2, in Equation (6.4) with the control force subjected to the limit, $u_{\max}$. In the URC design, the probability of failure, L_0, in Equation (6.10) is minimized through one optimization process with the control force limit. The peak drift ratio, DR, is used as an engineering demand parameter to assess the level of damage of the building. This ratio is defined as:

$$DR = \frac{\max(|x_1 - x_2|)}{H} \tag{6.11}$$

where H (= 4 m) is the story height. In the controlled state, the goal is to minimize the likelihood of the slight damage, thus the threshold of 0.2% according to Ghobarah (2004) is considered for DR in the design of the control strategies. In the stochastic averaging method, the system is described in terms of total energy; therefore, a mapping from drift to energy is performed using modal analysis to derive a critical energy that approximately

corresponds to 0.2% drift level in the system. In the next step for the CRC strategy, the value function, $V'(e)$ in Equation (6.3b), is calculated based on a predefined cost function, L_1 in Equation (6.3c), with $R = 1$ and $\theta(e) = s_1 e + s_2 e^2$. For the URC method, the optimization is conducted based on the function $g(e)$ in Equation (6.8) with R = 1 and $g(e) = j_0 + j_1 e + j_2 e^2$. For both control approaches, the force per unit mass capacity of the actuator is derived and capped at the maximum control force per unit mass u_{max} of 0.4 g. In addition, the root mean square (RMS) of the control force u_{rms} can be determined using:

$$\overline{u}_{\mathrm{rms}} = \sqrt{\int_0^{\infty} 1/2R^2 f_e(e)^2 \emptyset_0(e)\, p(e) de} \tag{6.12}$$

where the function $f_e(e)$ is equal to $\mathrm{d}V'/de$ for CRC and $\mathrm{g}(e)$ for URC. Equation (6.12) are enforced to be within 0.15 g to reduce sudden changes in the control force. The iterations within the optimization processes for the shape of the function $\mathrm{d}V'/de$ are shown in Figure 6-2a with the converged optimal solution shown in bold lines. This optimal solution satisfies the maximum and RMS force requirements stated previously. Furthermore, the optimal solutions for CRC ($\mathrm{d}V'/de$) and URC $\left(g(e)\right)$ are compared in Figure 6-2c. It appears that the optimal solution for URC has a steeper slope than that for CRC. In addition for low energy values, the optimal gain and hence the applied control force for URC are smaller than the corresponding quantities for CRC. This pattern is reverse for medium to large energy levels. The steep positive slope is expected to ensure a dissipative force since the function $g(e)$ is free and is not governed by the HJB equation.

As mentioned previously, this result yields a negative nonlinear gain in Equation (6.8) and provides response reduction and dissipation.

In order to evaluate the performance of the proposed controllers for highly nonlinear systems, the Bouc-Wen model parameter, γ_{BW}, that controls the shape of the hysteresis loops is increased by five times. The new structure model is called the modified system. The force versus the lateral foundation displacement of this structure for the uncontrolled and URC states under Kobe ground motion is shown in Figure 6-1b. In comparison to the original system, similar trends of $dV'(e)/de$ and $g(e)$ are observed for the modified system as shown in Figure 26b and Figure 26d.

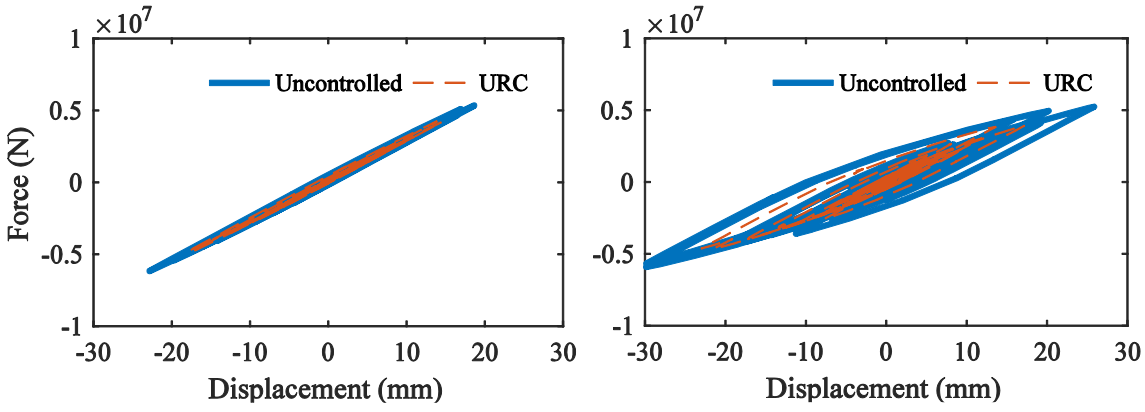

Figure 6-1 The nonlinear foundation response under Kobe earthquake for (a) the original system (b) the modified system.

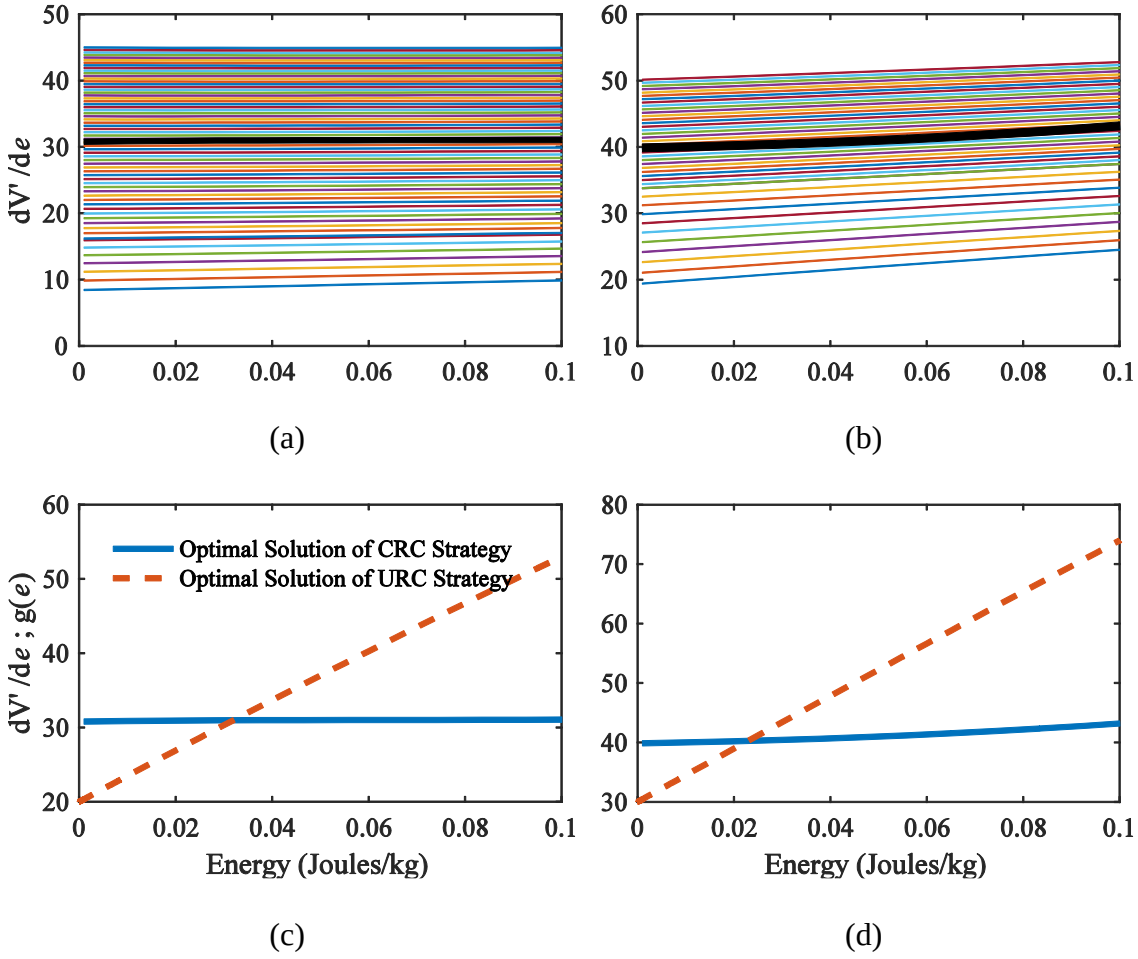

Figure 6-2 The iterations of dV'/de for the CRC optimization for (a) original and (b) and modified systems, and the optimal gain functions (dV'/de ; g(e)) for the constrained and unconstrained reliability-based optimizations for (c) original and (d) modified systems.

6.3.2 Discussion

Before analyzing the time history results, the PDF of the energy of the system e for the uncontrolled, CRC, and URC states are derived using the analytical enhanced stochastic averaging and Monte Carlo simulation (MCS) methods and the results are shown in Figure 6-3a and 6-3b. A very good agreement is observed between results obtained using analytical and numerical techniques for the uncontrolled and controlled cases. The first and

second order moment of energy, $E(e)$ and $E(e^2)$, for the case of γ_{BW} = 29.1 m^{-1} are compared here for different states. For the uncontrolled case, MCS and ESA estimates for $E(e)$ are 0.112 Joules/kg and 0.116 Joules/kg, and for $E(e^2)$ are 0.0198 $Joules^2/kg^2$ and 0.021 $Joules^2/kg^2$, respectively. Estimates of $E(e)$ through ESA and MCS techniques are 0.033 Joules/kg and 0.031 Joules/kg for the CRC state and 0.030 Joules/kg and 0.0298 Joules/kg for the URC state, respectively. Estimates of the second order moment of energy derived using ESA and MCS techniques are 0.0016 $Joules^2/kg^2$ and 0.0019 $Joules^2/kg^2$ for the CRC state and 0.0013 $Joules^2/kg^2$ and 0.0017 $Joules^2/kg^2$ for the URC state, respectively. All these results indicate the high accuracy of enhanced stochastic averaging of energy envelope in estimating probabilistic characteristics of system responses. Moreover, both CRC and URC techniques appear to significantly reduce the mean and standard deviation of system energy as shown in Figure 6-3.

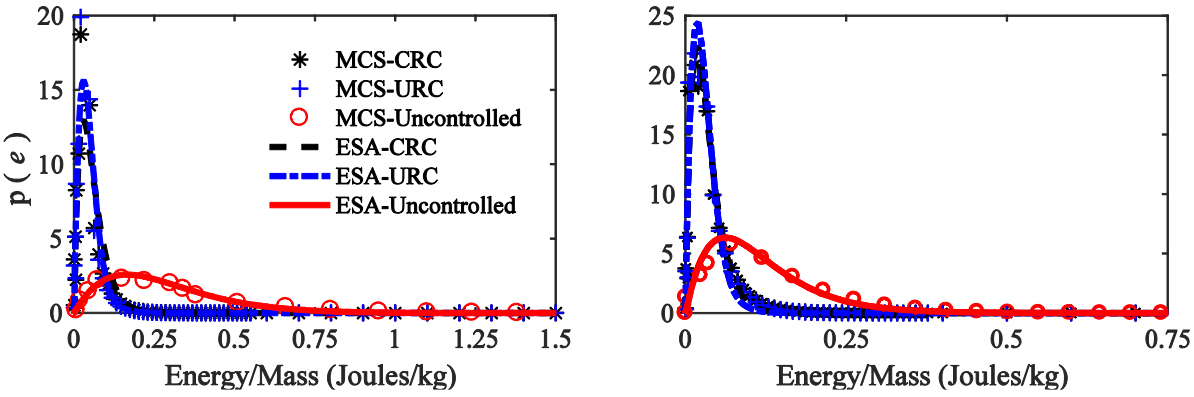

(a) (b)

Figure 6-3 The PDF of controlled and uncontrolled cases for (a) original system and (b) modified system under white noise (σ_0 = 0.32 g).

Prior to the simulations, the analytical forms of the control force for the proposed control methods are derived and therefore, no computationally demanding operation is required to determine the control force during the simulations or actual implementations. For the case study system, functions $V'(e)$ and $g(e)$ are determined beforehand as shown in Figure 6.2c and Figure 6.2d; these functions are represented by polynomial functions of the energy of the system. During the simulations, the energy of the system is computed based on its responses, and the aforementioned functions $V'(e)$ and $g(e)$ are evaluated to determine in real-time control forces for the CRC case using Equation (18b) and for the URC case via Equation (26). To examine the reliability of the controlled systems, the probabilities of failure based on energy $P(e \geq e_c)$ and drift $P(DR \geq 0.20\%)$ are obtained for white noise input excitation with the intensity of 0.32 g, and the results are presented in Table 6-1 for the original and modified systems. It should be noted that $P(e \geq e_c)$ is the cost function L_2 in Equation (23) for CRC approach and the cost function L_0 in Equation (28) for URC approach. Results indicate that control systems in general considerably improve the reliability of the structure. For the original system, the extent of improvement achieved using proposed CRC and URC techniques with respect to stochastic linear quadratic regulator (SLQR) in Section 5.3 is 23% and 41% based on $P(e \geq e_c)$ and 40% and 55% based on $P + (DR \geq 0.2\%)$, respectively. For the case of the modified system (the system with higher extent of nonlinearity), CRC and URC techniques improve the reliability of the structure with respect to SLQR by 26% and 38% based on $P(e \geq e_c)$ and 56% and 72% based on $P(DR \geq 0.20\%)$, respectively. The control algorithm in El-Khoury and Shafieezadeh (2016) is based on solving the Hamilton-Bellman-Jacobi equation to reduce the expected energy of the system and the control objective function

does not involve the probability of failure of the system. For the original system (γ_{BW} = 5.82 m^{-1}) equipped with ESA-based control algorithm, $P(e \geq e_c)$ and $P(DR \geq 0.20\%)$ are 0.1308 and 0.1617, respectively; these probabilities for the modified system (γ_{BW} = 29.1 m^{-1}) are 0.086 and 0.104, respectively. In addition to improvements in the reliability of the structure, proposed controllers can further reduce some of the structural responses compared to the ESA-based control method. For example, URC method reduces the relative displacement of the original system under Kobe ground motion by 8% compared to ESA-based control method.

γ_{BW} = 5.82 m^{-1}				
Reliability Measures	**URC**	**CRC**	**SLQR**	**Uncontrolled**
$P(e \geq e_c)$	0.074	0.097	0.126	0.864
$P(DR \geq 0.20\%)$	0.087	0.116	0.192	0.600
γ_{BW} = 29.1 m^{-1}				
Reliability Measures	**URC**	**CRC**	**SLQR**	**Uncontrolled**
$P(e \geq e_c)$	0.048	0.058	0.078	0.608
$P(DR \geq 0.20\%)$	0.035	0.054	0.123	0.416

Table 6-1 MCS results of reliability-based measures at an intensity level of 0.32 g.

Moreover for the original and modified systems, the three controlled and the uncontrolled systems are subjected to white noise excitations with intensities of 0.12 g, 0.2 g, and 0.32 g as well as recorded ground motions for Northridge, El Centro, and Kobe earthquakes. Peak and root mean square of system responses including the relative displacement of the structure with respect to foundation, foundation displacement, and acceleration of the structure are presented in Tables 6-3 and 6-4 for the original and modified systems, respectively. For the original system, the only ground motion where the

SLQR case yields the lowest DR is the Northridge ground motion where DR equals 1.37%, 0.93%, 0.95%, and 0.91% (DR < 1.00%) for uncontrolled, URC, CRC, and SLQR cases, respectively (Tables 6-3 and 6-4). In all other cases including white noise excitations of different intensity levels and El Centro and Kobe ground motions, URC performed the best in terms of reducing the relative displacement of the structure with respect to foundation which is the engineering demand parameter for reliability analysis. For instance for the original structure under Kobe ground motion, the normalized peak drift displacement with respect to the SLQR case is 0.78 and 0.81 for the URC and CRC cases, respectively. The ratios of peak foundation displacement for URC and CRC cases with respect to SLQR are 0.89 and 0.88, respectively. For the modified system under Northridge ground motion, DR equals 0.93%, 0.81%, 0.79%, and 0.79% for uncontrolled, URC, CRC, and SLQR cases, respectively. Similar to the case of the original system, considerable improvements in responses of the modified system are observed when the system is subjected to Kobe ground motion. For example, the normalized peak drift displacement with respect to SLQR is 0.76 and 0.84 for the URC and CRC cases, respectively and the normalized peak foundation displacement with respect to SLQR is 0.78 and 0.79 for the URC and CRC cases, respectively. Time histories of drift and control force for the three controlled systems are shown in Figure 6.4 for the original system under Kobe Earthquake. These results highlight the improvements achieved in system responses using proposed reliability-based methods compared to SLQR, while using comparable level of control forces.

Based on the results presented here, it can be observed that the URC method reduces the probabilities of failure the most compared to other techniques. Moreover, controllers

exhibit similar performance trends under white noise and actual ground motions. As seen in Table 6-2 for the original and in Table 6-3 modified structures, the URC method yields the least peak relative displacements which correlates with damage for two thirds of 12 cases that involve white noise excitations of varying intensities and actual ground motions.

White Noise (0.12 g)	Peak/RMS			**White Noise (0.2 g)**	Peak/RMS		
State	$(x_2 - x_1)$ (mm)	x_2 (mm)	$\ddot{x}_{1A}$ (m/sec^2)	State	$(x_2 - x_1)$ (mm)	x_2 (mm)	$\ddot{x}_{1A}$ (m/sec^2)
Uncontrolled	21/6.5	14.1/4.2	13.26/4.10	Uncontrolled	32.5/10.1	22.3/6.6	20.53/6.35
URC	7.1/2.1	6.1/1.6	5.08/1.46	URC	10.3/3.2	9.9/2.6	8.21/2.29
CRC	7.0/1.9	5.8/1.6	4.98/1.36	CRC	11.6/3.2	9.7/2.6	8.25/2.26
SLQR	8.5/2.3	6.2/1.6	5.45/1.48	SLQR	14.1/3.8	10.3/2.7	9.01/2.46
White Noise (0.32 g)	Peak/RMS			**Northridge**	Peak/RMS		
State	$(x_2 - x_1)$ (mm)	x_2 (mm)	$\ddot{x}_{1A}$ (m/sec^2)	State	$(x_2 - x_1)$ (mm)	x_2 (mm)	$\ddot{x}_{1A}$ (m/sec^2)
Uncontrolled	47.7/14.8	33.8/9.9	30.20/9.30	Uncontrolled	54.9/10.7	44.3/7.3	34.82/6.79
URC	18.9/4.8	15.1/4.1	15.10/3.50	URC	37.3/4.7	33.6/3.6	25.30/2.97
CRC	19.8/5.1	15.7/4.2	14.20/3.60	CRC	38.0/4.6	33.5/3.5	25.77/3.01
SLQR	22.4/6.1	16.7/4.4	14.50/3.90	SLQR	36.3/4.6	34.7/3.5	26.31/2.93
El-Centro	Peak/RMS			**Kobe**	Peak/RMS		
State	$(x_2 - x_1)$ (mm)	x_2 (mm)	$\ddot{x}_{1A}$ (m/sec^2)	State	$(x_2 - x_1)$ (mm)	x_2 (mm)	$\ddot{x}_{1A}$ (m/sec^2)
Uncontrolled	23.4/3.6	15.9/3.5	14.79/3.48	Uncontrolled	28.6/5.0	22.9/3.7	18.06/3.17
URC	9.0/1.4	7.1/1.2	6.53/1.23	URC	17.0/3.2	18.1/3.0	14.34/2.26
CRC	8.3/1.5	7.3/1.3	6.34/1.27	CRC	17.7/3.4	18.0/3.0	12.84/2.29
SLQR	10.5/1.5	7.5/1.3	6.88/1.30	SLQR	21.9/3.7	20.3/3.1	14.43/2.41

Table 6-2 Simulation results for control cases for the original system ($\gamma_{BW} = 5.82$ m^{-1}).

White Noise (0.12 g)	Peak/RMS			**White Noise (0.2 g)**	Peak/RMS		
State	$(x_2 - x_1)$ (mm)	x_2 (mm)	$\ddot{x}_{1A}$ (m/sec^2)	State	$(x_2 - x_1)$ (mm)	x_2 (mm)	$\ddot{x}_{1A}$ (m/sec^2)
Uncontrolled	15.2/4.8	11.6/3.3	9.61/3.02	Uncontrolled	21.8/6.9	18.3/5.0	13.81/4.37
URC	5.9/1.8	6.0/1.6	4.43/1.29	URC	8.5/2.7	10.2/2.6	7.19/2.04
CRC	5.9/1.6	5.8/1.5	4.41/1.25	CRC	9.4/2.7	10.0/2.6	7.09/2.04
SLQR	7.4/2.1	6.2/1.6	4.90/1.38	SLQR	11.8/3.4	10.6/2.7	7.87/2.24
White Noise (0.32 g)	Peak/RMS			**Northridge**	Peak/RMS		
State	$(x_2 - x_1)$ (mm)	x_2 (mm)	$\ddot{x}_{1A}$ (m/sec^2)	State	$(x_2 - x_1)$ (mm)	x_2 (mm)	$\ddot{x}_{1A}$ (m/sec^2)
Uncontrolled	29.7/9.5	28.6/7.2	18.74/6.00	Uncontrolled	37.0/5.9	54.9/5.2	23.45/3.73
URC	15.4/4.0	16.4/4.2	12.91/3.12	URC	32.2/4.0	46.9/4.1	22.51/2.62
CRC	15.7/4.2	16.7/4.3	12.12/3.20	CRC	31.4/3.9	46.3/4.1	21.67/2.60
SLQR	17.7/5.2	17.7/4.4	12.12/3.46	SLQR	31.4/3.8	47.7/4.1	22.46/2.57
El-Centro	Peak/RMS			**Kobe**	Peak/RMS		
State	$(x_2 - x_1)$ (mm)	x_2 (mm)	$\ddot{x}_{1A}$ (m/sec^2)	State	$(x_2 - x_1)$ (mm)	x_2 (mm)	$\ddot{x}_{1A}$ (m/sec^2)
Uncontrolled	16.1/3	14/2.7	10.16/2.70	Uncontrolled	27.9/5.5	29.9/5.0	17.60/3.50
URC	7.1/1.4	7.7/1.2	5.85/1.16	URC	15.2/3.0	23.0/3.4	12.72/2.18
CRC	7.8/1.4	7.6/1.1	6.03/1.15	CRC	16.7/3.2	23.3/3.4	12.81/2.12
SLQR	9.6/1.8	7.1/1.5	6.47/1.22	SLQR	20.0/3.5	29.6/3.6	13.71/2.35

Table 6-3 Simulation results for control cases for the modified system ($\gamma_{BW} = 29.1$ m^{-1}).

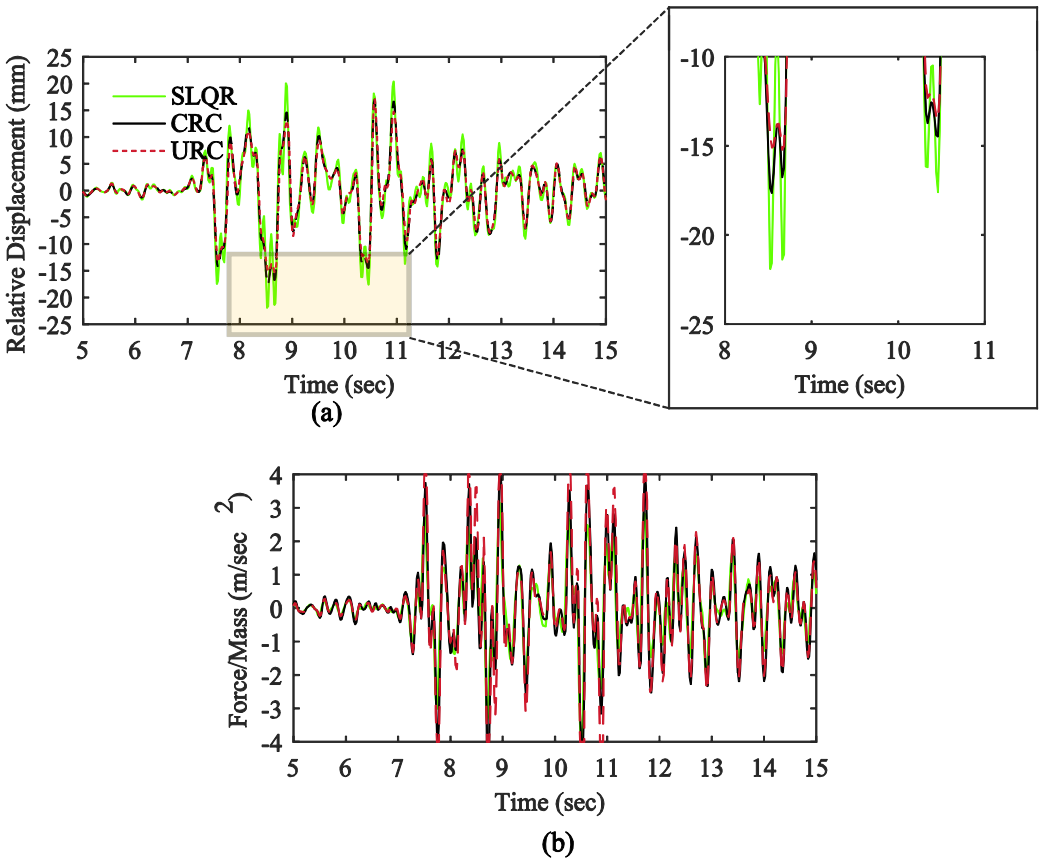

Figure 6-4 (a) The relative displacement of the structure with respect to foundation for CRC compared to SLQR; and (b) applied control forces for CRC compared to SLQR under Kobe ground motion for the modified system of the original system.

6.4 Closure

This chapter proposes reliability-based control algorithms using enhanced stochastic averaging of energy envelope to minimize the probability of system failure against stochastic excitations. Two new control techniques are developed: constrained reliability-based control (CRC) and unconstrained reliability-based control (URC) designs. These algorithms address current limitations in integration of reliability measures in design of control methods for nonlinear hysteretic systems. First, the Itô stochastic equation of

energy for the uncontrolled system is derived using enhanced stochastic averaging method to yield probability distribution function of system's energy. This initial step entails deriving an equivalent nonlinear stochastic system with an equivalent excitation intensity and modified damping parameters by applying the method of weighted residuals. The method of weighted residuals determines those parameters in terms of high order moments of system velocities. The proposed CRC design employs first-level analytical optimization based on Hamilton-Jacobi-Bellman equation for a given objective function and second-level numerical optimization to find optimal parameters of the objective function such that the probability of failure that is derived through enhanced stochastic averaging is minimized. In the URC design, a flexible dissipative form for the control force is considered and a numerical optimization is used to find the parameters of the control gain such that the probability of failure is minimized.

Chapter 7: Risk-Based Control Algorithms for Seismically Excited Nonlinear Systems

7.1 Introduction

Conventional performance-based control designs (e.g., a linear quadratic regulator) achieve their results by minimizing the variance in response variables such as roof displacement and inter-story drifts in multi-story buildings. However, the damage to structures due to seismic activity is best minimized by reducing the expected cost due to loss at different damage states, hence minimizing the risk of damage by natural hazards on structures. From this point of view, life cycle cost is considered a common measure for representing such risk: it includes both the initial cost and the maintenance cost following the earthquake through the remaining life of the structure, as described in Section 2.5. Taflanidis and Beck (2009) and Gidaris and Taflanidis (2015) implemented life cycle cost measure for design of passive systems, however those methods have not been extended to active or semi-active control designs. Moreover, those methods are computationally very demanding and their potential extension to active and semi-active strategies will require significantly more computational resources.

A comprehensive and computationally efficient framework is developed based on life cycle cost criteria for design of active controllers for seismically excited nonlinear multi-story buildings. This framework models loss based on damage states due to inter-story

drifts, and the expected costs are identified accordingly. The probabilistic properties of uncertain parameters of the system and the probability of exceedance of seismic activity are both considered in the framework. Computation and assessment of life cycle cost follow the approach established in Fereshtehnejad and Shafieezadeh (2016), where the failure probability abides by the crossing rate theory (Lutes and Sarkani, 1997), the stochasticity of uncertain parameters is embedded in the risk estimates, and nonlinearity of the system is accounted for based on stochastic linearization (El-Khoury et al., 2016).

This chapter is divided as follows. Section 7.2 develops the risk-based control framework. Section 7.2.1 derives the representation of the uncontrolled system, and the computations and assumptions of corresponding costs due to damage. Section 7.2.2 introduces two analytical control frameworks: the risk-based linear quadratic regulator (R-LQR) and the unconstrained risk-based regulator (URR). R-LQR optimization obtains the control gain matrix by applying the conventional LQR solution and then minimizing the life cycle cost. In contrast, URR optimization obtains the control gain matrix by directly minimizing the life cycle cost. Section 7.3 discusses the numerical example (nonlinear multi-story building subjected to seismic excitations) and analyzes the results from different control cases: an uncontrolled case and a controlled case equipped with R-LQR, URR, and conventional linear quadratic regulator. The results are generated using stochastic simulations (Latin hypercube sampling) for artificial and real seismic excitations. Section 7.4 summarizes and concludes the research study.

7.2 Methodology

This section introduces the risk-based control framework based on the total probability theorem and crossing rate technique (Lutes and Sarkani, 1997). The following sections present a general infrastructure system then further develop the framework for multi-story buildings. The damage is expressed in terms of inter-story drift. Given the stochastically linearized system, the optimization is applied to minimize the life cycle cost. In this regard, the uncontrolled system is presented in subsection 7.2.1. In section 7.2.2, two control algorithms are depicted for the controlled state: risk-based linear quadratic regulator and unconstrained risk-based regulator.

7.2.1 Uncontrolled System

The status-quo system corresponding to the uncontrolled system is presented in state space form as:

$$\dot{\mathbf{X}} = \boldsymbol{G}_{\mathbf{state}}(\mathbf{X}) + \mathbf{F_e} \approx \mathbf{A}_{\text{state}}\mathbf{X} + \mathbf{F_e} \tag{7.1}$$

where the state space vector $\mathbf{X}$ consists of the displacement, velocity, and other nonlinear response variables of the entire system, and $\mathbf{A}_{\text{state}}$ is the state matrix. The excitation vector $\mathbf{F_e}$ identifies a particular hazard; for a seismic activity, the vector includes the ground motion acceleration $\ddot{x}_g$. The state function, $\boldsymbol{G}_{\mathbf{state}}(\mathbf{X})$, includes the full nonlinear behavior of the system (e.g., hysteretic behaviors in a multi-story building). The nonlinear term $\boldsymbol{f}_{\mathbf{state}}(\mathbf{X})$ is linearized to the term $\mathbf{A}_{\text{state}}\mathbf{X}$ based on stochastic linearization, as mentioned earlier. For this purpose, the Lyapunov equation, presented later as Equation (7.18), is solved to determine the covariance matrix of the state vector $\mathbf{X}$ (Wen, 1980; Robert and

Spanos, 2003) and to further compute probabilities of failure and life cycle cost (Lutes and Sarkani, 1997).

In this research, the life cycle cost (LCC) for *n* years is defined as:

$$\mathrm{LCC} = \mathrm{ICC} + P(\mathrm{EQ}) \times K_{\gamma}^{n} \times \mathrm{E}(\mathrm{Loss}) + K_{\gamma}^{n} \times \mathrm{AMC} \tag{7.2}$$

where ICC is the initial construction cost and is considered to be 0.91 times the replacement cost (RC); the unit cost of construction is considered to be 75 \$/ft^2 (Jalayer et al., 2011; Fereshtehnejad and Shafieezadeh, 2016); and $P(\mathrm{EQ})$ is the annual probability of earthquake occurrence. The unit construction cost is the sum of the cost of constructing the building and is given per square foot (Jalayer et al., 2011). The annual maintenance cost (AMC) is considered to be 1% of ICC (Jalayer et al., 2011). K_{γ}^{n} is the cumulative discount factor for *n* years, and is defined as:

$$K_{\gamma}^{n} = \sum_{t=1}^{n-1} {\gamma_{\mathrm{df}}}^{t} \tag{7.3}$$

where the discount factor γ_{df} is defined as:

$$\gamma_{\mathrm{df}} = \left(\frac{1}{1+\delta_{\mathrm{dr}}}\right) \tag{7.4}$$

where δ_{dr} represents the discount rate. Notably, the controlled state includes the initial cost and maintenance cost of the control device in addition to the aforementioned costs of the uncontrolled system. Assuming a Poisson distribution, the annual probability of at least one earthquake occurrence $P(\mathrm{EQ})$ is expressed as:

$$P(\mathrm{EQ}) = 1 - \exp\left(-v_{EQ}\right) \tag{7.5}$$

where v_{EQ} is the mean annual rate of hazard occurrence. $\mathrm{E}(\mathrm{Loss})$ is the total annual loss or alternatively average annual repair cost associated with the damage induced by the

hazard on the system. Based on the total probability theorem and the conditional probability chain rule, $\mathrm{E}(\mathrm{Loss})$ is expressed as:

$$\mathrm{E}(\mathrm{Loss}) = \int_{IM} \sum_{i=0}^{4} \mathrm{E}(\mathrm{Loss}|DS_i) \times P(DS_i|IM)\, f(IM) dIM \tag{7.6}$$

where $\mathrm{E}(\mathrm{Loss}|DS_i)$ is the average cost of the estimated loss or equivalently the repair cost required to restore the structure to its initial condition for a particular damage state i (DS_i). The losses include those due to damage to structural components, nonstructural drift sensitive components, nonstructural acceleration sensitive components, and contents as a percentage of replacement cost (FEMA, 2003):

$$\mathrm{E}(\mathrm{Loss}|DS_i) = \mathrm{E}(\text{Repair Cost}|DS_i) = \%\text{ of RC} \tag{7.7}$$

The index i (= 0…4) corresponds to the damage state: 0 for intact, 1 for light, 2 for moderate, 3 for extensive, and 4 for collapse states. Intuitively, the higher the damage state, the greater the loss is. In this framework, the cost of human casualties is not considered.

The probability of damage state $P(DS_i|IM)$ is calculated using the crossing rate technique, as shown later in Equation (7.9). $f(IM)$ is the annual probability density function of the intensity measure IM. The intensity measure IM is the peak ground acceleration (PGA), and the corresponding probability is denoted by $P(\mathrm{PGA})$. The annual probability $P(\mathrm{PGA})$ is determined as follows (Kiureghian, 2005; Fereshtehnejad and Shafieezadeh, 2016):

$$P(\mathrm{PGA}) = \frac{\Delta\lambda_{\mathrm{AR}}(\mathrm{PGA})}{\nu_{EQ}} \tag{7.8}$$

The mean annual rate of exceedance $\lambda_{\mathrm{AR}}(\mathrm{PGA})$ can be determined from probabilistic seismic hazard analysis. For simplicity herein, the continuous probability distribution

$P(\text{PGA})$ is discretized and a summation operator substitutes the integration operator in Equation (7.6), giving:

$$\text{E(Loss)} = \sum_{\text{PGA}} \sum_{i=0}^{4} E(\text{Loss}|DS_i) \times P(DS_i|\text{PGA})\, P(\text{PGA}) \tag{7.9}$$

Noticeably, $\sum_{\text{PGA}} P(\text{PGA})$ equals 1 across the whole domain. While the loss due to DS_0 is considered to be zero, the probability of the damage state $P(DS_h|\text{PGA})$ is determined for the four damage levels 1 to 4 as follows:

$$P(DS_h|\text{PGA}) = P(b_{h-1} \leq DR \leq b_h)\ ;\ h = 1 \ldots 4 \tag{7.10}$$

The extent of damage defined in Equation (10) is based on drift (DR) levels. The seismic drift ranges are 0.00-0.20% for intact, 0.20-0.40% for light, 0.40-1.00% for moderate, 1.00-1.80% for extensive, and ≥ 1.80% for collapse damage states (Abad et al., 2013). b_{h-1} and b_h are the lower and upper bounds, respectively of drifts at the *h*th damage level (e.g. for the light damage level DS_1, b_0 and b_1 are 0.20% and 0.40% respectively). The probability of failure corresponding to the *h*th damage level (i.e. 1…4) due to drift can be expanded as:

$$P(DS_h|\text{PGA}) = \int \ldots \int P_{\emptyset}(b_{h-1} \leq DR \leq b_h) \times g_p(\emptyset_1, \ldots, \emptyset_s)\mathrm{d}\emptyset_1 \ldots d\emptyset_s \tag{7.11a}$$

$$\int \ldots \int g_p(\emptyset_1, \ldots, \emptyset_s)\mathrm{d}\emptyset_1 \ldots d\emptyset_s = 1 \tag{7.11b}$$

$g_p(\emptyset_1, \ldots, \emptyset_s)$ is the probability density function of the uncertain parameters $(\emptyset_1, \ldots, \emptyset_s)$ (Scruggs et al., 2006). The uncertain parameters may include the stiffness, mass, and damping variables of the given system. Assuming a Gaussian distribution of the drift response, the probability of failure $P_{\emptyset}(b_{h-1} \leq DR \leq b_h)$ within time T corresponds to the

probability of a drift ranging between b_{h-1} and b_h. T is equal to 30 seconds to present seismic excitation (Scruggs et al., 2006). The failure probability follows a Poisson distribution and is achieved using the crossing rate technique (Lutes and Sarkani, 1997; Casciati and Roberts, 1996), shown by:

$$P_{\emptyset}(b_{h-1} \leq DR \leq b_h) = P_{\emptyset}(DR \geq b_{h-1}) - P_{\emptyset}(DR \geq b_h) = \Big(1 - \exp\Big(-v_{\mathrm{CR}}(\emptyset)_{\Sigma_{b_{h-1}}}(T)\Big) - \Big(1 - \exp\Big(-v_{\mathrm{CR}}(\emptyset)_{\Sigma_{b_h}}T\Big)\Big)\Big) = \exp\Big(-v_{\mathrm{CR}}(\emptyset)_{\Sigma_{b_h}}T\Big) - \exp\Big(-v_{\mathrm{CR}}(\emptyset)_{\Sigma_{b_{h-1}}}T\Big) \tag{7.12}$$

The drift is considered to be a stationary Gaussian variable. Substituting Equation (7.12) in (7.11a), the probability of failure corresponding to the *h*th damage is:

$$P(DS_h|IM) = \int \ldots \int \exp\left(-v_{\mathrm{CR}}(\emptyset)_{\Sigma}^{\ b_h}T\right) - \exp\left(-v_{\mathrm{CR}}(\emptyset)_{\Sigma}^{b_{h-1}}T\right) \times g_p(\emptyset_1, \ldots, \emptyset_s)\mathrm{d}\emptyset_1 \ldots d\emptyset_s \tag{7.13}$$

The total crossing rate $v_{\mathrm{CR}}(\emptyset)_{\Sigma_{b_{h-1}}}$ is the summation of p failures due to b_{h-1} drift assuming the failures are unlikely or highly uncorrelated (Scruggs et al., 2006), defined as:

$$v_{\mathrm{CR}}(\emptyset)_{\Sigma}^{b_{h-1}} = v_{\Sigma}^{b_{h-1}} = \sum_{m=1}^{\mathrm{p}} v_{b_{h-1}}^{m} \tag{7.14}$$

It is noteworthy that the assumptions of stationary, uncorrelated, and Gaussian variables may induce error for realistic systems. In the future research, the frameworks will be expanded to include nonstationary correlated variables. On the other hand, the evaluation of the multiple integrals in Equation (7.13) is not trivial and its dimension grows significantly with the number of uncertain parameters. For simplicity, the integral is approximated by applying the first order second moment method, as follows:

$$P(DS_h|IM) = \int \ldots \int \exp\left(-v_{\mathrm{CR}}(\emptyset)_{\Sigma}^{b_h} T\right) - \exp\left(-v_{\mathrm{CR}}(\emptyset)_{\Sigma}^{b_{h-1}} T\right) \tag{7.15}$$

$$\times g_p(\emptyset_1, \ldots, \emptyset_s)\mathrm{d}\emptyset_1 \ldots . d\emptyset_s$$

$$\approx \left(\exp\left(-\bar{v}_{\mathrm{DR}}(\emptyset)_{\Sigma}^{b_h} T\right) - \exp\left(-\bar{v}_{\mathrm{DR}}(\emptyset)_{\Sigma}^{b_{h-1}} T\right)\right)$$

$$\times \int \ldots \int \times g_p(\emptyset_1, \ldots, \emptyset_s)\mathrm{d}\emptyset_1 \ldots . d\emptyset_s = \left(\exp\left(-\bar{v}_{\mathrm{DR}}(\emptyset)_{\Sigma}^{b_h} T\right)\right.$$

$$\left. - \exp\left(-\bar{v}_{\mathrm{DR}}(\emptyset)_{\Sigma}^{b_{h-1}} T\right)\right)$$

The averaged total crossing rate $\bar{v}_{\mathrm{DR}}\,(\emptyset)_{\Sigma}^{b_{h-1}}$ for b_{h-1} is denoted as:

$$\bar{v}_{\mathrm{DR}}\,(\emptyset)_{\Sigma}^{b_{h-1}} = \sum_{m=1}^{\mathrm{p}} \bar{v}_{b_{h-1}}^{m} \tag{7.16a}$$

$$\bar{v}_{b_{h-1}}^{m} = \frac{\mathrm{E}\left(\sigma_{\dot{DR}_m}\right)}{\pi\ \mathrm{E}\left(\sigma_{DR_m}\right)} \exp\left(-\frac{{b_{h-1}}^2}{2\mathrm{E}\left(\sigma_{\dot{DR}_m}\right)^2}\right) \tag{7.16b}$$

where the expectation of the standard deviations of drift $E\left(\sigma_{DR_m}\left(\overline{\emptyset}, \sigma\left(\overline{\emptyset}\right)\right)\right)$ and of the time differential $\mathrm{E}\left(\sigma_{\dot{DR}_m}\left(\overline{\emptyset}, \sigma\left(\overline{\emptyset}\right)\right)\right)$ of the mth node is determined using Taylor Series as:

$$\mathrm{E}\left(\sigma_{DR_m}\right) = \mathrm{E}\left(\sigma_{DR_m}\left(\emptyset = \overline{\emptyset} + \Delta\emptyset\right)\right)$$

$$= \mathrm{E}\left(\sigma_{DR_m}\left(\overline{\emptyset}\right)\right) + \mathrm{E}\left(\frac{1}{2}\sum_{i=1}^{p} \frac{\partial^2 \sigma_{DR_m}\left(\overline{\emptyset}\right)}{\partial \emptyset_i^2} \Delta\emptyset_i \Delta\emptyset_i\right) + \mathrm{HOT}$$

$$= \mathrm{E}\left(\sigma_{DR_m}\left(\overline{\emptyset}\right)\right) + \frac{1}{2}\sum_{i=1}^{p} \frac{\partial^2 \sigma_{DR_m}\left(\overline{\emptyset}\right)}{\partial \emptyset_i^2} E(\Delta\emptyset_i \Delta\emptyset_i) + \mathrm{HOT}$$

$$= \sigma_{DR_m}\left(\overline{\emptyset}\right) + \frac{1}{2}\sum_{i=1}^{p} \frac{\partial^2 \sigma_{DR_m}\left(\overline{\emptyset}\right)}{\partial \emptyset_i^2} \sigma_{\emptyset_i}^2 + \mathrm{HOT} \tag{7.17a}$$

$$\mathrm{E}\left(\sigma_{\dot{DR}_m}\right) = \mathrm{E}\left(\sigma_{\dot{DR}_m}\left(\overline{\emptyset}, \sigma_{\emptyset_i}^2, \mathrm{HOT}\right)\right)$$
$$= \sigma_{D\dot{R}_m}\left(\overline{\emptyset}\right) + \frac{1}{2}\sum_{i=1}^{p} \frac{\partial^2 \sigma_{D\dot{R}_m}\left(\overline{\emptyset}\right)}{\partial \emptyset_i^2} \sigma_{\emptyset_i}^2 + \mathrm{HOT} \tag{7.17b}$$

where $\overline{\emptyset}$ ($\overline{\emptyset}_1$ ... $\overline{\emptyset}_p$ **)** is the mean vector of uncertain parameters, ($\sigma_{\emptyset_i}$ ... $\sigma_{\emptyset_p}$) are the corresponding standard deviations and $\Delta\emptyset$ is defined as $\emptyset - \overline{\emptyset}$. The uncertain parameters here are considered to be uncorrelated. HOT includes higher order terms of Taylor's expansion. If HOT is incorporated, higher order moments of the uncertain parameters can be considered accordingly. The standard deviations, $\sigma_{DR_m}\left(\overline{\emptyset}\right)$ and $\sigma_{D\dot{R}_m}\left(\overline{\emptyset}\right)$, can be determined using the Lyapunov equation as follows:

$$\mathbf{0} = \mathbf{A_{state}S_{COV}} + \mathbf{S_{COV}A_{state}}^{\mathbf{T}} + \mathbf{T_e} \tag{7.18}$$

where $\mathbf{S_{COV}}$ defines the covariance matrix of the state vector and $\mathbf{T_e}$ is a vector that identifies the intensity level of the ground motion (El-Khoury et al., 2015a; El-Khoury et al., 2015b; El-Khoury et al., 2016).

7.2.2 Controlled System

The objective here is to introduce a control methodology that can explicitly alleviate the life cycle cost. The controlled system is represented as:

$$\dot{\boldsymbol{x}} = \boldsymbol{G_{state}}(\mathbf{X}) + \mathbf{Bu} + \mathbf{F_e} \approx \mathbf{A}_{\mathrm{state}}\mathbf{X} + \mathbf{Bu} + \mathbf{F_e} \tag{7.19}$$

The control force vector **u** is considered linear and equals to $\boldsymbol{K_u}\mathbf{X}$ where the gain matrix $\boldsymbol{K_u}$ is determined by minimizing the objective function representing the life cycle cost. **B** is the location matrix of controllers. The life cycle cost (LCC) for n years at the controlled state is defined as

$$\mathrm{LCC} = \mathrm{ICC} + P(\mathrm{EQ}) \times K_\gamma^n \times E(\mathrm{Loss}) + K_\gamma^n \times \mathrm{AMC} + \mathrm{C_{controller}} \tag{7.20}$$

where the controller cost $\mathrm{C_{controller}}$ is added to the life cycle cost. The controller cost $\mathrm{C_{controller}}$ is defined as:

$$\mathrm{C_{controller}} = \mathrm{ICo} + \mathrm{AMCC} \times K_\gamma^n \tag{7.21a}$$

$$\mathrm{MCC} = \mathrm{AMCC} \times K_\gamma^n \tag{7.21b}$$

where ICo is the initial controller cost and AMCC is the annual controller maintenance costs. The maintenance cost MCC includes the mobilization cost and the calibration cost of each actuator. The objective of this control design is to minimize the life cycle cost. For the uncontrolled case, the controller cost $\mathrm{C_{controller}}$ is zero, and the annual maintenance cost AMC and initial construction ICC of the building excluding the controller cost is assumed to be the same for both controlled and uncontrolled states. The objective is to evaluate the life cycle cost of the controlled case $\mathrm{LCC_{controlled}}$ and compare it with that of uncontrolled case ($<$ $\mathrm{LCC_{uncontrolled}}$).

Two control strategies are derived. The first control algorithm, risk-based linear quadratic regulator (R-LQR), employs two levels of optimization. The first level is based on LQR and minimizes the second order moment of inter-story drifts, and the second level searches for optimal gains to minimize the expected life cycle cost of the system. This is depicted as:

$$[\boldsymbol{K}_{\mathbf{u}}^*, {\theta_i}^*] = \arg\min\left(\sum_{i=0}^{n} \boldsymbol{R}^{\boldsymbol{T}} \mathbf{u} \boldsymbol{R} + \sum_{i=1}^{w} \theta_{\mathrm{r}_i} (x_i - x_{i-1})^2 \right)\Big|_{\boldsymbol{K}_{\mathbf{u}}, \theta_{\mathrm{r}_i}} \tag{7.22a}$$

$$\left[\boldsymbol{K}_{\mathbf{u}}^*, {\theta_{\mathrm{r}_i}}^*\right] = \arg\min(\mathrm{LCC})\big|_{\boldsymbol{K}_{\mathbf{u}}, \theta_{\mathrm{r}_i}} \tag{7.22b}$$

$$\mathbf{u} = \boldsymbol{K}_{\mathbf{u}}^* \mathbf{X} = -\boldsymbol{R}^{-1} \mathbf{B}^{\mathbf{T}} \boldsymbol{P}_{\mathbf{R-LQR}} \mathbf{X} \tag{7.22c}$$

where $\boldsymbol{K_u}$, θ_{r_i}, and $\boldsymbol{R}$ are the control gain, drift weights, and positive definite weighted matrix for control force, respectively. The asterisk symbol (*) corresponds to the optimal solution. w is the number of stories. The matrix $\boldsymbol{P_{R-LQR}}$ corresponds to the optimal positive definite symmetric matrix corresponding to the optimal θs (θ^*). The second algorithm, unconstrained risk-based regulator (URR), directly minimizes the expected life cycle cost as follows:

$$\boldsymbol{K_u^*} = \arg\min(\text{LCC})|_{\boldsymbol{K_u}} \tag{7.23a}$$

$$\boldsymbol{K_u^*} = -\boldsymbol{R^{-1}}\mathbf{B^T}\,\boldsymbol{P_{URR}}\mathbf{X} \tag{7.23b}$$

where $\boldsymbol{P_{URR}}$ corresponds to the optimal positive definite symmetric matrix to produce stable dissipative forces (Taflanidis et al., 2008). Controller capacity is defined by a maximum force ($u_{\max}$). An upper bound of the standard deviation of every control force is applied to the control algorithm to account for the maximum capacity of the corresponding control device. Because the control force is assumed to be a Gaussian variable, the ratio between the maximum and the standard deviation ($u_{\max}/\sigma_u$) is considered to be equal to 3.3, which corresponds to a 99.97% confidence interval (Kester, 2005; Moghimi, 2010).

The control design minimizes the losses due to seismic vibrations. The optimization process is carried out by analytically determining the covariance matrix of the system and further computing the objective function. The control gain is computed by either R-LQR or URR. Finally, Latin hypercube sampling is applied to calculate and compare the averaged LCC and study the performance for both the controlled and uncontrolled states (Figure 7-1).

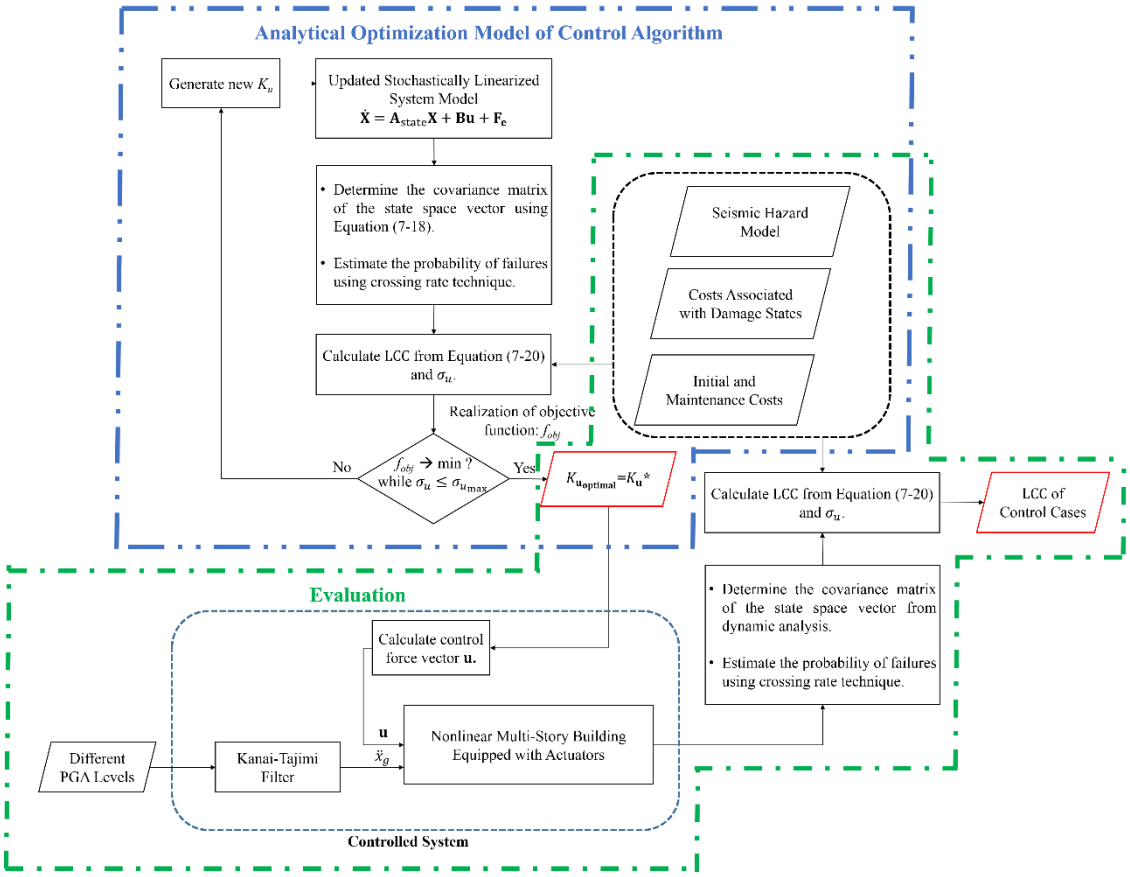

Figure 7-1 Risk-Based Control Framework.

7.3 Numerical Example

The proposed framework is applied and demonstrated for a four story nonlinear reinforced concrete frame building. The building is considered an office building and the floor plan and elevation sections are shown in Figure 7-2. The plan is composed of five bays in longitudinal direction and three bays in transverse direction. The dimensions of each bay are 24'× 24'. The story height is 12' throughout. The seismic design of the building complies with the Uniform Building Code (ICBO, 1988) and FEMA 273 (BSCC, 1997).

The fundamental period of the building is 0.30 seconds and the building has a classical damping of 5%. Further details of this design can be found in Gupta and Kunnath (2000).

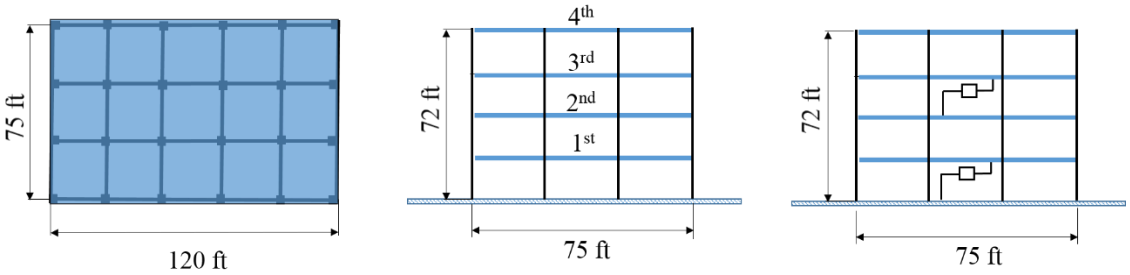

Figure 7-2 Four Story Concrete moment resisting frame (MRF) (Business/Office).

To characterize the system here, the story stiffnesses and mass are derived from performing a static pushover analysis that satisfies the following conditions: a fundamental period equals 0.30 seconds and an averaged slope of 0.50 for the normalized base shear and roof displacement as shown in Gupta and Kunnath (2000). The system is further calibrated to characterize the post-yield behavior. This is achieved by matching the inter-story drifts (Figure 7-3a) for all stories subjected to fn Northridge, 1994, Newhall (LA13) (civil.eng.buffalo.edu/Sac_records) to the results shown in Gupta and Kenneth (2000). The hysteretic nonlinearity is characterized using the Bouc Wen model (Ikhouane et al., 2007; Ismail et al., 2009); the Bouc Wen model used here obeys class I, which is considered asymptotically dissipative and thermodynamically stable (Ikhouane et al., 2007). Figure 7-3a depicts the inter-story drifts of the system under LA13. The base shear forces and roof

displacements are shown in Figure 7-3b and a close match is observed relative to the results found in Gupta and Kunnath (2000).

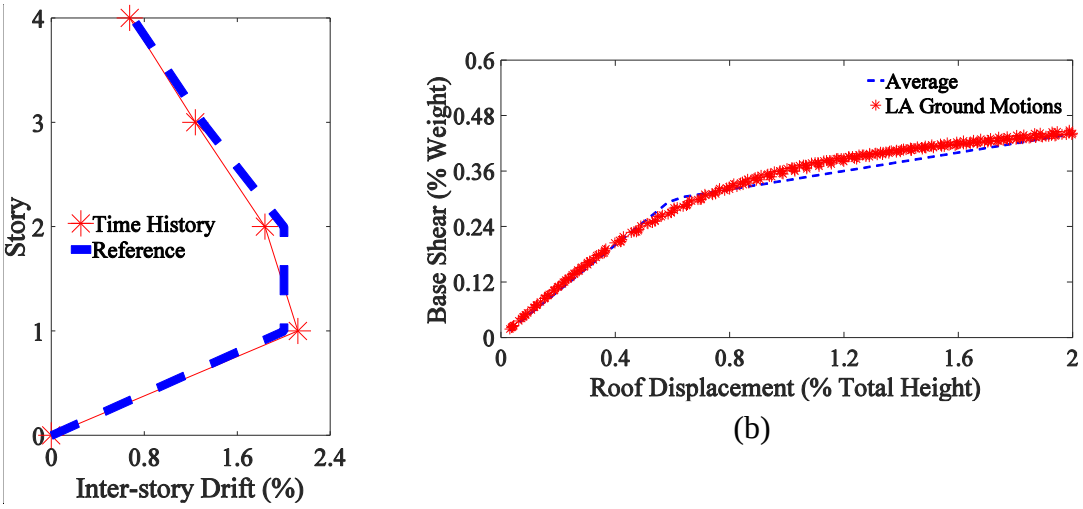

(a) (b)

Figure 7-3 (a) Inter-story drifts profiles for the four story building under fn Northridge, 1994, Newhall ground motion (Reference: Gupta and Kunnath, 2000) and (b) base shear versus roof displacement for the four story building (story mass and story stiffness are 1.037E+06 kg and 4.19E+08 N/m, respectively).

For this particular example, the objective is to minimize the life cycle cost defined in Equation (7.20). The risk-based control algorithms are demonstrated for different cases where the number and location of actuators are varied. The following six cases are adopted:

- Case-0 for uncontrolled state.
- Case-1 for one actuator on the first floor.
- Case-2 for two actuators installed on the first floor.
- Case-3 for two actuators installed on the first and third floors (See Figure 7-2c).

- Case-4 for three actuators installed on the first, second, and third floors.
- Case-5 for one actuator on every floor.

The control algorithms are compared to uncontrolled state and controlled state equipped with conventional linear quadratic regulator (LQR). The results are generated for artificial and historic ground motions. The artificial ground motions are simulated to determine and analyze the life cycle cost for all cases. The historic ground motions are extracted from SAC LA ground motions (civil.eng.buffalo.edu). In this respect, a pair of the historic ground motion are considered for fault-normal (fn) and fault-parrallel (fp) directions. The properties (peak ground acccleration, earthquake magnitude, time step, distance, and scale factor) of the LA ground motions comply with the values given in civil.eng.buffalo.edu/Sac_records/LA. The results are analyzed in the following section.

7.3.1 Results

After modeling the system, the control algorithms (R-LQR and URR) are designed and optimized analytically. The system is linearized using a classical Kanai-Tajimi filter and the Lyapunov equation (Equation (7.18)) is solved analytically. The classical Kanai-Tajimi filter is a good approach for generating artificial earthquakes and properties such as non-stationarity can be added to more closely approximate an actual earthquake (Amiri et al., 2007). Herein, the classical stationary Kanai-Tajimi filter (Kanai, 1957; Tajimi, 1960) is used and corresponds to a linear filter under white Gaussian noise $n(t)$, and is denoted as:

$$H(j\omega) = \frac{1 + 2\zeta_g j\left(\omega/\omega_g\right)}{1 - \left(\omega/\omega_g\right)^2 + 2\zeta_g j\left(\omega/\omega_g\right)} \tag{7.24a}$$

$$\ddot{x}_{KT} + 2\zeta_g\omega_g\dot{x}_{KT} + \omega_g^2 x_{KT}(t) = n(t) \tag{7.24b}$$

where $H(j\omega)$ is the frequency response function, j is $\sqrt{-1}$, and $\ddot{x}_{KT}$ is the artificially generated acceleration using the Kanai-Tajimi filter. The parameters ω_g (= 5 rad/sec) and ζ_g (= 0.2) are the angular frequency and the damping content, respectively for the soft soil conditions, and depend on the distance from the epicenter and the rigidity of the ground layer (Kiureghian and Neuenhofer, 1992). For R-LQR, the control gain is determined using Equation (7.22c), where the matrix $\boldsymbol{P}_{\mathbf{R-LQR}}$ is controlled by the LQR design. For URR, the control gain is determined using an unconstrained matrix $\boldsymbol{P}_{\mathbf{URR}}$ in the numerical optimization. For instance, the initial guess of $\boldsymbol{P}_{\mathbf{URR}}$ is equal to $\boldsymbol{P}_{\mathbf{R-LQR}}$; upper and lower bounds are enforced in the optimization to ensure adherence to the semi-positive definite requirement and the forces' upper bound. Both matrices should be positive definite to comply with stability conditions and generate dissipative forces.

From Section 7.2, the life cycle cost for uncontrolled and controlled states is represented for n-years (n = 100) as:

$$\mathrm{LCC}_{\mathrm{uncontrolled}} = \mathrm{ICC} + P(\mathrm{EQ}) \times K_\gamma^n \times E(\mathrm{Loss}) + K_\gamma^n \times \mathrm{AMC} \tag{7.25a}$$

$$\mathrm{LCC}_{\mathrm{controlled}} = \mathrm{ICC} + P(\mathrm{EQ}) \times K_\gamma^n \times E(\mathrm{Loss}) + K_\gamma^n \times \mathrm{AMC} + \mathrm{C}_{\mathrm{controller}} \tag{7.25b}$$

$$\mathrm{C}_{\mathrm{controller}} = \mathrm{ICo} + \mathrm{AMCC} \times K_\gamma^n \tag{7.25c}$$

$$\mathrm{ICo} = \mathrm{AC} + \mathrm{IAC} + \mathrm{WSC} + \mathrm{SHCC} \tag{7.25d}$$

The initial cost ICC and annual maintenance cost AMC are the same for uncontrolled and controlled cases. They are excluded here since they are assumed fixed and equal for both controlled and uncontrolled states. The initial controller cost ICo consists of the costs of the actuator, AC, the installation cost, IAC, the cost for a wireless data acquisition system, WSC, and the servo hydraulic controller cost, SHCC. The actuator cost AC at Shore

Western is approximately \$110 K. The installation cost IAC includes the labor cost (= \$2 K per day: 1 day for 1 actuator, 1.5 days for 2 actuators, 1.75 for 3 actuators, and 2 days for 4 actuators) and the mobilization cost (= \$1 K). The cost WSC is \$0.6 K per node (Kim et al., 2007). In this study, the wireless system is installed to support one accelerometer for each floor; therefore, four nodes are considered here. According to Shore Western, the cost of a servo hydraulic controller unit is \$20 K + (NA – 1) × \$13.3 K, where NA represents the number of actuators. Furthermore, new parameters are redefined as:

$$\mathrm{Re}_{\mathrm{COST}} = P(\mathrm{EQ}) \times K_{\gamma}^{n} \times E(\mathrm{Loss}) \tag{7.26a}$$

$$\mathrm{Sv} = \mathrm{LCC}_{\mathrm{uncontrolled}} - \mathrm{LCC}_{\mathrm{controlled}} \tag{7.26b}$$

$$\mathrm{MCC} = \mathrm{AMCC} \times K_{\gamma}^{n} \tag{7.26c}$$

The repair cost $\mathrm{Re}_{\mathrm{COST}}$ is the total cost to restore the building after an earthquake event. However, for evaluating the saving Sv of using different control cases and comparing them with the uncontrolled state, the controller cost $\mathrm{C}_{\mathrm{controller}}$ is added. MCC the maintenance controller cost spanned over *n*-years. The annual maintenance controller cost AMCC incorporates the cost to calibrate the actuators and maintain the wireless data acquisition system and a servo hydraulic controller. In consultation with Shore Western, hydraulic actuators are used in this research, with each actuator having the capacity of 1,000 kN. Based on those consultations, the maintenance cost of actuators including the costs of mobilization and calibration can be determined as:

$$\mathrm{AMCC} = \mathrm{MoC} + \mathrm{NA} * \mathrm{CCC}\ (\$) \tag{7.27}$$

MoC (= \$1,000) and CCC (= \$500) correspond to the mobilization cost and calibration cost per actuator, respectively. In Equation (7.7), $E(\text{Loss}|DS_i)$ is based on the replacement cost. These values are provided in Table 7-1 in FEMA (2003).

Repair Cost	Damage Level			
	Light	Moderate	Extensive	Collapse
Structural	0.4	1.9	9.6	19.2
Non-structural drift	0.9	4.8	14.4	47.9
Non-structural acceleration	0.7	3.3	16.4	32.9
Contents	0.5	2.3	11.4	22.8

Table 7- 1 Repair cost in terms of the percentage of replacement cost of the building (RC = \$2.85E+06).

As stated above, the aim of this research is: (1) to evaluate whether the use of controllers that explicitly minimize life cycle cost is superior to the status quo case; and (2) whether the proposed controller can further optimize life cycle cost relative to conventional strategies. As a result, in addition to the uncontrolled system, a system equipped with a conventional LQR is used for reference. The conventional LQR is designed based on minimizing the second order moments of inter-story drift, and the objective function is:

$$\boldsymbol{K}_{\mathbf{u}} = \arg\min\left(\sum_{i=0}^{n} \boldsymbol{R}^{\boldsymbol{T}}\mathbf{u}\boldsymbol{R} + \sum_{i=1}^{w} \theta_{\mathrm{r}_i}(x_i - x_{i-1})^2\right) \tag{7.28}$$

In R-LQR, those factors are optimized to minimize the life cycle cost. Here, θ_{r}s are chosen to provide a maximum force provided by the actuator (i.e., 1,000 kNs per actuator).

To analyze life cycle cost, the Kanai-Tajimi filter presented in Equation (7.24a) is applied to the system; the annual rate of exceedance λ is given in Figure 7-4 (geohazards.usgs.gov). Corresponding to this hazard curve, the mean annual rate v_{EQ} of earthquake occurrence is equal to 0.584. The mass, damping, and stiffness are varied

probabilistically for each of the realizations selected by Latin hypercube sampling. The variation coefficient is applied to the mass, damping, and stiffness matrices as follows:

$$\mathbf{M_d} = £_{LHF} * \mathbf{M_p} \tag{7.29}$$

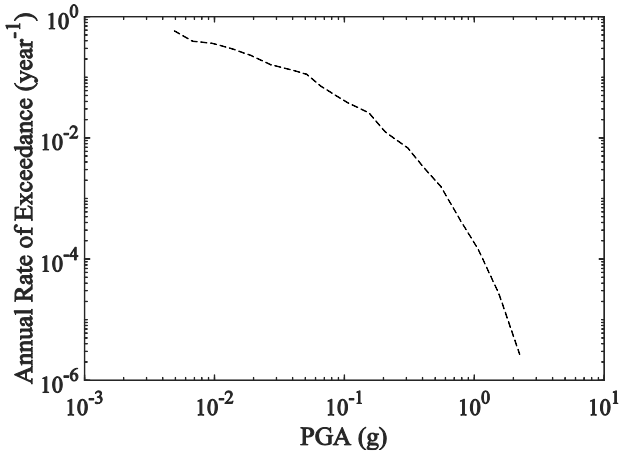

Figure 7-4 The annual rate of exceedance versus PGA (geohazards.usgs.gov) in Los Angeles (34.0522°, 118.2437°).

The results of $\mathrm{Re_{COST}}$ and Sv are described in Table 7-2 for conventional LQR and R-LQR. As mentioned above, different cases are analyzed in which the number of actuators NA and actuator location are varied. Use of more actuators for conventional LQR does not necessarily yield minimum repair costs (e.g. $\mathrm{Re_{COST}}$ in case-2 is lower than that in case-4 and case-5) and maximum savings (e.g. for case-4 and case-5 Sv < \$0), as shown in Table 7-2. Moreover, in case-2 for conventional LQR, the repair cost $\mathrm{Re_{COST}}$ is reduced by \$97.7 K and the saving is reduced by \$37.0 K relative to case-1, where one actuator is installed. The stakeholder may therefore decide to go with one actuator and adopt case-1 for a conventional-LQR, since an additional amount needs to be paid for an actuator in case-2. To optimize case-1 further, R-LQR is adopted and an improvement of \$32.0 K and \$245.6

K is achieved over the conventional LQR and uncontrolled cases, respectively. In addition, case-3 and case-2 correspond to the same controller cost $C_{controller}$, but the location of the actuators is different. In the conventional LQR and R-LQR cases, case-2 is superior to case-3, as shown in Table 7-2. As a result, case-3 may not be an optimal solution for stakeholders. For case-2, the conventional LQR approach provides a better Sv value of \$176.6 K compared to the uncontrolled state (Sv = \$0). Case-2 is further optimized using the R-LQR approach, and the savings are increased by \$113.0 K. Meanwhile, the conventional LQR designs of case-4 and case-5 are not economic (Sv < 0). In case-4 ($NA = 3$), the R-LQR design saves \$113.2 K with respect to case-5 ($NA = 4$, one per story). Applying the R-LQR strategy, the savings are increased significantly as depicted in Table 7-2. Additionally, a reliability measure defined by the probability of exceeding 1.00% drift (*DR*) P(*DR* $\geq$ 1.00%) is defined in Table 7-2 (i.e., this region corresponds to the extensive damage and collapse states). Case-5 yields the smallest probability of failure for R-LQR. Case-2 results in the smallest probability of failure for conventional LQR and the highest savings for R-LQR, as shown in Table 7-2 and Figure 7-5b. Although case-5 of R-LQR approach corresponds to the lowest repair cost (Figure 7-5a), its Sv value is the lowest among all controlled cases (Figure 7-5b). Overall, it can be seen for all cases that R-LQR yields higher savings than the conventional LQR.

Considering the stakeholders are willing to purchase more than one actuator, case-1, case-2, case-3, and case-4 are selected to be further optimized using the URR approach (See Table 7-2). URR is a more flexible approach, since it is not restricted by the LQR objective function. The only condition for the URR approach is to search for a positive definite matrix, $\boldsymbol{P}_{\mathbf{URR}}$, as mentioned previously. For case-1, the Re_{COST} of URR is equal to \$853.9

K, corresponding to a saving of $2.6 K when compared to the R-LQR approach, and the probability of failure P(DR ≥ 1.00%) is equal to 0.0282. For case-2, the Re_{COST} of URR is equal to $677.5 K, corresponding to a saving of $0.3 K when compared to the R-LQR approach, and the probability of failure P(DR ≥ 1.00%) is equal to 0.0225. For case-3, the Re_{COST} of URR is equal to $762.7 K, corresponding to a saving of $12.4 K when compared to the R-LQR approach, and the probability of failure P(DR ≥ 1.00%) is equal to 0.0221. For case-4, the Re_{COST} of URR is equal to $644.0K, corresponding to a saving of $5.6K, and the probability of failure P(DR ≥ 1.00%) is equal to 0.022.

Conventional LQR						
Re_{COST} ($)	Case-0	Case-1	Case-2	Case-3	Case-4	Case-5
	1268810	888539	790815	853158	1028090	1023967
ICo ($)	0	135400	259733	259733	383567	507400
MCC ($)	0	31260	41681	41681	52101	62521
P(DR ≥ 1.00%)	0.0414	0.0281	0.0242	0.0269	0.0342	0.0341
Sv ($)	0	213610	176581	114238	-194948	-325078
R-LQR						
Re_{COST} ($)	Case-0	Case-1	Case-2	Case-3	Case-4	Case-5
	1268810	856569	677791	775079	649468	642236
ICo ($)	0	135400	259733	259733	383567	507400
MCC ($)	0	31260	41681	41681	52101	62521
P(DR ≥ 1.00%)	0.0414	0.0283	0.0226	0.0258	0.0221	0.0219
Sv ($)	0	245580	289604	192317	183675	56653

Table 7-2 Results for risk-based parameters.

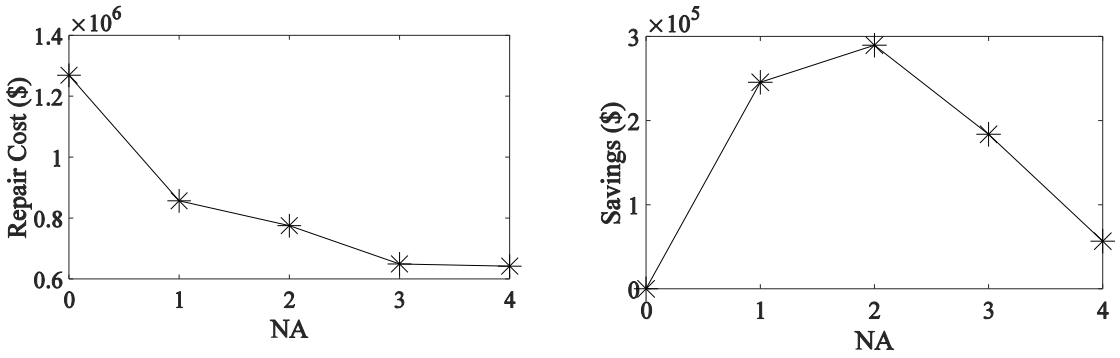

(a) (b)

Figure 7-5 (a) Repair cost versus NA. (b) Savings versus NA (R-LQR).

To analyze the peak performance of the control algorithms, the normalized drift J_{DR} is defined as follows:

$$J_{\mathrm{DR}} = \frac{\max(\mathrm{DR}_{\mathrm{controlled}})}{\max(\mathrm{DR}_{\mathrm{uncontrolled}})} \tag{7.30}$$

Using Latin hypercube sampling, random realizations are generated for the stiffness, damping, and mass, as mentioned in Equation (7.29). The averaged peak drift is defined as:

$$E(J_{\mathrm{DR}}) = E\left(\frac{\max(\mathrm{DR}_{\mathrm{controlled}})}{\max(\mathrm{DR}_{\mathrm{uncontrolled}})}\right) \tag{7.31}$$

The averaged peak drift is determined for the controlled and uncontrolled systems under LA ground motions (See Table 7-3). An improvement ($J_{\mathrm{DR}} < 1$) is recorded in most cases (i.e., for case-2, and the maximum inter-story drift decreases by 27.6% for the system equipped with R-LQR compared to the uncontrolled system under fp Northridge, 1994, Sylmar). Similar trends are reported for various controlled systems and different cases. For

case-3 with the URR approach, the maximum and minimum values of J_{DR} are 0.976 for fn North Palm Springs and 0.829 for fp Loma Prieta, 1989. For case-4 with the URR approach, the maximum and minimum values of J_{DR} are 1.044 for fp 1995 Kobe ground motion and 0.855 for fp Northridge, 1994, respectively. The stakeholder may therefore decide to select case-2 where two actuators are needed, achieving a significant improvement in savings (R-LQR is equal to \$289.6K; URR is equal to \$289.9K) and a J_{DR} value smaller than one for all ground motions except fn North Palm Springs, 1986.

Case (**LQR**)	fn Imperial Valley, 1940, El Centro	fp Imperial Valley, 1940, El Centro	fn Northridge, 1994, Newhall	fp Northridge, 1994, Newhall	fn Northridge, 1994, Sylmar	fp Northridge, 1994, Sylmar	fn North Palm Springs, 1986	fp North Palm Springs, 1986	fn 1995 Kobe	fp 1995 Kobe	fn 1989 Loma Prieta	fp 1989 Loma Prieta	fn 1994 Northridge	fp 1994 Northridge
1	0.923	0.913	0.898	0.895	0.885	0.900	0.994	0.915	0.919	0.878	0.919	0.876	0.861	0.917
2	0.898	0.822	0.966	0.859	0.794	0.805	1.034	0.820	0.841	0.770	0.849	0.749	0.742	0.835
3	0.928	0.891	0.911	0.886	0.881	0.903	0.997	0.910	0.926	0.883	0.924	0.867	0.859	0.921
4	1.070	0.890	0.989	0.960	0.826	0.862	1.058	0.782	0.859	0.807	0.855	0.757	0.802	0.877
5	1.074	0.893	0.993	0.950	0.824	0.863	1.052	0.781	0.863	0.802	0.859	0.756	0.802	0.879
Case (**R-LQR**)	fn Imperial Valley, 1940, El Centro	fp Imperial Valley, 1940, El Centro	fn Northridge, 1994, Newhall	fp Northridge, 1994, Newhall	fn Northridge, 1994, Sylmar	fp Northridge, 1994, Sylmar	fn North Palm Springs, 1986	fp North Palm Springs, 1986	fn 1995 Kobe	fp 1995 Kobe	fn 1989 Loma Prieta	fp 1989 Loma Prieta	fn 1994 Northridge	fp 1994 Northridge
1	0.923	0.900	0.901	0.885	0.883	0.884	0.963	0.904	0.920	0.878	0.919	0.859	0.869	0.900
2	0.949	0.754	0.921	0.850	0.775	0.749	0.974	0.799	0.869	0.774	0.831	0.724	0.757	0.787
3	0.928	0.883	0.905	0.865	0.878	0.867	0.971	0.888	0.931	0.887	0.928	0.826	0.875	0.889
4	1.021	0.905	0.939	0.976	0.928	0.860	0.912	1.011	1.055	0.997	1.003	0.923	0.933	0.898
5	0.985	0.893	0.919	0.977	0.903	0.836	0.903	1.003	1.062	1.007	0.977	0.913	0.916	0.880
Case (**URR**)	fn Imperial Valley, 1940, El Centro	fp Imperial Valley, 1940, El Centro	fn Northridge, 1994, Newhall	fp Northridge, 1994, Newhall	fn Northridge, 1994, Sylmar	fp Northridge, 1994, Sylmar	fn North Palm Springs, 1986	fp North Palm Springs, 1986	fn 1995 Kobe	fp 1995 Kobe	fn 1989 Loma Prieta	fp 1989 Loma Prieta	fn 1994 Northridge	fp 1994 Northridge
1	0.923	0.901	0.901	0.885	0.882	0.883	0.963	0.905	0.920	0.878	0.919	0.860	0.868	0.900
2	0.966	0.760	0.918	0.857	0.779	0.746	0.981	0.800	0.868	0.773	0.834	0.725	0.755	0.787
3	0.921	0.876	0.912	0.870	0.876	0.857	0.976	0.885	0.933	0.887	0.929	0.829	0.875	0.882
4	1.015	0.896	0.931	0.972	0.931	0.855	0.922	1.000	1.044	0.990	0.997	0.914	0.927	0.896

Table 7-3 Results for peak normalized inter-story drift under LA ground motions.

7.4 Closure

This research introduces on risk-based control algorithms with life cycle cost taken as the performance objective, a common measure for assessing potential damage and loss following an earthquake. The process here entails: (1) estimating the life cycle cost, and (2) optimizing the controller's performance. The life cycle cost includes the initial cost and the expected losses due to seismic events. Cost is described as stochastic and is approximated as a linear function of system repair costs. Repair costs are estimated based on the severity of the damage, which in turn is quantified in terms of probability for each damage level, defined as intact, light, moderate, extensive, and collapse. The probability of damage is calculated based on the total probability theorem and using the crossing rate technique. The stochasticity of the system is incorporated in terms of higher order moments of the corresponding parameters (stiffness, mass, and damping), and system uncertainty is based on fragility curves for the properties of ground motion in a particular region. After defining the life cycle cost, two control algorithms are designed. The first control algorithm, risk-based linear quadratic regulator (R-LQR), employs two levels of optimization, where the first level is based on LQR and minimizes the second order moment of inter-story drifts, and the second level obtains optimal gains to minimize the expected life cycle cost of the system. The second algorithm, unconstrained risk-based regulator (URR), directly minimizes the expected life cycle cost.

The framework is applied to a nonlinear multi-story building subjected to earthquake hazard. The control optimizations are performed on the stochastically linearized model of the system. These designs are compared to the status quo option and the structure equipped

with a conventional LQR control strategy. The number of controllers and their locations are varied in multiple cases. Results show that the proposed control methods reduce the life cycle cost and the extent of expected damage significantly when compared to the status quo (savings ranging from $180-290 K) (including actuator and maintenance costs for controlled systems) and compared to conventional LQR (savings ranging from $32-382 K). Additional results are presented for LA ground motions, and reasonable improvements are observed in the proposed control algorithms (i.e., for the system equipped with two actuators—located on the first and second floors and using the URR approach—subjected to the historical Imperial Valley, 1940, El Centro earthquake, the maximum displacement drift was reduced by 22% compared to the uncontrolled case). This proposed framework was capable of minimizing the lifecycle cost compared to conventional control states and the uncontrolled state. This is promising, considering the current framework and the possibility of expanding it to different structural systems subjected to various hazard types.

Chapter 8: Summary and Future Recommendations

This chapter summarizes the course of the research for the proposed control methodologies. Moreover, it presents the studies of every chapter in Section 8.1. Based on the research findings, the future directions are highlighted in Section 8.2.

8.1 Summary

This dissertation focused on two stages in structural control: (1) modeling nonlinear behavior in systems in response to stochastic excitations and (2) control design including dynamics and constraints of control devices. For modeling the nonlinearity and stochasticity, a method known as stochastic linearization (Chapter 3) was used and a stochastic averaging method was adopted and extended to enhanced stochastic averaging method (Chapter 4). State space control design based on nonlinear sliding mode control was developed (Chapter 3). In addition, a stochastic control method using enhanced stochastic averaging was introduced and was further extended to optimize reliability of systems. Multiple civil engineering applications subjected to seismic excitations were considered, including a nonlinear multi-span bridge (Chapter 3), a structure with nonlinear soil structure interactions (Chapters 4-6), and a nonlinear multi-story building (Chapter 7). Various control objective functions were studied such as drift, acceleration, pounding, energy, probability of failure, and life cycle cost.

Chapter 3 enhanced linear sliding mode control to nonlinear sliding mode control using concepts from optimal polynomial control. This method considered higher order weighting functions which consequently provides designers with more flexibility to achieve design objectives. The developed methodology was applied to a multi-span bridge equipped with semi-active MR dampers. The stochastically linearized model of the nonlinear system incorporated the dynamics of the control device, and a clipped optimal strategy was enforced for lower and upper bounds of control inputs. This methodology was shown to be successful in reducing pounding and excessive gap openings in adjacent structures. However, for larger systems and higher extents of nonlinearity, stochastic linearization may not be a good solution to characterize the system and design an optimal control algorithm.

To avoid linearization of the system, stochastic averaging of energy envelope was presented in Chapter 4 in order to characterize nonlinearity and uncertainty in the system and the excitation. The existing stochastic averaging of energy envelope was extended to enhanced stochastic averaging (ESA) to address limitations of these methods in dealing with damping in multi-DOF coupled nonlinear hysteretic systems and independent treatment of stochastic excitations. The averaging method was implemented in a single-story building with soil-structure interactions. To evaluate this method, the probabilistic measures of energy (e.g. probability distribution function and first and second order moments) were determined and compared with Monte Carlo simulations and the conventional stochastic averaging of energy envelope method (Chapter 4). Results indicated significant improvements in the accuracy of predictions using ESA compared to existing stochastic averaging method. Furthermore, Chapter 5 proposed a stochastic control

algorithm based on enhanced stochastic averaging of energy envelope. This strategy enables proper consideration of the stochastic nonlinear behavior of systems in the optimization process of the control design. The active control algorithm was implemented in a system with SSI, verified, and compared with linear quadratic regulator based on stochastic linearization.

Chapter 6 extended the stochastic control algorithm presented in Chapter 5 to explicitly optimize reliability of structures. Two variations of reliability-based control methods were proposed including constrained reliability-based control (CRC) and unconstrained reliability-based control (URC) algorithms. The CRC design employed first- and second-level optimizations sequentially, where the first-level optimization solved the Hamilton-Jacobi-Bellman equation and the second-level optimization searched for optimal objective function parameters to minimize the probability of failure. In the URC design, a single optimization minimized the probability of failure by directly searching for the optimal control gain. Considerable improvements were observed in structure's performance under stochastic excitations as discussed in Section 6.3. The proposed control methods have the potential to be used for control of other structures and dynamic systems.

Chapter 7 presented a stochastic risk-based framework for design as well as performance evaluation of controlled systems. The objective of the control design was to directly minimize the life cycle cost, which is evaluated through total probability theorem and crossing rate technique. Two control strategies were developed. The first control algorithm, called risk-based linear quadratic regulator (R-LQR), employs two levels of optimization where the first level is based on LQR and minimizes the second order moment of inter-story drifts, and the second level searched for optimal gains to minimize the

expected life cycle cost of the system. The second algorithm, called unconstrained risk-based regulator (URR), directly minimized the expected life cycle cost. These methods were applied to a nonlinear multi-story building subjected to earthquake excitations. Analytical optimizations were performed on the stochastically linearized model of the system. Uncertainties in system parameters and excitations were incorporated in the evaluation stage via Latin hypercube sampling method. These designs were compared with the status-quo option and the structure equipped with conventional LQR control strategy. Results showed that the proposed control methods reduced the life cycle cost and the extent of expected damage significantly compared with the status-quo option. In comparison to conventional LQR, R-LQR and URR reduced the life cycle cost of the system by $32.0-382.0K (including actuator and maintenance costs for controlled systems) as depicted in Table 7-2. This active control framework is a promising methodology to explicitly minimize the risk to structures under seismic events.

8.2 Future Research Directions

The presented computational and experimental research studies span two areas: hazard mitigation of civil engineering structures and treatment of system nonlinearity and stochasticity of hazard excitation. This research aims at developing control strategies that reduce the life cycle cost of structures that includes initial cost, the cost of maintaining and upgrading infrastructures, and repair costs in case of damage to structures following hazards. Other objectives include minimizing casualties and improving residents' comfort; all these enable achieving more resilient systems. Potential future research directions based on developments and findings of this research are listed below.

- Expanding the enhanced stochastic averaging method to higher DOFs under external excitations.
- Developing adaptive frameworks for disaster management and recovery of infrastructure systems and applying them to alleviate the likelihood and extent of damage to nonlinear structures under various hazard excitations.
- Integrating other risk measures to the risk-based framework discussed in the Chapter 7 by releasing the assumptions and limitations listed earlier.
- Implementing proposed control frameworks for other applications (e.g. irregular structures, quarter car model) and diverse hazard types (e.g. wind).
- Introducing a bounded optimization framework, which provides bounded optimal solutions versus clipped solutions for the constraints and dynamics of active and semi-active controllers.
- Conducting shaking table experiments to test proposed control strategies for realistic systems (e.g. systems with soil structure interactions).
- Optimizing the placement of control devices in large structures to maximize efficiency and performance on one hand and minimize cost on the other hand.

Appendix A: Derivation of Stochastic Averaging of Energy Envelope

Equations (4.16a-b) and Equation (4.17a-b) are fully derived here. First, the term, $\emptyset_1$, in Equation (4.16a), is

$$\emptyset_1 = \iiint_{\Upsilon} \frac{\dot{x}_1\dot{x}_2}{\dot{x}_2} \mathrm{d}x_1\mathrm{d}x_2\mathrm{d}\dot{x}_1 = \left(\iint \int_{-\sqrt{(2e-2u(x_1,x_2)-2u_2(z_2))}}^{\sqrt{(2e-2u(x_1,x_2)-2u_2(z_2))}} \dot{x}_1 d\dot{x}_1 dx_2 dx_1 \right|_{\dot{x}_2^+} + \iint \int_{-\sqrt{(2e-2u(x_1,x_2)-2u_2(z_2))}}^{\sqrt{(2e-2u(x_1,x_2)-2u_2(z_2))}} \dot{x}_1 d\dot{x}_1 dx_2 dx_1 \Big|_{\dot{x}_2^-} = \iint \frac{\dot{x}_1^2}{2} \Big|_{\sqrt{(2e-2u(x_1,x_2)-2u_2(z_2))}}^{\sqrt{(2e-2u(x_1,x_2)-2u_2(z_2))}} dx_2 dx_1 \Big|_{\dot{x}_2^+} + \iint \frac{\dot{x}_1^2}{2} \Big|_{-\sqrt{(2e-2u(x_1,x_2)-2u_2(z_2))}}^{\sqrt{(2e-2u(x_1,x_2)-2u_2(z_2))}} dx_2 dx_1 \Big|_{\dot{x}_2^-} \Bigg) = 0 \tag{A1}$$

To compute $\emptyset_2$ in Equation (4.16b), the differential equation for hysteresis is introduced. In that respect, the evolutionary variable, z_2, is governed by the Bouc-Wen model as

$$\dot{z}_2 = \mathrm{A_{BW}} - \gamma_{\mathrm{BW}}(\dot{x}_2|z_2| + z_2|\dot{x}_2|) \tag{A2}$$

where $\mathrm{A_{BW}}$ and γ_{BW} are parameters that control the shape of the loop. The nonlinear differential equation in Equation (A2) can be solved as

$$z_2(x_2) = \begin{cases} \begin{cases} \mathrm{A_{BW}}(x_2 + x_0) & -a \le x_2 \le -x_0 \\ \dfrac{\mathrm{A_{BW}}}{2\gamma_{\mathrm{BW}}}\left(1 - \exp\left(-2\gamma_{\mathrm{BW}}(x_2 + x_0)\right)\right) & -x_0 \le x_2 \le a \end{cases} & (\dot{x}_2 \ge 0) \\ \begin{cases} \dfrac{\mathrm{A_{BW}}}{2\gamma_{\mathrm{BW}}}\left(-1 + \exp\left(2\gamma_{\mathrm{BW}}(x_2 - x_0)\right)\right) & -a \le x_2 \le x_0 \\ \mathrm{A_{BW}}(x_2 - x_0)x_0 \le x_2 \le a \end{cases} & (\dot{x}_2 < 0) \end{cases} \tag{A3}$$

where a and x_0 are parameters the maximum amplitude and residue respectively. Then, the differential of $z_2$with respect to x_2,

$$\frac{dz_2(x_2)}{dx_2} = \begin{cases} \begin{cases} \mathrm{A_{BW}} & -a \le x_2 \le -x_0 \\ \mathrm{A_{BW}}\exp\left(-2\gamma_{\mathrm{BW}}(x_2 + x_0)\right) & -x_0 \le x_2 \le a \end{cases} & (\dot{x}_2 \ge 0) \\ \begin{cases} \mathrm{A_{BW}}\exp\left(-2\gamma_{\mathrm{BW}}(x_2 - x_0)\right) & -a \le x_2 \le x_0 \\ \mathrm{A_{BW}}x_0 \le x_2 \le a \end{cases} & (\dot{x}_2 < 0) \end{cases} \tag{A4}$$

Recall Equation (4.16b) is defined as

$$\emptyset_2 = \iiint_{\Upsilon} \frac{(1-\alpha_z)k_2 z_2 \frac{dz_2}{dx_2}\dot{x}_2}{\dot{x}_2}\, \mathrm{d}x_1 \mathrm{d}x_2 \mathrm{d}\dot{x}_1 = \iiint_{\Upsilon} (1-\alpha_z)k_2 z_2 \frac{dz_2}{dx_2}\, \mathrm{d}x_1 \mathrm{d}x_2 \mathrm{d}\dot{x}_1 \tag{A5}$$

Substituting Equation (A3) and Equation (A4) in Equation (A5), the integrand of $\emptyset_2$, is evaluated and integrated as

$$\begin{aligned} \int (1-\alpha_z)\, k_2 z_2 \frac{dz_2}{dx_2} dx_2 &= \int (1-\alpha_z)\, k_2 z_2 \frac{dz_2}{dx_2} dx_2\Big|_{\dot{x}_2^-} + \int (1-\alpha_z)\, k_2 z_2 \frac{dz_2}{dx_2} dx_2\Big|_{\dot{x}_2^+} \\ &= \int_{a(x_1,\dot{x}_1)}^{-a(x_1,\dot{x}_1)} (1-\alpha_z)\, k_2 z_2 \frac{dz_2}{dx_2} dx_2 + \int_{-a(x_1,\dot{x}_1)}^{a(x_1,\dot{x}_1)} (1-\alpha_z) k_2 z_2 \frac{dz_2}{dx_2} dx_2 \\ (1-\alpha_z)k_2 \Bigg(&\int_{a(x_1,\dot{x}_1)}^{x0} \mathrm{A_{BW}}^2 (x_2 - x_0)\, dx_2 \\ &+ \int_{x0}^{-a(x_1,\dot{x}_1)} \frac{-\mathrm{A_{BW}}^2}{2\gamma_{\mathrm{BW}}}\left(\exp\left(2\gamma(x_2 - x_0)\right) - \exp\left(4\gamma_{\mathrm{BW}}(x_2 - x_0)\right)\right) dx_2 \Bigg) \\ +(1-\alpha_z)k_2 \Big(&\int_{-a(x_1,\dot{x}_1)}^{-x0} \mathrm{A_{BW}}^2 (x_2 + x_0)\, dx_2 + \\ &\int_{-x0}^{a(x_1,\dot{x}_1)} \frac{\mathrm{A_{BW}}^2}{2\gamma_{\mathrm{BW}}}\left(\exp\left(-2\gamma(x_2 + x_0)\right) - \exp\left(-4\gamma_{\mathrm{BW}}(x_2 + x_0)\right)\right) dx_2 \Big) = 0 \end{aligned} \tag{A6}$$

The terms in Equations (4.18a-b) are obtained as:

$$\emptyset_3 = \iiint_{\Upsilon} \frac{\dot{x}_1^2}{\dot{x}_2} \mathrm{d}x_1 \mathrm{d}x_2 \mathrm{d}\dot{x}_1 = \iint \int_{-¥}^{¥} \frac{\dot{x}_1^2}{\dot{x}_2} d\dot{x}_1 dx_2 dx_1 \Big|_{\dot{x}_2^+} + \iint \int_{-¥}^{¥} \frac{\dot{x}_1^2}{\dot{x}_2} d\dot{x}_1 dx_2 dx_1 \Big|_{\dot{x}_2^-}$$

$$= \int_{-\sqrt{2e}}^{\sqrt{2e}} \int_{\varphi}^{-\varphi} \int_{-¥}^{¥} \frac{\dot{x}_1^2}{-\sqrt{(2e - 2u(x_1, x_2) - \dot{x}_1^2)}} d\dot{x}_1 \mathrm{d}x_1 \mathrm{d}x_2$$

$$+ \int_{-\sqrt{2e}}^{\sqrt{2e}} \int_{-\varphi}^{\varphi} \int_{-¥}^{¥} \frac{\dot{x}_1^2}{\sqrt{(2e - 2u(x_1, x_2) - \dot{x}_1^2)}} d\dot{x}_1 \mathrm{d}x_1 \mathrm{d}x_2$$

$$= \iint 2 \int_{-¥}^{¥} \frac{\dot{x}_1^2}{\sqrt{(2e - 2u(x_1, x_2) - \dot{x}_1^2)}} d\dot{x}_1 \mathrm{d}x_1 \mathrm{d}x_2$$

$$= \iint \pi\big(2e - 2u(x_1, x_2) - 2u_2(z_2)\big) \, \mathrm{d}x_1 \mathrm{d}x_2 \tag{A7}$$

$$\emptyset_4 = \iiint_{\Upsilon} \frac{\dot{x}_2^2}{\dot{x}_2} \mathrm{d}x_1 \mathrm{d}x_2 \mathrm{d}\dot{x}_1$$

$$= \iint \int_{-¥}^{¥} \frac{\dot{x}_2^2}{\dot{x}_2} d\dot{x}_1 dx_1 dx_2 \Big|_{\dot{x}_2^+} + \iint \int_{-¥}^{¥} \frac{\dot{x}_2^2}{\dot{x}_2} d\dot{x}_1 dx_1 dx_2 \Big|_{\dot{x}_2^-}$$

$$= \iint 2 \int_{-¥}^{¥} \sqrt{(2e - 2u(x_1, x_2) - \dot{x}_1^2)} d\dot{x}_1 \, \mathrm{d}x_1 \mathrm{d}x_2 \tag{A8}$$

$$= \iint \pi\big(2e - 2u(x_1, x_2) - 2u_2(z_2)\big) \, \mathrm{d}x_1 \mathrm{d}x_2$$

$$¥ = \sqrt{\big(2e - 2u(x_1, x_2) - 2u_2(z_2)\big)} \tag{A9}$$

$$\varphi = \sqrt{\big(2e - 2u(x_1, 0)\big)} \tag{A10}$$

References

Abad, J., Ulrich, T., Réveillere, A., & Gehl, P. (2013, August). Development of damage state-dependent fragility functions for a MDOF structure through dynamic analyses with successive un-scaled time-histories. In *Vienna Congress on Recent Advances in Earthquake Engineering and Structural Dynamics 2013 (VEESD 2013)* (pp. Paper-ID).

Adhikari, R., & Yamaguchi, H. (1997). Sliding mode control of buildings with ATMD. *Earthquake engineering & structural dynamics*, *26*(4), 409-422.

Agrawal, A. K., Yang, J. N., & He, W. L. (2003). Applications of some semiactive control systems to benchmark cable-stayed bridge. *Journal of Structural Engineering*, *129*(7), 884-894.

Alavinasab, A., Moharrami, H., & Khajepour, A. (2006). Active Control of Structures Using Energy-Based LQR Method. *Computer‐Aided Civil and Infrastructure Engineering*, *21*(8), 605-611.

Aldemir, U., Yanik, A., & Bakioglu, M. (2012). Control of structural response under earthquake excitation. *Computer‐Aided Civil and Infrastructure Engineering*, *27*(8), 620-638.

Aly, A. M., Zasso, A., & Resta, F. (2011). On the dynamics of a very slender building under winds: response reduction using MR dampers with lever mechanism. *The structural design of tall and special buildings*, *20*(5), 539-551.

Amini, F., Hazaveh, N. K., & Rad, A. A. (2013). Wavelet PSO-Based LQR Algorithm for Optimal Structural Control Using Active Tuned Mass Dampers. *Computer-Aided Civil and Infrastructure Engineering*, *28*(7), 542-557.

Amini, F., & Shadlou, M. (2011). Embedment effects of flexible foundations on control of structures. *Soil Dynamics and Earthquake Engineering*, *31*(8), 1081-1093.

Amiri, G. G., Bagheri, A., & Fadavi, M. (2007). New method for generation of artificial ground motion by a nonstationary Kanai-Tajimi model and wavelet transform. *Structural Engineering and Mechanics*, *26*(6), 709-724.

Anh, N. D., Hung, L. X., Viet, L. D., & Thang, N. C. (2015). Global-local mean square error criterion for equivalent linearization of nonlinear systems under random excitation. *Acta Mechanica*, *226*(9), 3011.

Bahar, A., Pozo, F., Acho, L., Rodellar, J., & Barbat, A. (2010). Hierarchical semi-active contro of base-isolated structures using a new inverse model of magnetorheological dampers. *Computers & structures*, *88*(7), 483-496.

Bajaj, H. M., Singh Birdi, G., & Ugale, B. A. (2014). Application of magnetorheological (MR) fluid damper and its social impact. *International Journal of Mechanical and Production Engineering*, *2*, 41-45.

Basili, M., & De Angelis, M. (2007). Optimal passive control of adjacent structures interconnected with nonlinear hysteretic devices. *Journal of sound and vibration*, *301*(1), 106-125.

Basili, M., De Angelis, M., & Fraraccio, G. (2013). Shaking table experimentation on adjacent structures controlled by passive and semi-active MR dampers. *Journal of Sound and Vibration*, *332*(13), 3113-3133.

Bellizzi, S., & Bouc, R. (1999a). Analysis of multi-degree of freedom strongly non-linear mechanical systems with random input: part I: non-linear modes and stochastic averaging. *Probabilistic Engineering Mechanics*, *14*(3), 229-244.

Bellizzi, S., & Bouc, R. (1999b). Analysis of multi-degree of freedom strongly non-linear mechanical systems with random input: Part II: equivalent linear system with random matrices and power spectral density matrix. *Probabilistic Engineering Mechanics*, *14*(3), 245-256.

Bellizzi, S., Guillemain, P., & Kronland-Martinet, R. (2001). Identification of coupled non-linear modes from free vibration using time-frequency representations. *Journal of Sound and Vibration*, *243*(2), 191-213.

Benjamin, J. R., & Cornell, C. A. (2014). *Probability, statistics, and decision for civil engineers*. Courier Corporation.

Berke, P., Smith, G., & Lyles, W. (2012). Planning for resiliency: Evaluation of state hazard mitigation plans under the disaster mitigation act. *Natural Hazards Review*, *13*(2), 139-149.

Bouc, R. (1971). A mathematical model for hysteresis. *Acta Acustica united with Acustica*, *24*(1), 16-25.

Bitaraf, M., & Hurlebaus, S. (2013). Semi-active adaptive control of seismically excited 20-story nonlinear building. *Engineering Structures*, *56*, 2107-2118.

Cai, G. Q. (2009). Application of stochastic averaging to non-linear ecosystems. *International Journal of Non-Linear Mechanics*, *44*(7), 769-775.

Cai, G. P., Huang, J. Z., Sun, F., & Wang, C. (2000). Modified sliding-mode bang–bang control for seismically excited linear structures. *Earthquake engineering & structural dynamics*, *29*(11), 1647-1657.

Casciati, F., & Roberts, B. (1996). *Mathematical models for structural reliability analysis* (Vol. 5). CRC Press.

Cha, Y. J., Zhang, J., Agrawal, A. K., Dong, B., Friedman, A., Dyke, S. J., & Ricles, J. (2013). Comparative studies of semiactive control strategies for MR dampers: pure simulation and real-time hybrid tests. *Journal of Structural Engineering*, *139*(7), 1237-1248.

Connor, J., & Laflamme, S. (2014). Applications of Active Control. In *Structural Motion Engineering* (pp. 347-386). Springer International Publishing.

Klebaner, F. C. (2005). *Introduction to stochastic calculus with applications*. World Scientific Publishing Co Inc.

Çeşmeci, Ş., & Engin, T. (2010). Modeling and testing of a field-controllable magnetorheological fluid damper. *International Journal of Mechanical Sciences*, *52*(8), 1036-1046.

Chakraborty, S., Debbarma, R., & Marano, G. C. (2012). Performance of tuned liquid column dampers considering maximum liquid motion in seismic vibration control of structures. *Journal of Sound and Vibration*, *331*(7), 1519-1531.

Chakraborty, S., & Roy, B. K. (2011). Reliability based optimum design of tuned mass damper in seismic vibration control of structures with bounded uncertain parameters. *Probabilistic Engineering Mechanics*, *26*(2), 215-221.

Chang, C. M., & Spencer, B. F. (2010). Active base isolation of buildings subjected to seismic excitations. *Earthquake Engineering & Structural Dynamics*, *39*(13), 1493-1512.

Chau, K. T., & Wei, X. X. (2001). Pounding of structures modelled as non-linear impacts of two oscillators. *Earthquake engineering & structural dynamics*, *30*(5), 633-651.

Chen, L. C., & Zhu, W. Q. (2009). Stochastic averaging of strongly nonlinear oscillators with small fractional derivative damping under combined harmonic and white noise excitations. *Nonlinear Dynamics*, *56*(3), 231-241.

Chen, L., & Zhu, W. Q. (2010). First passage failure of quasi non-integrable generalized Hamiltonian systems. *Archive of Applied Mechanics*, *80*(8), 883-893.

Chen, L., & Zhu, W. (2011). Stochastic jump and bifurcation of Duffing oscillator with fractional derivative damping under combined harmonic and white noise excitations. *International Journal of Non-Linear Mechanics, 46*(10), 1324-1329.

Cheng, H., Zhu, W. Q., & Ying, Z. G. (2006). Stochastic optimal semi-active control of hysteretic systems by using a magneto-rheological damper. *Smart materials and structures, 15*(3), 711.

Chiou, B. J., & Youngs, R. R. (2008). An NGA model for the average horizontal component of peak ground motion and response spectra. *Earthquake Spectra, 24*(1), 173-215.

Chopra, A. K. (2007). Dynamics of structures: theory and applications to earthquake engineering. 2007.

Christenson, R. E., & Emmons, A. T. (2005). Semiactive structural control of a nonlinear building model: Considering reliability. In *Proc., Structures Congress 2005: Session on Semiactive Control of Civil Structures*. Reston, Va: ASCE.

Christofides, P. D., & El-Farra, N. (2005). *Control of nonlinear and hybrid process systems: Designs for uncertainty, constraints and time-delays* (Vol. 324). Springer Science & Business Media.

Code, U. B. (1988). ICBO. In *International Conference of Building Officials*.

Corbi, O. T. T. A. V. I. A., Elattar, A. D. E. L., Saleh, A. H. M. E. D., & Zaghw, A. H. I. (2013). Protection of an Historical Islamic Minaret by Passive and Semi-Active Control

Strategies. In *WSEAS International Conference. Proceedings. Recent Advances in Computer Engineering Series* (No. 9). WSEAS.

Council, Building Seismic Safety (1997). NEHRP recommended provisions for seismic regulations for new buildings and other structures. *Washington, DC, 1*, 997.

Debbarma, R., Chakraborty, S., & Ghosh, S. K. (2010). Optimum design of tuned liquid column dampers under stochastic earthquake load considering uncertain bounded system parameters. *International Journal of Mechanical Sciences*, *52*(10), 1385-1393.

Deng, M. L., & Zhu, W. Q. (2011). Energy Transition Rate at Peptide-Bond Using Stochastic Averaging Method. In *IUTAM Symposium on Nonlinear Stochastic Dynamics and Control* (pp. 13-23). Springer Netherlands.

DesRoches, R., Comerio, M., Eberhard, M., Mooney, W., & Rix, G. J. (2011). Overview of the 2010 Haiti earthquake. *Earthquake Spectra*, *27*(S1), S1-S21.

Efraimiadou, S., Hatzigeorgiou, G. D., & Beskos, D. E. (2013). Structural pounding between adjacent buildings subjected to strong ground motions. Part I: The effect of different structures arrangement. *Earthquake Engineering & Structural Dynamics*, *42*(10), 1509-1528.

El-Khoury, O., Shafieezadeh, A., and Fereshtehnejad, E. (2017), "Risk-Based Control Based of Nonlinear Structures." Structural Control and Health Monitoring, In Preparation.

El-Khoury, O. and Shafieezadeh, A. (2017b), "Reliability-Based Control Strategies for Nonlinear Hysteretic Systems Using Enhanced Stochastic Averaging Approach." Earthquake Engineering and Structural Dynamics, Accepted.

El-Khoury, O. and Shafieezadeh, A. (2017a), "Enhanced Stochastic Averaging of Non-integrable Nonlinear System Subjected to Single White Noise." Soil Dynamics and Earthquake Engineering, In Review.

El-Khoury, O. and Shafieezadeh, A. (2016). A Stochastic Averaging-based Optimal Control Method for Nonlinear Systems: Application to a Building with Soil-structure Interactions. Engineering Structures, Vol. 127, No. 15, pp. 635-644.

El-Khoury, O., Shafieezadeh, A., Kim, C., Hur, J. E., and Heo, G. H. (2016), "Mitigation of the Seismic Response of Multi-Span Bridges Using MR Dampers: Experimental Study of a New SMC-Based Controller." Journal of Vibrations and Control, DOI: 10.1177/1077546316633540.

El-Khoury, O., Kim, C., Shafieezadeh, A., Hur, J. E., and Heo, G. H. (2015), "Experimental study of the semi-active control of a nonlinear two span bridge using stochastic optimal polynomial control." Smart Materials and Structures, Vol. 24, No.6, pp. 1-15.

El-Khoury, O. and Adeli, H. (2013), "Recent Advances on Vibration Control of Structures under Dynamic Loading." Archives of Computational Methods in Engineering, Vol. 20, No.4, pp.353-360.

Ellingwood, B. R. (2001). Earthquake risk assessment of building structures. *Reliability Engineering & System Safety, 74*(3), 251-262.

Fan, Y. C., Loh, C. H., Yang, J. N., & Lin, P. Y. (2009). Experimental performance evaluation of an equipment isolation using MR dampers. *Earthquake Engineering & Structural Dynamics, 38*(3), 285-305.

FEMA, H. (2003). Multi-hazard loss estimation methodology, earthquake model. *Washington, DC, USA: Federal Emergency Management Agency*.

Fereshtehnejad, E., & Shafieezadeh, A. (2016). Multiple hazard incidents lifecycle cost assessment of structural systems considering state-dependent repair times and fragility curves. *Earthquake Engineering & Structural Dynamics*, *45*(14), 2327-2347.

Fleming, W. H., & Soner, H. M. (2006). *Controlled Markov processes and viscosity solutions* (Vol. 25). Springer Science & Business Media.

Frangopol, D. M., & Ellingwood, B. R. (2010). Life-cycle performance, safety, reliability and risk of structural systems. *Structure magazine, 7*.

Fridman, L., Moreno, J., & Iriarte, R. (2011). Sliding modes after the first decade of the 21st century. *Lecture notes in control and information sciences, 412*.

Gajan, S., Raychowdhury, P., Hutchinson, T. C., Kutter, B. L., & Stewart, J. P. (2010). Application and validation of practical tools for nonlinear soil-foundation interaction analysis. *Earthquake Spectra*, *26*(1), 111-129.

Gencturk, B. (2013). Life-cycle cost assessment of RC and ECC frames using structural optimization. *Earthquake Engineering & Structural Dynamics*, *42*(1), 61-79.

Ghobarah, A. (2004, June). On drift limits associated with different damage levels. In *Performance-Based Seismic Design Concepts and Implementation: Proceedings of the International Workshop, Bled, Slovenia* (Vol. 28, pp. 321-332).

Gidaris, I., & Taflanidis, A. A. (2015). Performance assessment and optimization of fluid viscous dampers through life-cycle cost criteria and comparison to alternative design approaches. *Bulletin of Earthquake Engineering*, *13*(4), 1003-1028.

Guha-Sapir, D., Vos, F., Below, R., & Penserre, S. (2012). *Annual disaster statistical review 2011: the numbers and trends* (No. CRED/IRSS). UCL.

Gu, X. D., & Zhu, W. Q. (2014). Optimal bounded control of quasi-nonintegrable Hamiltonian systems using stochastic maximum principle. *Nonlinear Dynamics*, *76*(2), 1051-1058.

Gu, X. D., Zhu, W. Q., & Xu, W. (2012). Stochastic optimal control of quasi non-integrable Hamiltonian systems with stochastic maximum principle. *Nonlinear Dynamics*, *70*(1), 779-787.

Guo, A., Li, Z., Li, H., & Ou, J. (2009). Experimental and analytical study on pounding reduction of base-isolated highway bridges using MR dampers. *Earthquake Engineering & Structural Dynamics*, *38*(11), 1307-1333.

Gupta, B., & Kunnath, S. K. (2000). Adaptive spectra-based pushover procedure for seismic evaluation of structures. *Earthquake spectra*, *16*(2), 367-392.

Han, Q., Du, X., Liu, J., Li, Z., Li, L., & Zhao, J. (2009). Seismic damage of highway bridges during the 2008 Wenchuan earthquake. *Earthquake Engineering and Engineering Vibration*, *8*(2), 263-273.

Hover, F. S., & Triantafyllou, M. S. (2006). Application of polynomial chaos in stability and control. *Automatica*, *42*(5), 789-795.

Huang, Z. L., & Zhu, W. Q. (2004). Stochastic averaging of quasi-integrable Hamiltonian systems under bounded noise excitations. *Probabilistic Engineering Mechanics*, *19*(3), 219-228.

Huang, Z. L., & Zhu, W. Q. (2009). Stochastic averaging of quasi-generalized Hamiltonian systems. *International Journal of Non-Linear Mechanics*, *44*(1), 71-80.

Huo, Y., & Zhang, J. (2012). Effects of pounding and skewness on seismic responses of typical multispan highway bridges using the fragility function method. *Journal of Bridge Engineering*, *18*(6), 499-515.

Gao, W. (2006). Stochastically optimal active control of a smart truss structure under stationary random excitation. *Journal of Sound and Vibration*, *290*(3), 1256-1268.

Gerolymos, N., & Gazetas, G. (2007). A model for grain-crushing-induced landslides—Application to Nikawa, Kobe 1995. *Soil Dynamics and Earthquake Engineering*, *27*(9), 803-817.

Gidaris, I., & Taflanidis, A. A. (2015). Performance assessment and optimization of fluid viscous dampers through life-cycle cost criteria and comparison to alternative design approaches. *Bulletin of Earthquake Engineering*, *13*(4), 1003-1028.

Gu, X. D., & Zhu, W. Q. (2014). Optimal bounded control of quasi-nonintegrable Hamiltonian systems using stochastic maximum principle. *Nonlinear Dynamics*, *76*(2), 1051-1058.

Ikhouane, F., & Dyke, S. J. (2007). Modeling and identification of a shear mode magnetorheological damper. *Smart Materials and Structures*, *16*(3), 605.

Ikhouane, F., Hurtado, J. E., & Rodellar, J. (2007). Variation of the hysteresis loop with the Bouc–Wen model parameters. *Nonlinear Dynamics*, *48*(4), 361-380.

Isbiliroglu, Y., Taborda, R., & Bielak, J. (2015). Coupled soil-structure interaction effects of building clusters during earthquakes. *Earthquake Spectra*, *31*(1), 463-500.

Ismail, M., Ikhouane, F., & Rodellar, J. (2009). The hysteresis Bouc-Wen model, a survey. *Archives of Computational Methods in Engineering*, *16*(2), 161-188.

Iwan, W. D., & Spanos, P. T. (1978). Response envelope statistics for nonlinear oscillators with random excitation. *ASME, Transactions, Journal of Applied Mechanics*, *45*, 170-174.

Jankowski, R., Wilde, K., & Fujino, Y. (1998). Pounding of superstructure segments in isolated elevated bridge during earthquakes. *Earthquake engineering & structural dynamics*, *27*(5), 487-502.

Jalayer, F., Asprone, D., Prota, A., & Manfredi, G. (2011). Multi-hazard upgrade decision making for critical infrastructure based on life-cycle cost criteria. *Earthquake Engineering & Structural Dynamics*, *40*(10), 1163-1179.

Jia, G., Gidaris, I., Taflanidis, A. A., & Mavroeidis, G. P. (2014). Reliability-based assessment/design of floor isolation systems. *Engineering Structures*, *78*, 41-56.

Johnson, N., Ranf, R. T., Saiidi, M. S., Sanders, D., & Eberhard, M. (2008). Seismic testing of a two-span reinforced concrete bridge. *Journal of Bridge Engineering*, *13*(2), 173-182.

Kanai, K 1957 Semi-empirical formula for the seismic characteristics of the ground Bulletin of the Earthquake Research Institute University of Tokyo 35 309-25.

Karimi, H. R., Palacios-Quiñonero, F., Rossell, J. M., & Rubió-Massegú, J. (2013). Sequential design of multioverlapping controllers for structural vibration control of tall buildings under seismic excitation. *Proceedings of the Institution of Mechanical Engineers, Part I: Journal of Systems and Control Engineering*, *227*(2), 176-183.

Kausel, E. (2010). Early history of soil–structure interaction. *Soil Dynamics and Earthquake Engineering*, *30*(9), 822-832.

Kawashima, K., Takahashi, Y., Ge, H., Wu, Z., & Zhang, J. (2009). Reconnaissance report on damage of bridges in 2008 Wenchuan, China, earthquake. *Journal of Earthquake Engineering*, *13*(7), 965-996.

Kester, W. A. (Ed.). (2005). Data conversion handbook. Newnes.

Kiureghian, A. D. (2005). Non-ergodicity and PEER's framework formula. *Earthquake engineering & structural dynamics*, *34*(13), 1643-1652.

Kiureghian, A. D., & Neuenhofer, A. (1992). Response spectrum method for multi-support seismic excitations. *Earthquake Engineering & Structural Dynamics*, *21*(8), 713-740.

Kim, S. J., Holub, C. J., & Elnashai, A. S. (2010). Analytical assessment of the effect of vertical earthquake motion on RC bridge piers. *Journal of Structural Engineering*, *137*(2), 252-260.

Kim, Y., Bai, J. W., & Albano, L. D. (2013). Fragility estimates of smart structures with sensor faults. *Smart Materials and Structures*, *22*(12), 125012.

Kim, S., Pakzad, S., Culler, D., Demmel, J., Fenves, G., Glaser, S., & Turon, M. (2007, April). Health monitoring of civil infrastructures using wireless sensor networks. In *Proceedings of the 6th international conference on Information processing in sensor networks* (pp. 254-263). ACM.

Korkmaz, S. (2011). A review of active structural control: challenges for engineering informatics. *Computers & Structures*, *89*(23), 2113-2132.

Kwok, N. M., Ha, Q. P., Nguyen, M. T., Li, J., & Samali, B. (2007). Bouc–Wen model parameter identification for a MR fluid damper using computationally efficient GA. *ISA transactions*, *46*(2), 167-179.

Kwon, H. C., Kim, M. C., & Lee, I. W. (1998). Vibration control of bridges under moving loads. *Computers & Structures*, *66*(4), 473-480.

Leavitt, J., Bobrow, J. E., Jabbari, F., & Yang, J. N. (2006). Application of a high-pressure gas semi-active resettable damper to the benchmark smart base-isolated building. *Structural Control and Health Monitoring*, *13*(2-3), 748-757.

Lee, T. Y., & Chen, P. C. (2011a). Experimental and analytical study of sliding mode control for isolated bridges with MR dampers. *Journal of Earthquake Engineering*, *15*(4), 564-581.

Lee, T. Y., & Chen, P. C. (2011b). Sliding mode control for nonlinear isolated bridges. *Journal of Earthquake Engineering*, *15*(4), 582-600.

Lei, Y., Wu, D. T., & Lin, Y. (2012). A Decentralized Control Algorithm for Large-Scale Building Structures. *Computer-Aided Civil and Infrastructure Engineering*, *27*(1), 2-13.1

Li, Z., Deng, Z., & Gu, Z. (2010a, May). New sliding mode control of building structure using RBF neural networks. In *Control and Decision Conference (CCDC), 2010 Chinese* (pp. 2820-2825). IEEE.

Li, J., Peng, Y. B., & Chen, J. B. (2010b). A physical approach to structural stochastic optimal controls. *Probabilistic Engineering Mechanics*, *25*(1), 127-141.

Liel, A. B., Haselton, C. B., Deierlein, G. G., & Baker, J. W. (2009). Incorporating modeling uncertainties in the assessment of seismic collapse risk of buildings. *Structural Safety*, *31*(2), 197-211.

Lim, C. W., Chung, T. Y., & Moon, S. J. (2003). Adaptive bang–bang control for the vibration control of structures under earthquakes. *Earthquake engineering & structural dynamics*, *32*(13), 1977-1994.

Lin, Y. K., & Cai, G. Q. (2004). *Probabilistic structural dynamics: advanced theory and applications*. Mcgraw-hill Professional Publishing.

Liu, Z. H., & Zhu, W. Q. (2007). Stochastic averaging of quasi-integrable Hamiltonian systems with delayed feedback control. *Journal of Sound and Vibration*, *299*(1), 178-195.

Luo, M., & Zhu, W. Q. (2006). Nonlinear stochastic optimal control of offshore platforms under wave loading. *Journal of sound and vibration*, *296*(4), 734-745.

Lutes, L.D., Sarkani, S., 1997. Stochastic Analysis of Structural and Mechanical Vibrations. Prentice-Hall, New Jersey, USA.

Marano, G. C., Greco, R., Trentadue, F., & Chiaia, B. (2007). Constrained reliability-based optimization of linear tuned mass dampers for seismic control. *International Journal of Solids and Structures*, *44*(22), 7370-7388.

Mason, H. B., Trombetta, N. W., Chen, Z., Bray, J. D., Hutchinson, T. C., & Kutter, B. L. (2013). Seismic soil–foundation–structure interaction observed in geotechnical centrifuge experiments. *Soil Dynamics and Earthquake Engineering*, *48*, 162-174.

McKenna, F. (2011). OpenSees: a framework for earthquake engineering simulation. *Computing in Science & Engineering*, *13*(4), 58-66.

Metered, H., Bonello, P., & Oyadiji, S. O. (2010). The experimental identification of magnetorheological dampers and evaluation of their controllers. *Mechanical systems and signal processing*, *24*(4), 976-994.

Miranda, M. J., & Fackler, P. L. (2004). *Applied computational economics and finance*. MIT press.

Mishra, S. K., & Chakraborty, S. (2013). Performance of a base-isolated building with system parameter uncertainty subjected to a stochastic earthquake. *Int J Acoust Vibr*, *18*(1), 7-19.

Moghimi, R. (2010). Low Noise Signal Conditioning for Sensor-Based Circuits. *system*, *1*, 0-02.

Muravyov, A., Turner, T., Robinson, J., & Rizzi, S. (1999, January). A new stochastic equivalent linearization implementation for prediction of geometrically nonlinear vibrations. In *40th Structures, Structural Dynamics, and Materials Conference and Exhibit* (p. 1376).

Muthukumar, S., & DesRoches, R. (2006). A Hertz contact model with non-linear damping for pounding simulation. *Earthquake engineering & structural dynamics*, *35*(7), 811-828.

Naserkhaki, S., Aziz, F. N. A., & Pourmohammad, H. (2012). Earthquake induced pounding between adjacent buildings considering soil-structure interaction. *Earthquake Engineering and Engineering Vibration*, *11*(3), 343-358.

Nateghi-A, F., & Rezaei-Tabrizi, A. (2013). Nonlinear dynamic response of tall buildings considering structure–soil–structure effects. *The Structural Design of Tall and Special Buildings*, *22*(14), 1075-1082.

Ni, Y. Q., Spencer Jr, B. F., & Ko, J. M. (2001, July). Feasibility of active control of cable-stayed bridges: an insight into Ting Kau Bridge. In *SPIE's 8th Annual International Symposium on Smart Structures and Materials* (pp. 387-398). International Society for Optics and Photonics.

Norio, O., Ye, T., Kajitani, Y., Shi, P., & Tatano, H. (2011). The 2011 eastern Japan great earthquake disaster: Overview and comments. *International Journal of Disaster Risk Science*, *2*(1), 34-42.

Nguyen, Q. H., Choi, S. B., & Wereley, N. M. (2008). Optimal design of magnetorheological valves via a finite element method considering control energy and a time constant. *Smart Materials and Structures*, *17*(2), 025024.

Ohtori, Y., Christenson, R. E., Spencer Jr, B. F., & Dyke, S. J. (2004). Benchmark control problems for seismically excited nonlinear buildings. *Journal of Engineering Mechanics*, *130*(4), 366-385.

Ozbulut, O. E., & Hurlebaus, S. (2011). Re-centering variable friction device for vibration control of structures subjected to near-field earthquakes. *Mechanical Systems and Signal Processing*, *25*(8), 2849-2862.

Pamuk, A., Kalkan, E., & Ling, H. I. (2005). Structural and geotechnical impacts of surface rupture on highway structures during recent earthquakes in Turkey. *Soil Dynamics and Earthquake Engineering*, *25*(7), 581-589.

Pecker, A., Paolucci, R., Chatzigogos, C., Correia, A. A., & Figini, R. (2014). The role of non-linear dynamic soil-foundation interaction on the seismic response of structures. *Bulletin of Earthquake Engineering*, *12*(3), 1157-1176.

Peng, Y. B., Ghanem, R., & Li, J. (2010). Polynomial chaos expansions for optimal control of nonlinear random oscillators. *Journal of Sound and Vibration*, *329*(18), 3660-3678.

Peng, Y. B., Ghanem, R., & Li, J. (2013). Generalized optimal control policy for stochastic optimal control of structures. *Structural Control and Health Monitoring*, *20*(2), 187-209.

Prabakar, R. S., Sujatha, C., & Narayanan, S. (2013). Response of a quarter car model with optimal magnetorheological damper parameters. *Journal of Sound and Vibration*, *332*(9), 2191-2206.

Priestley, M. J. N., Calvi, G. M., & Kowalsky, M. J. (2007). Direct displacement-based seismic design of structures. In *2007 NZSEE conference*.

Raheem, S. E. A. (2009). Pounding mitigation and unseating prevention at expansion joints of isolated multi-span bridges. *Engineering Structures*, *31*(10), 2345-2356.

Rao, S. S., & Rao, S. S. (2009). *Engineering optimization: theory and practice*. John Wiley & Sons.

Rahman, M., Ong, Z. C., Chong, W. T., Julai, S., & Khoo, S. Y. (2015). Performance enhancement of wind turbine systems with vibration control: A review. *Renewable and Sustainable Energy Reviews*, *51*, 43-54.

Raychowdhury, P. (2011). Seismic response of low-rise steel moment-resisting frame (SMRF) buildings incorporating nonlinear soil–structure interaction (SSI). *Engineering Structures*, *33*(3), 958-967.

Roberts, J. B., & Spanos, P. D. (2003). *Random vibration and statistical linearization*. Courier Corporation.

Rofooei, F. R., Mobarake, A., & Ahmadi, G. (2001). Generation of artificial earthquake records with a nonstationary Kanai–Tajimi model. *Engineering Structures*, *23*(7), 827-837.

Saiidi, M. S., Vosooghi, A., & Nelson, R. B. (2012). Shake-table studies of a four-span reinforced concrete bridge. *Journal of Structural Engineering*, *139*(8), 1352-1361.

Scruggs, J. T., Taflanidis, A. A., & Beck, J. L. (2006). Reliability-based control optimization for active base isolation systems. *Structural Control and Health Monitoring*, *13*(2-3), 705-723.

Shafieezadeh, A., & Ryan, K. L. (2011). Demonstration of robust stability and performance of filter-enhanced H2/LQG controllers for a nonlinear structure. *Structural Control and Health Monitoring*, *18*(6), 710-720.

Shafieezadeh, A., Ryan, K., & Chen, Y. (2008). Fractional order filter enhanced LQR for seismic protection of civil structures. *Journal of Computational and Nonlinear Dynamics*, *3*(2), 021404.

Socha, L. (2005a). Linearization in analysis of nonlinear stochastic systems: recent results—part I: theory. *Applied Mechanics Reviews*, *58*(3), 178-205.

Socha, L. (2005b). Linearization in analysis of nonlinear stochastic systems, recent results—part II: applications. *Applied Mechanics Reviews*, *58*(5), 303-315.

Socha, L. (2007). *Linearization methods for stochastic dynamic systems* (Vol. 730). Springer Science & Business Media.

Soize, C. (1995). Stochastic linearization method with random parameters for SDOF nonlinear dynamical systems: prediction and identification procedures. *Probabilistic Engineering Mechanics*, *10*(3), 143-152.

Soize, C. (2013). Stochastic modeling of uncertainties in computational structural dynamics—recent theoretical advances. *Journal of Sound and Vibration*, *332*(10), 2379-2395.

Song, W. K., & Kim, S. E. (2007). Analysis of the overall collapse mechanism of cable-stayed bridges with different cable layouts. *Engineering Structures*, *29*(9), 2133-2142.

Soto, M. G., & Adeli, H. (2013). Tuned mass dampers. *Archives of Computational Methods in Engineering*, *20*(4), 419-431.

Soto, M. G., & Adeli, H. (2014). Optimum tuning parameters of tuned mass dampers for vibration control of irregular highrise building structures. *Journal of Civil Engineering and Management*, *20*(5), 609-620.

Spencer, B. F., Dyke, S. J., & Deoskar, H. S. (1998). Benchmark problems in structural control: part I-active mass driver system. *Earthquake Engineering and Structural Dynamics*, *27*(11), 1127-1140.

Spencer Jr, B. F., & Nagarajaiah, S. (2003). State of the art of structural control. *Journal of structural engineering*, *129*(7), 845-856.

Sun, H., Mordret, A., Prieto, G. A., Toksöz, M. N., & Büyüköztürk, O. (2017). Bayesian characterization of buildings using seismic interferometry on ambient vibrations. *Mechanical Systems and Signal Processing*, *85*, 468-486.

Stafford, P. J., Sgobba, S., & Marano, G. C. (2009). An energy-based envelope function for the stochastic simulation of earthquake accelerograms. *Soil Dynamics and Earthquake Engineering*, *29*(7), 1123-1133.

Sun, J. Q. (2006). *Stochastic dynamics and control* (Vol. 4). Elsevier.

Symans, M. D., Charney, F. A., Whittaker, A. S., Constantinou, M. C., Kircher, C. A., Johnson, M. W., & McNamara, R. J. (2008). Energy dissipation systems for seismic applications: current practice and recent developments. *Journal of structural engineering*, *134*(1), 3-21.

Tajimi, H. (1960). Statistical method of determining the maximum response of building structure during an earthquake. *Proc. of the 2nd WCEE, 2,* 781-798.

Tartakovsky, D. M. (1999). Stochastic modeling of heterogeneous phreatic aquifers. *Water Resources Research*, *35*(12), 3941-3945.

Taflanidis, A. A., Beck, J. L., & Angelides, D. C. (2007). Robust reliability-based design of liquid column mass dampers under earthquake excitation using an analytical reliability approximation. *Engineering Structures*, *29*(12), 3525-3537.

Taflanidis, A. A., & Beck, J. L. (2009). Life-cycle cost optimal design of passive dissipative devices. *Structural Safety*, *31*(6), 508-522.

Taflanidis, A. A., & Scruggs, J. T. (2010). Performance measures and optimal design of linear structural systems under stochastic stationary excitation. *Structural Safety*, *32*(5), 305-315.

Taflanidis, A. A., Scruggs, J. T., & Beck, J. L. (2008a). Reliability-based performance objectives and probabilistic robustness in structural control applications. *Journal of engineering mechanics*, *134*(4), 291-301.

Taflanidis, A. A., Scruggs, J. T., & Beck, J. L. (2008b). Probabilistically robust nonlinear design of control systems for base-isolated structures. *Structural Control and Health Monitoring*, *15*(5), 697-719.

To, C. W. (2000). *Nonlinear random vibration*. Swets & Zeitlinger.

To, C. W. S., & Li, D. M. (1991). Equivalent nonlinearization of nonlinear systems to random excitations. *Probabilistic engineering mechanics*, *6*(3-4), 184-192.

Todorov, E. (2006). Optimal control theory. *Bayesian brain: probabilistic approaches to neural coding*, 269-298.

Tse, K. T., Kwok, K. C. S., & Tamura, Y. (2012). Performance and cost evaluation of a smart tuned mass damper for suppressing wind-induced lateral-torsional motion of tall structures. *Journal of Structural Engineering*, *138*(4), 514-525.

Tu, J., Lin, X., Tu, B., Xu, J., & Tan, D. (2014). Simulation and experimental tests on active mass damper control system based on Model Reference Adaptive Control algorithm. *Journal of Sound and Vibration*, *333*(20), 4826-4842.

Utkin, V. I. (1977). Sliding mode control in the theory of variable structure systems.

Utkin, V. I. (1992). Sliding modes in optimization and control problems.

Wen, Y. K. (1976). Method for random vibration of hysteretic systems. *Journal of the engineering mechanics division*, *102*(2), 249-263.

Wen, Y. K. (1980). Equivalent linearization for hysteretic systems under random excitation. *Journal of Applied Mechanics*, *47*(1), 150-154.

Won, J. H., Mha, H. S., & Kim, S. H. (2015). Effects of the earthquake-induced pounding upon pier motions in the multi-span simply supported steel girder bridge. *Engineering Structures*, *93*, 1-12.

Wu, J. C., & Yang, J. N. (1997, June). Continuous sliding mode control of a TV transmission tower under stochastic wind. In *American Control Conference, 1997. Proceedings of the 1997* (Vol. 2, pp. 883-887). IEEE.

Xiang, P., & Nishitani, A. (2014). Seismic vibration control of building structures with multiple tuned mass damper floors integrated. *Earthquake Engineering & Structural Dynamics*, *43*(6), 909-925.

Xu, Y., Li, Y., Liu, D., Jia, W., & Huang, H. (2013). Responses of Duffing oscillator with fractional damping and random phase. *Nonlinear Dynamics*, *74*(3), 745-753.

Yang, M. G., & Cai, C. S. (2016). Longitudinal vibration control for a suspension bridge subjected to vehicle braking forces and earthquake excitations based on magnetorheological dampers. *Journal of Vibration and Control*, *22*(17), 3659-3678.

Yang, J. N., Li, Z., & Vongchavalitkul, S. (1994). Stochastic hybrid control of hysteretic structures. *Probabilistic Engineering Mechanics*, *9*(1-2), 125-133.

Yang, J. N., Agrawal, A. K., Samali, B., & Wu, J. C. (2004). Benchmark problem for response control of wind-excited tall buildings. *Journal of Engineering Mechanics*, *130*(4), 437-446.

Yang, J. N., Wu, J. C., & Agrawal, A. K. (1995a). Sliding mode control for seismically excited linear structures. *Journal of engineering mechanics*, *121*(12), 1386-1390.

Yang, J. N., Wu, J. C., & Agrawal, A. K. (1995b). Sliding mode control for nonlinear and hysteretic structures. *Journal of Engineering Mechanics*, *121*(12), 1330-1339.

Yang, J. N., Wu, J. C., Reinhorn, A. M., Riley, M., Schmitendorf, W. E., & Jabbari, F. (1996). Experimental verifications of H∞ and sliding mode control for seismically excited buildings. *Journal of Structural Engineering*, *122*(1), 69-75.

Yau, J. D. (2009). Response of a train moving on multi-span railway bridges undergoing ground settlement. *Engineering Structures*, *31*(9), 2115-2122.

Ye, K., Li, L., & Zhu, H. (2009). A modified Kelvin impact model for pounding simulation of base-isolated building with adjacent structures. *Earthquake Engineering and Engineering Vibration*, *8*(3), 433-446.

Yıldız, A. S., Sivrioğlu, S., Zergeroğlu, E., & Çetin, Ş. (2015). Nonlinear adaptive control of semi-active MR damper suspension with uncertainties in model parameters. *Nonlinear Dynamics*, *79*(4), 2753-2766.

Ying, Z. G., Zhu, W. Q., & Soong, T. T. (2003). A stochastic optimal semi-active control strategy for ER/MR dampers. *Journal of Sound and Vibration*, *259*(1), 45-62.

Ying, Z. G., Ni, Y. Q., & Ko, J. M. (2004). Non-linear stochastic optimal control for coupled-structures system of multi-degree-of-freedom. *Journal of Sound and Vibration*, *274*(3), 843-861.

Ying, Z. G., Ni, Y. Q., & Ko, J. M. (2005). Semi-active optimal control of linearized systems with multi-degree of freedom and application. *Journal of Sound and Vibration*, *279*(1), 373-388.

Ying, Z. G., Ni, Y. Q., & Ko, J. M. (2007). A bounded stochastic optimal semi-active control. *Journal of Sound and Vibration*, *304*(3), 948-956.

Yoshida, O., & Dyke, S. J. (2005). Response control of full-scale irregular buildings using magnetorheological dampers. *Journal of Structural Engineering*, *131*(5), 734-742.

Yoshida, O., Dyke, S. J., Giacosa, L. M., & Truman, K. Z. (2003). Experimental verification of torsional response control of asymmetric buildings using MR dampers. *Earthquake engineering & structural dynamics*, *32*(13), 2085-2105.

Yuen, K. V., & Beck, J. L. (2003). Reliability-based robust control for uncertain dynamical systems using feedback of incomplete noisy response measurements. *Earthquake engineering & structural dynamics*, *32*(5), 751-770.

Zeng, Y., & Zhu, W. Q. (2011). Stochastic averaging of quasi-nonintegrable-Hamiltonian systems under Poisson white noise excitation. *Journal of Applied Mechanics*, *78*(2), 021002.

Zhang, J., Huo, Y., Brandenberg, S. J., & Kashighandi, P. (2008). Effects of structural characterizations on fragility functions of bridges subject to seismic shaking and lateral spreading. *Earthquake Engineering and Engineering Vibration*, *7*(4), 369-382.

Zhao, M., & Zhu, W. Q. (2011). Stochastic optimal semi-active control of stay cables by using magneto-rheological damper. *Journal of Vibration and Control*, *17*(13), 1921-1929.

Zhu, W. Q. (2006). Nonlinear stochastic dynamics and control in Hamiltonian formulation. *Applied Mechanics Reviews*, *59*(4), 230-248.

Zhu, W. Q., Deng, M. L., & Huang, Z. L. (2002). First-passage failure of quasi-integrable Hamiltonian systems. *Journal of applied mechanics*, *69*(3), 274-282.

Zhu, W. Q., & Ying, Z. G. (2002). Nonlinear stochastic optimal control of partially observable linear structures. *Engineering Structures*, *24*(3), 333-342.

Zhu, W. Q., Ying, Z. G., & Soong, T. T. (2001). An optimal nonlinear feedback control strategy for randomly excited structural systems. *Nonlinear Dynamics*, *24*(1), 31-51.

Zhu, W. Q., Luo, M., & Ying, Z. G. (2004). Nonlinear stochastic optimal control of tall buildings under wind loading. *Engineering Structures*, *26*(11), 1561-1572.

Zhu, W. Q., Ying, Z. G., Ni, Y. Q., & Ko, J. M. (2000). Optimal nonlinear stochastic control of hysteretic systems. *Journal of engineering mechanics*, *126*(10), 1027-1032.

Zhu, C. X., & Zhu, W. Q. (2011). Feedback control of nonlinear stochastic systems for targeting a specified stationary probability density. *Automatica*, *47*(3), 539-544.